



HAL
open science

Bulk TiO₂ vs alternative Ti-based photocatalysts for the mild aerobic oxidation of alcohols

Diaa Obaid

► **To cite this version:**

Diaa Obaid. Bulk TiO₂ vs alternative Ti-based photocatalysts for the mild aerobic oxidation of alcohols. Theoretical and/or physical chemistry. Université Pierre et Marie Curie - Paris VI, 2017. English. NNT : 2017PA066578 . tel-01913747

HAL Id: tel-01913747

<https://theses.hal.science/tel-01913747>

Submitted on 6 Nov 2018

HAL is a multi-disciplinary open access archive for the deposit and dissemination of scientific research documents, whether they are published or not. The documents may come from teaching and research institutions in France or abroad, or from public or private research centers.

L'archive ouverte pluridisciplinaire **HAL**, est destinée au dépôt et à la diffusion de documents scientifiques de niveau recherche, publiés ou non, émanant des établissements d'enseignement et de recherche français ou étrangers, des laboratoires publics ou privés.

Université Pierre et Marie Curie

Ecole doctorale 397 - Physique et Chimie des Matériaux

Laboratoire de Réactivité de Surface / Equipe Catalyse

***Bulk TiO₂ vs alternative Ti-based photocatalysts
for the mild aerobic oxidation of alcohols***

Par Diaa OBAID

Thèse de doctorat de Chimie

Dirigée par Franck LAUNAY

Présentée et soutenue publiquement le 26 Octobre 2017

Devant un jury composé de :

MARCI Giuseppe, Associate Professor, Universita di Palermo	Rapporteur
VALANGE Sabine, Maître de Conférences HDR, Université de Poitiers	Rapporteur
EL ROZ Mohamad, Chargé de Recherches, CNRS Normandie	Examineur
GALVEZ PARRUCA Elena, Maître de Conférences HDR, UPMC	Examinatrice
LAUNAY Franck, Professeur, UPMC	Directeur de thèse

Dédicace

Acknowledgments

I am sincerely grateful to the staff and members of Surface Reactivity Laboratory, CNRS-Pierre and Marie Curie University, that broadens my research scopes in many areas and developed my visions in many aspects of the world. Many individuals provided help and support, I would like to express my gratitude for them, mostly, **Pr. Helene Pernot, Pr. Christian Bonhomme, and Dr. Catherine Louis** for kind support and encouragement during my PhD course. Without them, my graduate life will be much less wonderful.

I offer my first heartfelt thanks and eternally grateful to Prof. Dr. Franck Launay, the best advisor one could find, who teach me scientific thinking of the highest caliber. who supported and encouraged me with no limits of time. His keenness about knowing the basics and about questioning assumptions is an important lesson, which I shall carry with me throughout my career. He molded me from being just a student to, hopefully, being a researcher. Besides being a good professor, he has been a warm, delighted, and hilarious person.

I would like to thank the members of the chair of my PhD thesis jury for their useful comments and suggestions for the work included in this thesis, **special thanks for Pr. Dr. Leonardo Palmisano, Pr. Dr. Giuseppe Marci, Dr. Sabine Valange, Dr. Elena Galvez Parruca, Dr. Mohamad El Roz**, and would appreciate their cooperation.

I am thankful for the financial support I received from the French Government for giving me valuable advice and also an opportunity to do PhD in France.

I also deeply appreciate and extremely enjoyed working with **Dr. Asma Mayoufi** for her great cooperation during the course of my research.

I am very grateful to **Dr. Anne Davidson**, who has shown considerable interest in my work. Also, I am thankful to **Mdm. Patricia Beaunier**, for TEM micrographs.

To All and friends, they left me with memories of enlightening moments to be treasured forever.

My heartfelt regards and deepest thanks to the closest persons of my life who have given me all I could ask for and much more that can ever be expressed in words, **my parents** for their warmth and

affection. My mother and father are among the kindest and the most patient people I know. I will be eternally indebted to them for constantly arousing in me a sense of curiosity and wonder about both the physical and the human world. who have provided me with immense intellectual and moral inspiration.

“To live is to change, and to be perfect is to have changed often”

“A man would do nothing if he tried to do it so well that nobody would find fault with what he has done”

John Henry Newman

Summary

Introduction.....	1
Part I - Mild oxidation of alcohols using dioxygen in combination with photocatalysts.....	5
Chapter 1: Bibliography survey	7
Chapter 2 : Experimental results.....	33
Part II - New photocatalysts for alcohol oxidation based on the deposition of stable TiO₂ colloids onto mesoporous silica	57
Chapter 3: Bibliography survey	59
Chapter 4 : Experimental results.....	73
Conclusion générale.....	93
Annex 1	97
Annex 2	111

INTRODUCTION

For many years, a lot of attention has been paid to the development of heterogeneous catalytic systems that use clean, cheap, readily available and atom efficient oxidants such as molecular oxygen under mild conditions [1-8]. From the thermodynamic point of view, oxidation reactions with molecular oxygen are favorable. However, due to kinetic reasons, very few convincing studies have been reported in selective oxidation reactions involving O₂. Partial oxidation of molecules is very difficult knowing that the formed products are usually more reactive than the reactants themselves. In this field, the main challenge consists in designing resistant catalysts allowing a sufficient decrease of the activation energy. The way biological catalysts (enzymes) work *i.e.* through the activation of O₂ with the formation of reduced forms is a source of inspiration for chemists in this field. **This manuscript will focus on the oxidation of alcohols** which is a reaction often involved in chemical transformations used both for laboratory-scale experiments and in manufacturing processes [9-11]. Unfortunately, methods requiring stoichiometric amounts of oxidants such as dichromate, permanganate salts, peroxy acids are often used. However, such reactants are usually hazardous, corrosive, expensive and generate large quantities of useless by-products [12].

One pathway for O₂ activation is photocatalysis. Due to its wide band gap, unique electronic, morphological and optical properties, titanium dioxide, TiO₂, is an ideal photocatalyst for applications performed under UV-light irradiation. One of the most active photocatalyst is titanium dioxide P25 which is in fact a mixture of the rutile and anatase crystal forms of TiO₂. The latter has proved to be efficient in many pollutant degradation tests (*i.e.* mineralization of organics) [13-18]. Up to now, **such approach has been very little studied for selective oxidation and more work is needed in order to understand the role of dioxygen and of the solvents used as well as of the irradiance.** The problem is that this type of material is characterized by very low specific surface area. We believe that it would be desirable to improve it. As in other fields of catalysis, it would be interesting, in our opinion, **to design mesoporous catalysts in order to optimize heterogeneous catalysis processes.** Such materials prepared by simple methods could be interesting for the oxidation of relatively large molecules. **Working with nanoparticles of titanium oxide represents another pathway to reach high surface area.** The chemical structural properties of materials obtained from titania colloids have motivated a substantial research effort in their preparation. Sol-gel, solvothermal and hydrothermal derived titanium dioxide nanoparticles with controlled size distribution, well-defined shape and morphology are of great interest for many applications [19-25]. However, the main problem with nanoparticles is to avoid their aggregation. One of the means to benefit from the increase of the

specific surface area linked to the use of nanoparticles without agglomeration consists in depositing them on a porous support. In the case of materials with meso-structured porosity, included oxide nanoparticles are usually generated by the further transformation of precursor salts previously introduced into the pores by impregnation pathways. In these cases, it has often been found that this step plays a key role in the final dispersion of the nanoparticles. Indeed, it is not sufficient to have supports with large specific surfaces, the precursors have to be anchored preferentially on the internal surface to the detriment of the external one. An original method in the case of water-soluble precursors consists in introducing the quantity of aqueous precursor solution just necessary to fill the porosity, the remaining part of the solvent being constituted by a non-miscible hydrophobic solvent. This route known as “two-solvents” method, has been mainly used starting from aqueous metal salts [26, 27]. In the present work, **we would like to transpose it to TiO₂ colloids prepared in aqueous suspension.**

The present manuscript consists of two main parts each consisting of two chapters (chapters 1 and 2 for Part 1; chapter 3 and 4 for Part 2).

- **Chapter 1** will present the photocatalysis concept, the main mechanisms proposed for selective oxidation especially with TiO₂. The use of some other photocatalysts will be discussed too. Some strategies used to minimize electron/hole recombination and shift the absorption energy to wavelengths in the visible range will be detailed. Chapter 1 will also address the pathways available to get photocatalytically active mesoporous materials (mainly TiO₂) using either soft or hard templating methods. In this last part of the chapter, the discussion will focus on the different types of benefits that can be derived in terms of photocatalytic activity.

- **Chapter 2** will propose a systematic study of the oxidation of benzyl alcohol under oxygen atmosphere and UV irradiance. Various metal oxides, such as TiO₂, CeO₂, and ZrO₂, will be tested and TiO₂ P25 selected for a detailed examination, under comparable conditions, of the influence of the solubility of dioxygen, of the solvent and of the addition of scavengers or promoters. Results dealing with i) the oxidation of other benzylic alcohols or aliphatic ones and ii) the oxidative cleavage of C-C bonds will be presented. Attempts aiming at replacing P25 by mesoporous titania obtained by an hard templating pathway will be exposed.

- **Chapter 3** will describe the main preparation methods and phase behavior of TiO₂ NPs/colloidal particles. The importance to control the colloidal nucleation and growth steps to get monodisperse particles and eventually particular morphologies will be emphasized as well as some potential applications of these colloids in material science.

- **Chapter 4** will be focused on the comparison of a conventional impregnation method and of the

“two-solvents” one for the incorporation of pre-formed TiO₂ nanoparticles into silicic supports of the SBA-15 type with different porosity networks. Prior to the deposition study, the parameters of the TiO₂ colloid synthesis, already described in the group [28], will be studied more deeply in order to better control their size and their stability over time. DLS, HR-TEM, BET, TGA, UV-vis spectroscopy and BET measurements performed either on the NPs or on the TiO₂ NP@SBA-15 materials will be discussed prior to the tests. The photocatalytic activity of TiO₂ NP@SBA-15 materials will be examined in the oxidation of benzylalcohol in acetonitrile under UV irradiation for comparison with the P25 reference catalyst described in chapter 2.

Two annexes are proposed. **The first** one is the result of a collaborative work with the University of Guelma (Algérie) dealing with the synthesis and use of Ru(0) NPs supported on an Algerian clay, DD3, as an oxidation catalyst also for the aerobic oxidation of benzyl alcohol into benzaldehyde. **The second** one gathers experimental details for the characterization of the samples in the whole manuscript.

Attention: Chapters 2 and 4, as well as the experimental annex 1, are written in the form of publications. We apologize in advance for repetitions.

References

- [1] A.H. Lu, W.C. Li, Z. Hou, F. Schueth, Chem. Commun., 10 (2007) 1038.
- [2] H. Tsunoyama, H. Sakurai, N. Negishi, T. Tsukuda, J. Am. Chem. Soc. 127 (2005) 9374.
- [3] M. Turner, V.B. Golovko, O.P.H. Vaughan, P. Abdulkin, A. Berenguer-Murcia, M.S. Tikhov, B.F.G. Johnson, R.M.G. Lambert, Nature, 454 (2008) 981.
- [4] A. Abad, C. Almela, A. Corma, H. Garcia, Chem. Commun., (2006) 3178.
- [5] D.I. Enache, J.K. Edwards, P. Landon, B. Solsona-Espriu, A.F. Carley, A.A. Herzing, M. Watanabe, C. J. Kiely, D. W. Knight, G.J. Hutchings, Science, 311 (2006) 362.
- [6] Y. H. Ng, S. Ikeda, T. Harada, Y. Morita, M. Matsumura, Chem. Commun., (2008) 3181.
- [7] R. A. Sheldon, I. W. C. E. Arends, A. Dijkstra, Catal. Today, 57 (2000) 157.
- [8] R. A. Sheldon, I. W. C. E. Arends, A. Dijkstra, Acc.Chem. Res., 35 (2002) 774.
- [9] G. J. Brink, I.W.C.E. Arends, R.A. Sheldon, Science 287 (2000) 1636.
- [10] T. Mallat, A. Baiker, Chem. Rev., 104 (2004) 3037.
- [11] M. Nechab, C. Einhorn, J. Einhorn, Chem. Commun., (2004) 1500.
- [12] R. Noyori, S. Hashigushi, Acc. Chem. Res., 30 (1997) 97.
- [13] U. R. Pillai, E. S. Demessie, J. Catal., 211 (2002) 434.
- [14] J. Chen, D. F. Ollis, W. H. Rulkens, H. Bruning, H. Water Res. 33 (1999) 661.
- [15] D. S. Muggli, J. T. Mccue, J. L. Falconer, J. Catal., 173 (1998) 470.
- [17] J. L. Falconer, K. A. M. Bair, J. Catal., 179 (1998) 171.
- [18] F. H. Hussein, G. Pattenden, R. Rudham, J. J. Russell, Tetrahedron Lett., 25 (1984) 3363.
- [19] A. V. Zdravkova, Yu. S. Kudryashovaa, G. F. Pruglob, N. N. Khimich 59 (2014) 1003.
- [20] L. Chen, B. Yao, Y. Cao, K. Fan, J. Phys. Chem. C, 111 (2007) 11849.
- [21] V. Kalousek, J. Tschirch, D. Bahnemann, J. Rathousky, Superlattices Microstruct., 44 (2008) 506.
- [22] T. Sugimoto, X. P. Zhou, J. Colloid Interface Sci., 252 (2002) 347.
- [23] G. Tian, H. Fu, L. Jing, B. Xin, K. Pan, J. Phys. Chem. C, 112 (2008) 3083.
- [24] V. F. Stone, R. J. Davis, Chem. Mater., 10 (1998) 1468.

- [25] T. W. Kim, H. W. Ha, M. J. Paek, S. H. Hyun, I. H. Baek, J. H. Choy, S. J. Hwang, *J. Phys. Chem. C*, **112** (2008) 14853.
- [26] I. Lopes, N. El Hassan, H. Guerba, G. Wallez, A. Davidson, *Chem. Mater.*, **18** (2006) 5826.
- [27] D. Peng, T. T. Yan, X. X. Yu, Z.M. Bai, M. Z. Wu, *Nanoscale Res. Lett.*, **11** (2016) 226.
- [28] C. Salameh, J.-P. Nogier, F. Launay, M. Boutros, *Catal. Today*, **257** (2015) 35.

Part I

Mild oxidation of alcohols using dioxygen in combination with photocatalysts

Chapter 1: Bibliographical survey

Chapter 2: Experimental results

I. Applications of photocatalysis to the controlled oxidation of alcohols

Photocatalysis has become increasingly important in the last two decades and should provide very promising sustainable technologies for the purpose of decolorization of dyes, removal of toxic pollutants, water treatment [1-3]. Discovering innovative catalytic materials that can be activated by sun light which includes 45% of visible light and 4% of ultraviolet (UV) light, as seen in figure I.1, is the driving force behind a whole research field that aims to reduce environmental problems induced by conventional processes.

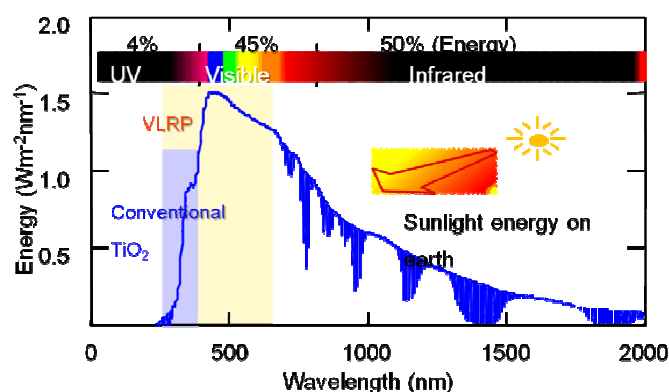


Figure I.1: Composition of solar energy on earth.

In this bibliographic part, we first describe the oxidation of benzyl alcohol in the presence of TiO_2 under UV irradiation, mainly in water and acetonitrile. Different mechanisms described in the literature are confronted before presenting the possible strategies to improve the use of photons and to move the energy absorbed towards the visible part of the emission spectrum.

I.1. Photocatalysis with TiO_2 for selective oxidation reactions

TiO_2 is regarded as the most efficient and environmentally benign photocatalyst. It is of a great interest due to its electronic and optical properties such as photochemical stability, high oxidative power, large band gap (c.a. 3.2 eV), as well as its non-toxicity, low cost, abundance [4-8]. The performances of TiO_2 for the photolysis of water have been firstly discovered by Honda and Fujishima in 1972 [5].

The photocatalytic properties of TiO_2 are derived from the formation of photogenerated charge carriers (holes and electrons) which occurs upon the absorption of ultraviolet light corresponding to the band gap (see Fig. I.2) [9-12]. The photogenerated holes in the valence band are known to diffuse to the TiO_2 surface and react with adsorbed water molecules, forming hydroxyl radicals (OH^*). The photogenerated holes and the hydroxyl radicals oxidize nearby organic molecules on the TiO_2

surface. Meanwhile, electrons in the conduction band typically participate in reduction processes, which are typically reaction with molecular oxygen in the air to produce superoxide radical anions ($O_2^{\cdot-}$).

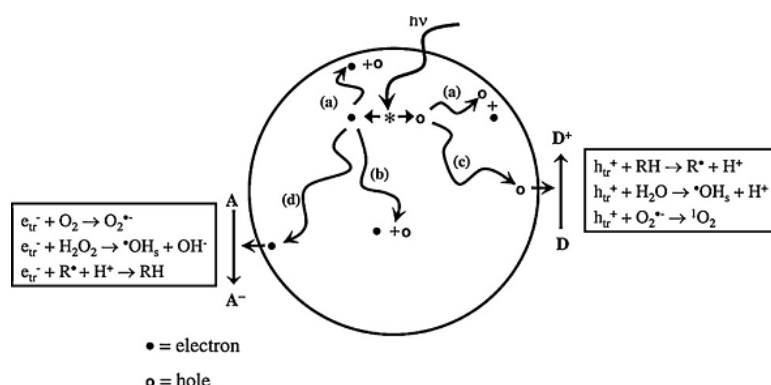
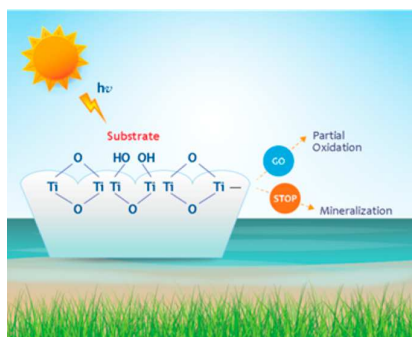


Figure 1.2: Principle of photocatalysis in the presence of excited TiO_2 [10].

Major radical reactive species produced are HO^{\cdot} and $O_2^{\cdot-}/^{\cdot}OOH$. Both are relatively short-lived but highly reactive. $^{\cdot}OH$ is the most reactive oxygenated radical with a very high standard potential $E^{\circ}(^{\cdot}OH, H^+/H_2O)$ of 2.18 V vs. NHE at pH 7. It is generally thought that due to these active radicals, photocatalytic reaction over TiO_2 under UV light is somewhat non-selective. Hence, the utilization of O_2 as oxidant and irradiance by UV/Vis as the driving force is usually exploited in order to mineralize organics. Since, TiO_2 mediated photooxidation has been used for environmental remediation, in which low concentrations of toxic materials can be photocatalytically converted to “harmless” oxidation products such as CO_2 and H_2O . Particularly, there are many publications that describe the use of TiO_2 oxide in photodegradation of dyes and air pollutants (mineralization) [13, 14].

In the field of photocatalysis, much less examples are dealing with selective oxidation. The challenge here consists to overcome the overoxidation of the primary products (scheme I.1). The task is not easy. In 2015, there were approximately 2000 papers published dealing with TiO_2 and oxidation, but only 200 were related to selective oxidation.

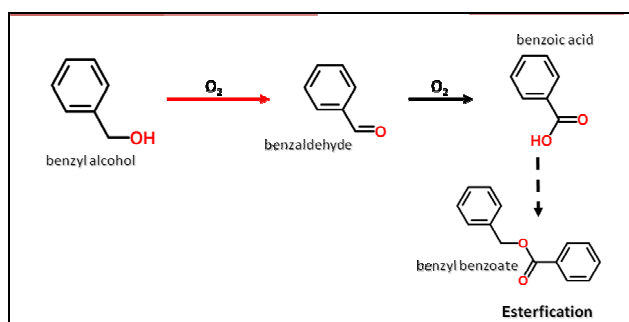


Scheme I.1: Mineralization versus selective oxidation [15].

One interesting example of application is the oxidation of primary and secondary alcohols to their corresponding aldehydes and ketones. Such reaction is still often carried out using stoichiometric

reagents based on chromium (VI), manganese (VII) which generates toxic/copious wastes. Alternatives are needed, for example to get aldehydes which are used in a wide variety of foods, beverages, in pharmaceutical industries and as raw materials for many important chemicals such as dyes, resins, and fragrances.

To achieve the goal of potential application of oxidation reactions by TiO₂ photocatalysis at ambient O₂ pressure and room temperature, a delicate balance between reactivity and selectivity is required. The kinetic issue represents a major challenge in future practical utilization of these systems. Benzyl alcohol has received substantial attention as a probe molecule. The selective, partial oxidation of benzyl alcohol to benzaldehyde would be achieved at low oxygen surface concentrations and take place through dehydrogenation of the alcohol to form benzaldehyde via a benzyloxy (C₆H₅-CH₂O-) intermediate [16] (Scheme I.2). While in this case, atomic oxygen plays solely a dehydrogenating role, at higher concentrations it would lead to the formation of intermediates from benzaldehyde, producing benzoic acid and CO₂. Facile ester (benzyl benzoate) formation also occurs at low oxygen concentrations, which indicates that benzoic acid is not a precursor of further oxidation of the ester. Instead, the ester would be produced by the coupling of adsorbed benzyloxy and benzaldehyde. Key to the high selectivity seen at low oxygen concentrations is the fact that the production of the aldehyde (and esters) is kinetically favored over the production of benzoic acid.

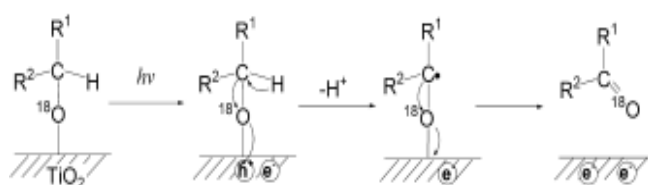


Scheme I.2: Oxidation reaction pathway of benzyl alcohol (products distribution) [16].

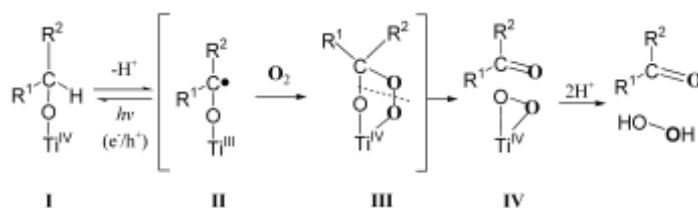
Recently, Higashimoto *et al.* reported that the photocatalytic oxidation of benzyl alcohol and its derivatives into the corresponding aldehydes could be achieved over TiO₂ in acetonitrile under the irradiation of both UV and visible light, observing that visible light response of TiO₂ could be attributed to the characteristic surface complex formed by the adsorption of the benzyl alcoholic compound on the TiO₂ surface [17, 18].

One question arises about the way oxygen atoms of dioxygen are transferred into the oxidation products. In noble-metal catalysis systems, dioxygen has been proven to oxidize the reduced noble-metal center (for example, M⁰ or Mⁿ⁺ hydride species) without any O-atom transfer from dioxygen to the products. A report made by M. Zhang [19] showed an oxygen isotope effect in the photocatalytic oxidation of alcohols over TiO₂ (pure anatase, 10 nm in diameter, 210 m² g⁻¹) dispersed in

benzotrifluoride (BTF) and illuminated with a 100 W-high-pressure Hg lamp under O₂ (0.1 MPa). Under normal conditions, the alcohol conversion was 42% and the selectivity in benzaldehyde of 30%. Using TiO₂ pretreated by H₂¹⁸O (98% ¹⁸O) under UV irradiation for 12 h, it was found that the oxygen atom in the alcohol substrate is completely replaced by one of the oxygen atoms of dioxygen in the corresponding aldehyde. This involves a selective cleavage of the C-O bond of the alcohol with concomitant formation of a new C=O bond in the product aldehyde in which the O atom comes from dioxygen. Such observation implies that the O atom transferred into the product did not originate from the surface-bound water or OH groups of TiO₂ as illustrated in the scheme I.3 for a two-electron transfer (TET). In fact, a concerted cleavage of the C-O bond of the alcohol and the O-O bond of dioxygen through a peroxo bridged structure, as shown in scheme I.4, is more likely.



Scheme I.3: Two-electron transfer mechanism in the oxidation of alcohols in the absence of O₂ [19].



Scheme I.4: Oxygen transfer process in the TiO₂ photocatalytic oxidation of alcohols in BTF solvent in the presence O₂ [19].

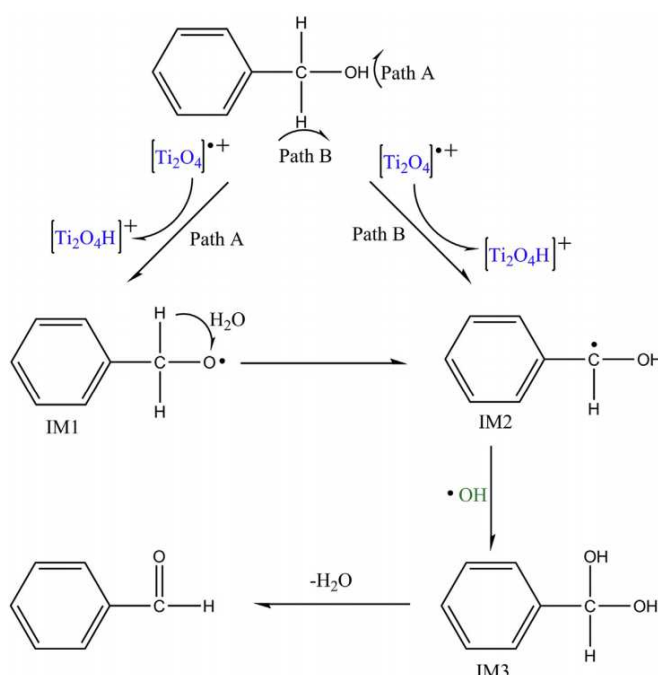
In an other context, Abdel-Wahab *et al.* studied anatase TiO₂ in the photocatalytic oxidation of 1-phenylethanol in dry acetonitrile illuminated by UV light and hypothesized that the rate-determining step is the reaction between the superoxide and the alcohol radical cation over the surface [20].

L. Zhao and co-workers [21] have investigated the oxidation of benzylalcohol in aqueous solution in the presence of TiO₂-P25 exposed to UV light (500 W Hg lamp) and N₂. Bubbling of the inert gas was done in order to suppress the formation of O-based radical species. Under these conditions, the yield of benzaldehyde was 36% after 5 h irradiation.

- With addition of hole scavenger such as sodium oxalate, benzaldehyde yield did not change.
- However, using KBrO₃, as an electron capturer, the yield of benzaldehyde was increased significantly to 60%. This could be attributed to the holes which may directly participate in the oxidation process or more holes generated after the electrons had been captured by KBrO₃.

- To clarify the role of $\cdot\text{OH}$ radical, *i*-PrOH was used as $\cdot\text{OH}$ radical capturer and it was found that the yield of benzaldehyde decreased 10% after 5 h, emphasizing that $\cdot\text{OH}$ are formed mainly from dissolved O_2 when the hole is captured, and as well from the holes when an electron capturer is added.
- To test the role of dissolved O_2 in the oxidation process, benzoquinone was used to trap O_2^- and it was found that the amount of benzaldehyde increased about 30% after 1 h which suggests that the dissolved O_2 is generating $\cdot\text{OH}$ radicals to some extent.

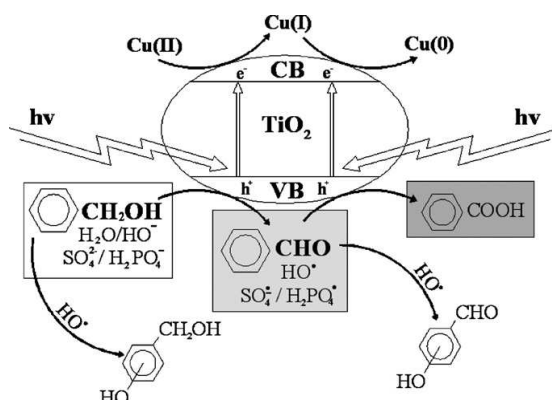
The photocatalytic oxidation mechanism of benzyl alcohol can be summarized as shown in scheme I.5. Firstly, the hole initiates the reaction by abstracting -H from -OH (path A) and -CH (path B), along with the formation of compounds IM1 and IM2, respectively. IM1 is less stable and tends to change into IM2. Subsequently, IM2 combines with $\cdot\text{OH}$ to form IM3. Finally, benzaldehyde is obtained through the intermolecular dehydration reaction of IM3. Thus, the holes $[\text{Ti}_2\text{O}_4]^{*\text{+}}$ and $\cdot\text{OH}$ radicals were found to be the major active species. However, it is not clear how $\cdot\text{OH}$ is formed.



Scheme I.5: Probable photocatalytic oxidation mechanism of benzyl alcohol into benzaldehyde in the presence of TiO_2 under UV light [21].

This latter mechanism, which does not involve surface species, has similarities to that seen in scheme I.4. Both agree for an activation of the benzylic C-H bond. In both cases, the oxygen atom introduced originates from the dioxygen of the air either directly (scheme I.4) or indirectly via $\cdot\text{OH}$. In this last step, the authors can hardly prove the nature of the species involved. The evidence is indirect: either by isotopic labeling or by the action of traps.

The photoreaction results are strongly dependent on many factors such as substrate adsorption, the reactivity of the intermediates, catalysts type and dosage and illumination intensity. A too rapid recombination rate of the photogenerated electrons and holes can greatly affect the performance of the photocatalyst. Some techniques used to overcome this are based on the mediation of the photogenerated charge carriers away from the TiO_2 surface. Such process prolongs their lifetime, and gives electrons and holes sufficient time to initiate reduction and oxidation reactions, respectively. Hence, the electron-hole separation can improve significantly the photocatalytic performance. In some articles, compounds are added to modify the mechanism in order to make the transformation more selective. This is the case of Cu(II) ions which are oxidants strong enough to be reduced by the electrons generated by the photocatalysis process. The idea here is to avoid the formation of superoxide ions and then of hydrogen peroxide (successive reductions) since these compounds are sources of $\cdot\text{OH}$ radicals [22]. Marotta *et al.*, have investigated the selective oxidation of benzyl alcohol to aldehydes in aqueous medium using $\text{TiO}_2 / \text{Cu(II)}$ / solar UV photocatalytic system under acidic conditions with varying operating conditions. The best result found, in terms of yield, was of 35% for benzaldehyde with respect to the initial benzyl alcohol concentration [23]. The effects of the catalyst loading, the addition of inorganic cations (Cu(II)), anions (SO_4^{2-} , H_2PO_4^-), the initial Cu(II) concentration and pH of the solution have been studied. A decrease of benzyl alcohol oxidation and benzaldehyde formation rates by increasing the pH from 2.0 to 4.0 has been observed. It was demonstrated that copper (II) was reduced by the photogenerated electrons to copper(0), which could be re-oxidized to Cu(II) , in the dark, in the presence of oxygen (scheme I.6).

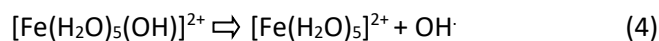
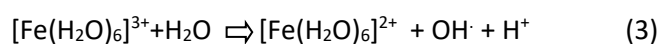
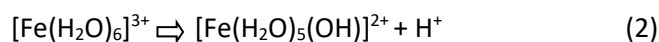
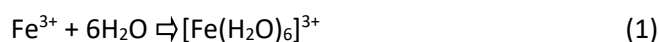


Scheme I.6. Probable mechanism of selective oxidation of benzyl alcohol by $\text{TiO}_2/\text{Cu(II)}/\text{UV}$ [23].

Whereas Cu^{II} ions were reduced to Cu^0 , it was found that SO_4^{2-} , H_2PO_4^- species compete with benzyl alcohol and benzaldehyde for the reaction with positive holes on the catalyst surface and act as scavengers towards HO radicals (scheme I.6).

Some attempts have been focused on selective photo-oxidation of benzyl alcohol in aqueous media under mild conditions using only transition metal cations as photocatalysts, and especially those are

very cheap and of low toxicity. Hence, Spasiano *et al.* [24] did obtain benzaldehyde from benzylalcohol with a conversion of 40% and a selectivity of 80% in aqueous solution using oxygen as an oxidant and UV-solar simulated radiation of Fe(III) salts. Only ferric complexes $[\text{Fe}(\text{H}_2\text{O})_6]^{3+}$ and $[\text{Fe}(\text{H}_2\text{O})_5(\text{OH})]^{2+}$ were detected under UV-light irradiation in these conditions. According to the authors, hydroxyl radicals would be generated by charge transfer reactions from water orbitals to ferric centered ones, whereas benzyl radicals would be produced through direct reactions of charge transfer in the outer solvation sphere of the excited state of the hexa-aquoiron(III)-benzyl alcohol complexes following the mechanism below:

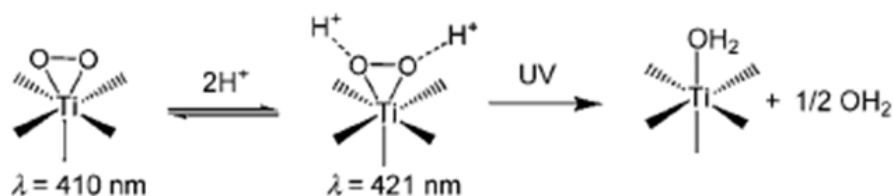


On another hand, Meng *et al.* was found that homogeneous CuCl_2 led to an aldehyde selectivity higher than 95% using molecular oxygen as an oxidant. The formation of a visible light responsive complex between Cu(II) and the solvent seemed to be responsible for the occurrence of the oxidation of benzyl alcohol and isotopic tracer experiments showed that molecular oxygen did not transfer to benzaldehyde [25].

Other benzyl alcohol derivatives have been studied by TiO_2 photocatalysis. Vijaikumar *et al.* [26] reported the formation of benzophenone from the oxidation of the corresponding secondary alcohol (benzhydrol) in oxygen-purged acetonitrile irradiated with UV light ($\lambda > 350$ nm). According to the authors, benzhydrol would be oxidized by a hole giving rise to the radical cation and benzophenone would be produced by the subsequent reaction of this intermediate with a superoxide radical anion produced by the transfer of a conduction band electron to oxygen. It was found that with an increase of light intensity, the yield of benzophenone increased. While, Wang *et al.* [27] showed that another secondary alcohol, 1-phenyl ethanol, is selectively photooxidised to acetophenone using Fe or V doped titanium dioxide (TiO_2) under exposure to UV irradiance. The yield of acetophenone was 40% instead of 16% with pure TiO_2 . With increased doping concentrations of both Fe and V, the crystal structure and the morphology of the catalyst turned out to change, and as the particle size decreased, the total catalyst surface area increased and the photogenerated electron density on the surface of each particle increased. This could be at the origine of the enhanced photocatalytic activity upon TiO_2 doping. Interestingly, the reactivity of ring-substituted benzyl alcohols in CH_3CN can be influenced by the preferential adsorption of the OH group with respect to the aromatic ring on TiO_2 photocatalyst. In particular, electron abstraction by the photogenerated hole is from the aromatic

ring in the presence of electron-donating groups whereas it is from the hydroxyl moiety in the presence of electron-withdrawing groups.

Previously, it was found that one oxygen atom is transferred from molecular oxygen to alcohols during the TiO₂ photo-oxidation process and a Ti intermediate with a side-*on* peroxide was proposed using ¹⁸O-labeling experiments [19]. Wang *et al.* [28] reported for the first time the dramatical acceleration of the photocatalytic oxidation of benzyl alcohol, diphenyl methanol, 1-phenyl ethanol, and cyclohexanol into their corresponding aldehydes and ketones upon the pre-treatment of TiO₂ by a simple adsorption of a Brønsted acid. This occurred without any loss of selectivity in benzotrifluoride purged with O₂ (0.1 MPa) using UV light at room temperature. Such a unique effect of protons in the reaction was attributed to the promotion of the decomposition of the surface Ti/peroxide species and the resulting regeneration of Ti sites in the photocatalytic transformation of alcohols as seen in scheme I.7.



Scheme I.7: Role of proton in acceleration of the disproportionate decomposition [28].

To develop photocatalytic oxidation as a green oxidation route for organic synthesis, a high selectivity towards the desired product is a key point to be achieved. Actually, photocatalytic oxidation of alcohols in water suspensions affords a rather poor selectivity to carbonyl compounds due to the generation of a lot of non-selective OH radicals [29, 30]. One trend is to avoid the use of solvent or additives and it has been easily demonstrated that the complete oxidation of benzyl alcohol to CO₂ can be efficiently suppressed under solvent-free conditions when the formation of OH radicals can be avoided.

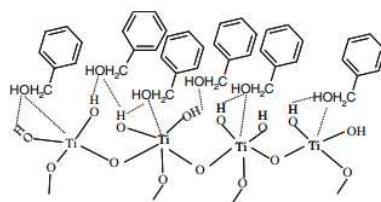
I.2. Modifications of photocatalysts

It is known that anatase TiO₂ is excited only by UV light ($\lambda < 380$ nm) because of its large band gap energy of 3.0-3.4 eV. This requirement limits the effective use of solar light to drive the photocatalytic transformations of organic compound. Thus, to address this issue, different strategies have been proposed to extend the photon response of titania to the visible light region, including doping with metal ions or non metal elements, sensitization with dyes or addition of noble metals and coupling with a narrow band gap semiconductor [31-36]. In the past decades, enormous efforts have been devoted to improve the optical properties of TiO₂ such as metal ion doping (Fe³⁺ or Ag⁺

etc.), semiconductor coupling $\text{TiO}_2\text{-CdS}$ and dye sensitizing. Such modification of TiO_2 usually resulted in poor thermal and chemical stability and/or lower UV activity.

Several organic dyes which are of low toxicity, low cost such as Eosin Y, Rose Bengal, Merocyanine, Cresyl violet and Riboflavin have been employed for spectral sensitization of semiconductors photocatalysts [37, 38]. Al-Zahra *et al.* [39] have studied the influence of different sensitizers for the selective photocatalytic oxidation of benzyl alcohol using a suspension of titanium dioxide (anatase) under an oxygen atmosphere using low pressure mercury lamp. The effect of sensitizers on the activity of TiO_2 for photo-conversion of benzyl alcohol to benzaldehyde was as in the following sequence: riboflavin > safranin O > naked TiO_2 . The differences in activities of dyes reflect their ability to absorb light and inject electrons to the conduction band of TiO_2 . Riboflavin and safranin O turned out to have good overlapping of their spectrum with that of TiO_2 .

Anpo *et al.* [40] reported that both TiO_2 and fluorinated surface of $\text{TiO}_2\text{-HF}$ (400°C) which exhibited absorption in the UV, but also in the visible light region. This could be attributed to the formation of surface complexes formed by the interaction of benzyl alcohol with the coordinately unsaturated Ti sites of the TiO_2 , as shown in scheme I.8.



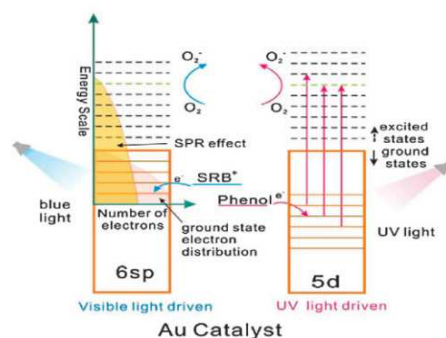
Scheme I.8. Surface structures of benzyl alcohol adsorbed- TiO_2 [40].

Higashimoto *et al.* [41] have investigated the use of surface-modified TiO_2 loaded with several metal ions such as iron, silver, cerium, platinum or copper for the oxidation of benzyl alcohol in acetonitrile using pure O_2 (1 atm) under visible-light irradiation. Among the different materials prepared, the iron(III) ion-modified TiO_2 was found to exhibit the highest photocatalytic performance in terms of benzylalcohol conversion and benzaldehyde selectivity (>99%). In this case, the contribution of the Fe^{3+} ions on TiO_2 were attributed to a synergetic effect related to efficient electronic transitions between the energy level constructed by the O 2p orbitals of the alcoholate species hybridized with the occupied Fe 3d orbitals and the energy level of the conduction band of TiO_2 , as well as subsequent electron transfer to the unoccupied Fe 3d orbitals as the acceptor levels followed by O_2 reduction. On the other hand, rhodium(III) ion-modified titanium(IV) oxide (Rh(III)/TiO_2) studied in the photocatalytic oxidation of benzyl alcohols in aqueous suspensions in the presence of O_2 irradiated with visible light showed photoabsorption in the visible light region as the result of the charge transfer from Rh^{3+} to the conduction band of TiO_2 .

Long *et al.* [42] designed a metal-semiconductor hybrid system in which Pd nanocrystals enclosed by {100} facets are deposited on TiO₂ supports (Pd–TiO₂ hybrid structures) revealing that the plasmonics of Pd may force a large number of electrons to undergo reverse migration from Pd to the conduction band of TiO₂ under strong illumination, thus lowering the electron density of the Pd surface as a side effect, which enables optimization of O₂ activation and thus, improvement of the efficiency of catalytic glucose oxidation by shedding appropriate light on the Pd–TiO₂ hybrid structures.

Recently, it was found that Pt nanoparticles absorb the light in the visible region due to the interband transition of 5d band e⁻ to the sp conduction band of the TiO₂ support. As a result, Pt nanoparticles deposited on anatase TiO₂ (Pt/anatase) efficiently promote aerobic photo-oxidation under visible light irradiation. The apparent quantum yield for the reaction was *c.a.* 7% which is higher than that obtained with the Au catalyst (*c.a.* 4%). The superior activity would be due to the strong affinity between Pt nanoparticles and the anatase surface. This would facilitate an efficient e⁻ transfer from the photoactivated Pt particles to anatase, but, for bimetallic alloy nanoparticles consisting of Pt and copper (Cu) supported on anatase TiO₂, this system significantly enhance aerobic oxidation under visible light. The apparent quantum yield for the reaction, 17%, is more than the double of that obtained with monometallic Pt catalyst (*c.a.* 7%) [43-45].

Although gold nanoparticles have surface Plasmon Resonance SPR absorption in the visible domain, they also exhibit a strong absorption of ultraviolet light. In fact, UV absorption produces a much larger surface photocurrent than that induced by the SPR absorption under visible light irradiation. The interband absorption (UV) results in a much larger proportion of electron transfer from the Au-NPs to dioxygen than the intraband SPR absorption (visible). Consequently, more positive charges are left in lower energy levels (in 5d band) of the Au-NPs when they are exposed to UV light. Given the relatively high electronegativity of gold, the Au-NPs can capture electrons from the organic molecules adsorbed on them to neutralize the positive charges, oxidizing the organic compound, achieving selective oxidation with high selectivity [46-49]. The transfer mechanism has been proposed to explain these photocatalytic observations with the Au-NPs as illustrated in Scheme I.9.



Scheme I.9: Selective oxidation of alcohols over Au- under Visible light irradiation [49].

Tsukamoto *et al.* [50] have reported that small Au particles loaded on a mixture of anatase and rutile particles with Au size diameter < 5 nm, exhibited a very good catalytic activity under visible light. Indeed, plasmon activation of the Au particles promotes consecutive e^- transfer from the Au particles to rutile and then to anatase and efficient O_2 reduction on the anatase surface.

Similarly, gold nanoparticles supported on cerium (IV) oxide powder showed a strong absorption at around 550 nm due to surface plasmon resonance that was also exploited for the oxidation of aromatic alcohols to corresponding aldehydes in an aqueous suspension under irradiation of green light [51]. It has to be noted that the rate of photocatalytic benzaldehyde formation under visible light irradiation exhibited a linear dependency on the external surface area of Au loaded on CeO_2 . As a result, an important challenge for the improvement of the plasmonic photocatalysts is related to the increase of their specific surface. In the plasmonic reaction, the charge separation is facilitated by the reduction of O_2 on the catalyst surface with the e^- transferred from the photoactivated metal particles. The anatase surface is active for O_2 reduction, whereas rutile surface is inactive. In contrast, photoactivated Au particles scarcely transfer e^- to anatase, probably due to the weak Au/anatase interaction, but the e^- transfer to rutile does occur.

Pt particles show also absorption band in the visible region due to the intraband transition of electrons from sp band valence band to the sp conduction band (SPR absorption) and the interband transition of electrons from d band to sp conduction band. The intensity of this absorption is much weaker than that of Au particles. Thus, photocatalysis driven by visible light activation of Pt particles should be investigated [43]. Hence, Yasuhiro *et al.* [44] has demonstrated that Pt nanoparticles (3-4 nm) supported on anatase titanium dioxide (TiO_2) promote aerobic oxidation. In this case, the relatively large number of perimeter Pt atoms produced at the Pt/anatase heterojunction creates a relatively low Schottky barrier which would facilitate smooth Pt→anatase electron transfer, resulting in very high photocatalytic activity.

M. Qamar *et al.* [52] reported that Pt-modified nanoporous hierarchical Bi_2WO_6 spheres in water under simulated sunlight (W tungsten-halogen lamp) show a high activity for the photooxidation of 4-methoxybenzyl and 4-nitrobenzyl alcohol into their corresponding aldehydes. These authors considered that the reduction site of the semiconductor photocatalysts is more pivotal to obtain high selective oxidation. Furthermore, such photocatalyst was chemically stable and showed efficient recyclability.

Furthermore, the rapid recombination of photoinduced electrons and holes sharply decreases the quantum efficiency. Therefore, it is also of great interest to improve the generation and separation of

charge carriers in catalytic system for selective oxidation reactions. It was found that the synthesis of semiconductor heterostructures could help for this system [53-55]. When magnetic oxides are involved, they also make it possible to facilitate the recovery of the catalysts at the end of the reaction. Such type of photocatalysts has been prepared by Xuan *et al.* [56] in the form of well-defined hollow spherical $\text{Fe}_3\text{O}_4 / \text{TiO}_2$ materials. They showed good photocatalytic activity for the degradation of Rhodamine B under UV light irradiation and could be recycled six times by magnetic separation without major loss of activity. Similarly, Colmenares *et al.* [57] reported the preparation of magnetically separable $\text{TiO}_2 / \text{MAGSNC}$ (maghemite-silica nanocomposites) solids that exhibited good performances in the photocatalytic oxidation of benzyl alcohol in acetonitrile or water for 4 h under UV-light (125 W lamp) with air bubbling flow. The conversion and selectivity in benzaldehyde were of 50 and 90% in acetonitrile suspension, whereas they were of 99 and 10%, respectively in water. Better photoactivity than Evonik P25- TiO_2 was observed which was attributed to the existence of an heterojunction between TiO_2 and Fe_2O_3 . According to the authors, the latter would increase the sensitization and decrease the band gap of TiO_2 .

Interestingly, Feng *et al.* [58] examined a solvent-free selective photocatalytic oxidation of benzyl alcohol into benzaldehyde using TiO_2 and modified TiO_2 with Ir clusters prepared by photodeposition (Ir/TiO_2) under a 250 W high pressure Hg lamp. Under these conditions, TiO_2 gave a reaction rate of $325 \text{ mmol h}^{-1} \text{ gcat}^{-1}$ but Ir/TiO_2 showed a remarkably higher activity with an average reaction rate of $14538 \text{ mmol h}^{-1} \text{ gcat}^{-1}$. According to the authors, this dramatical enhancement was due to the presence of iridium clusters on TiO_2 which efficiently suppress the recombination of photogenerated holes and electrons and also favor the activation of molecular oxygen thus promoting the participation of molecular oxygen in selective oxidation. Quite recently, Ru/TiO_2 was studied intensively [59-61] and it was reported that under irradiation of light, electron transfer from TiO_2 to Ru NPs occurred due to the Schottky barrier effect at the metal-oxide interface. However, the preparation routes of Ru/TiO_2 nano-composites are very complicated and it is hard to control the size distribution of Ru NPs. Therefore, Ru NPs had to be dispersed on large surface area within support to achieve high mass activity and to prevent aggregation. One-dimensional (1D) TiO_2 nanostructures were selected due to their stability, their large surface area and fast electron transfer properties, as well as the possibility to gather easily metal or metal oxide to form heterostructures based on Schottky barrier effect [62, 63]. Tiana *et al.* prepared one dimensional (1D) TiO_2 nanobelts (NB) with diameter of 8 nm, then, modified their surface with Ru nanoparticles deposited by a photo-reduction method. SEM image shows that the TiO_2 consists of uniform belts with width of 50– 200 nm, and a length of up to several of micrometers, and the average size of the obtained Ru clusters was 1.5 nm (Fig. I.3). The conversion of benzyl alcohol into benzaldehyde was rather small with *ca.*

11% for TiO₂-NB nanobelts and 72% for the corresponding Ru/TiO₂ heterostructure. According to the authors, Ru/TiO₂ exhibited superior activity due to the tiny particle size and high density of the supported Ru NPs on the surface as well as to the Schottky barrier effect of Ru NPs which efficiently harvests the electrons of TiO₂ and increase the separation of photogenerated electron-hole pairs [64].

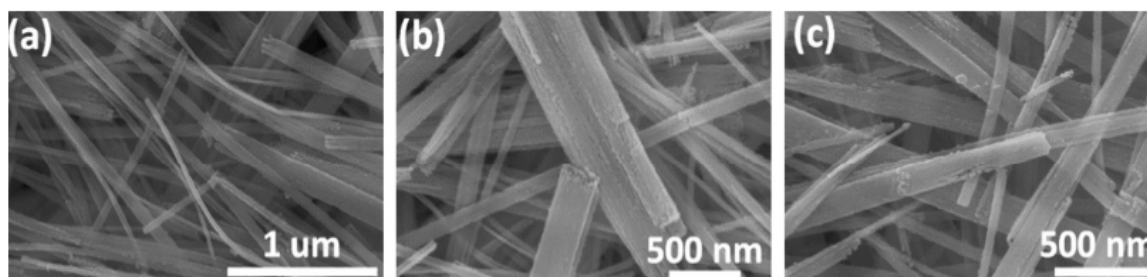


Figure 1.3: SEM images of (a, b) TiO₂ NBs and (c) Ru/TiO₂ NB heterostructures [64].

The atom efficiency of photocatalytic selective oxidation of benzyl alcohol involving O₂ never reaches 100% because a stoichiometric amount of H₂O is formed as a by-product. Formation of benzaldehyde by simple dehydrogenation should be much more interesting because the reaction gives H₂ which is an alternative energy carrier. However, it is hard to eliminate hydrogen atoms of alcohol as H₂ due to thermodynamic reasons but, for oxidant-free dehydrogenation reactions carried out in the liquid phase, it is easier to remove H₂ from the liquid phase due to its low solubility. Accordingly, Imamura *et al.* [65] have investigated the photocatalytic oxidation of alcohols such as benzyl alcohol, methyl-, methoxy- and chloro- benzyl alcohols into their corresponding aldehydes in acetonitrile suspensions of Pt-loaded titanium (IV) oxide under various conditions with exposure to UV irradiance under Ar at room temperature. Benzaldehyde and dihydrogen (H₂) were produced with a molar ratio of 1:1 from benzyl alcohol with high quantum efficiency of 38% at 366 nm. Moreover, it was found that the benzaldehyde yield in dehydrogenation under deaerated conditions was much higher (> 99%) than that (53%) obtained by dehydrogenation of benzyl alcohol in the presence of dioxygen, leading to the formation of water instead of H₂.

1.3. Crystallinity and surface/bulk defects of TiO₂ nanoparticles

For hydrogen production from water splitting, the mixed-phase TiO₂ (rutile (20%) / anatase (80%)), Degussa P25 was shown to exhibit higher photocatalytic activity in comparison to pure phase anatase or rutile. Li *et al.* [66] have proposed that this difference was directly related to the surface phase structure and the phase junction formed between anatase and rutile. The exposed facet of TiO₂ crystal is an important factor. Lu *et coll.* found that the {001} facets of anatase TiO₂ with high energy show more reactivity than the thermodynamically stable {101} facets for water splitting reactions

[67]. Surface/bulk defect on TiO_2 is also a very important parameter influencing its photocatalytic performance. Hence, Li *et al.* [68] demonstrated that the relative concentration ratio of bulk defects to surface defects in TiO_2 nanocrystals can improve the separation of photogenerated electron-hole and therefore can enhance photocatalytic efficiency. The sole effect of surface/bulk defects of nano-sized anatase and rutile TiO_2 samples on their photocatalytic activity was investigated. In the case of a TiO_2 crystal free of any defects, the photogenerated electrons and holes undergo quick recombination both in the bulk phase and on the surface, while in the case of TiO_2 with surface/bulk defects, the photo-generated holes could be trapped by the bulk defects through electrostatic interaction. Holes can also be trapped by surface defects, *i.e.* oxygen vacancies, and the separation of photo-generated electron-hole pairs is facilitated. Moreover, the photo-generated holes trapped by surface defects are ready to react with electron donors, thus the photocatalytic reaction can be promoted as emphasized by Yan *et al.* [69].

Generally, the photocatalytic activity of TiO_2 samples can be influenced by their physico-chemical properties, in particular, crystalline phases, exposed crystal facets and surface/bulk defects. However, a direct correlation of the physico-chemical properties with photocatalytic performance is still difficult and hot research for chemists. Palmisano *et coll.* [29, 30] synthesized rutile TiO_2 at low temperature and evaluated it in the photocatalytic oxidation of aromatic alcohols into aldehydes in water medium under UV irradiation, emphasizing that crystallinity of the sample appeared to be a key factor in controlling the product selectivity. Moreover, the introduction of substituents into the aromatic alcohols could change the photocatalytic oxidation rate and product selectivity.

1.4. Use of other oxides

Various oxide and non-oxide 1D nanostructured materials were used as photocatalysts in the oxidation of alcohols. ZnO is also a semiconductor material with a characteristic wide bandgap of 3.3 eV in its bulk form. To date, many methods were employed for the synthesis of 1D ZnO nanorods, such as hydrothermal and solvothermal processes [70-75]. Some authors, *e.g.* Tang *et al.* [76], have prepared such nanorods with $20 < \text{diameters} < 30$ nm *via* a facile surfactant-free hydrothermal method. According to the authors, the resulting 1D ZnO exhibited a higher selectivity to aldehydes compared to commercial ZnO in benzotrifluoride (BTF) using dioxygen and UV light irradiation. Such results were attributed to the 1D morphology of ZnO nanorods, a stronger adsorptivity toward alcohols compared to aldehydes, and a fast and long-distance transport of electrons compared to bulk ZnO. Moreover, 1D ZnO nanorods were shown to be beneficial for the activation of molecular

oxygen due to their easy trapping by very accessible electrons photogenerated along the 1D dimension of the photocatalyst.

Among the metal oxides used in photocatalysis applications, niobium (V) oxide (Nb_2O_5) is characterized by a gap energy of 3.4 eV which is similar to that of TiO_2 (3.2 eV). Therefore, it could have been expected to get a similar photocatalytic activity. However, there have been very few studies on photocatalysis by Nb_2O_5 . Since the potential conduction band edge of Nb_2O_5 was reported to lie close to the H^+/H_2 (0 V at pH 0) redox potential, it is also an interesting point whether an Nb_2O_5 photocatalyst can produce H_2 from water or not. Thus, the use of Nb_2O_5 as a catalyst may be a new alternative for the photocatalytic oxidation of alcohols.

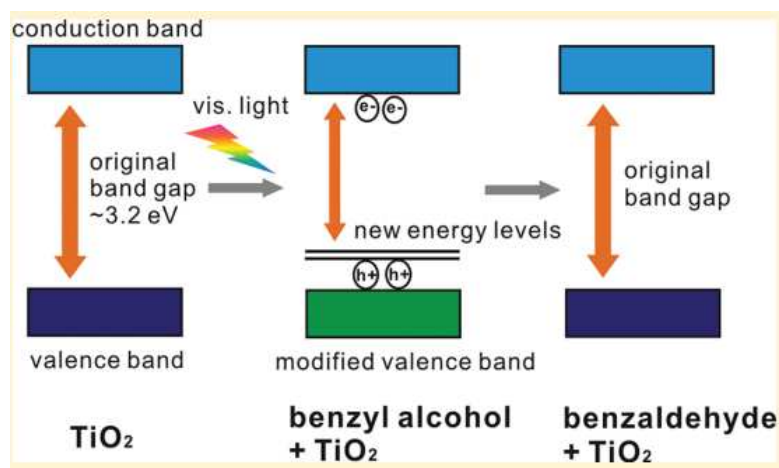
II. Mesoporous photocatalysts

This part will focus on the strategies implemented for the synthesis of mesoporous photocatalysts and more particularly of titanium dioxide. The advantages of these materials are described, essentially for the degradation reactions of various organic molecules since few examples of applications in selective oxidation catalysis have been listed up to now.

Ordered mesoporous oxides are interesting materials for both scientific and technological concerns. They have a large series of potential applications, such as in catalysis, gas sensing and energy storage due to their ordered pore networks, large surface areas and large pore volumes, which reduce mass diffusion within frameworks. One of their main advantages is to make easier the accessibility of bigger molecules to the internal surface than microporous solids.

However, thermal stability of mesoporous structures is often a critical parameter for catalytic applications. Indeed, metastable-to-stable transformation of oxides is associated always with sharp decrease in surface area and/or porosity. Therefore, several attempts have been done to stabilize the pore structure of these metastable oxides. Furthermore, the walls of these synthesized mesoporous materials are amorphous [77-83]. Silica or aluminosilica of the MCM-41 type [84] were the first examples of ordered mesoporous solids prepared. They were obtained from the deposition of silica (or alumino-silica) precursors on the surface of micelles of cetyltrimethylammonium bromide (CTAB). Mesoporous metal oxides synthesized using surfactants (e.g. CTAB, Pluronic P123, and F127) as templates are noncrystalline because the soft templates cannot tolerate the high temperature required for crystallization of metal oxides. Several attempts using similar synthetic routes have been employed to obtain different mesostructured metal oxides such TiO_2 [85-89].

In 2011, Li *et al.* [90] got high yield of benzaldehyde *ca.*90 % from the benzyl alcohol oxidation transformation over mesoporous crystalline TiO₂ under mild conditions under visible-light irradiation with/without molecular oxygen. DFT calculations proposed an explanation for the efficiency of visible light in this case. Indeed, the antibonding π molecular orbitals of adsorbed benzyl alcohol can hybridize with the O 2p atomic orbitals of TiO₂, creating new energy levels located in the band gap (scheme I.10), where holes can be generated under visible-light irradiation.



Scheme I.10: Mechanism of mesoporous TiO₂ in photooxidation of benzyl alcohol under visible light, with creating new energy levels [90].

II.1. Use of soft templates

In 2006, Fan *et al.* [91] published a new sol gel system route for the preparation of homogeneous, ordered, thermally stable, multicomponent mesoporous metal oxides. The growth kinetics of the different metal alkoxides could be controlled by the judicious addition of complexing ligands, such that particle size and condensation kinetics of the quite different precursors could be matched allowing for complex metal oxide stoichiometries. Hence, ordered mesoporous metal oxides (e.g., Al₂O₃, TiO₂, ZrO₂, Nb₂O₅, and Ta₂O₅) or mixed metal oxides (e.g., 4ZrO₂-P₂O₅, SiO₂-Al₂O₃, CaO-TiO₂, YbO-2TiO₂, NiO-2SiO₂-2ZrO) were prepared from acetic acid sol-gel system using alkoxides as inorganic precursors (Figure I.4). In all these cases, mesostructured materials having a p6m symmetry with uniform size distribution (8.5-10 nm), high surface area (86-265 m².g⁻¹) and high porosity volumes (0.38-0.45 cm³. g⁻¹) were obtained.

Niobium-based oxide materials have interesting properties for heterogeneous catalysis. Hence Nb₂O₅ can be used as a photocatalyst of selective oxidation under visible light whereas hydrated niobium oxide (Nb₂O₅ · 3nH₂O; niobic acid) exhibits both Lewis acid sites and relatively strong Brønsted acid sites on its surface even in the presence of water that makes this material attractive for industrial use [92,93]. Despite this, very few reports have dealt to date with the preparation of ordered mesoporous niobium oxides. For instance, Nakajima *et al.* [94] reported on the synthesis of

mesoporous $\text{Nb}_2\text{O}_5 \cdot n\text{H}_2\text{O}$ using different amphiphilic block copolymers such as L64, P103, and P123 acting as structure-directing agents. Under these synthesis conditions, it was found that the pore size in the prepared materials increased with increasing molecular weight of the block copolymer in the following order: P123 > P103 > L64 keeping the weight percentage of ethylene oxide groups constant between all the attempts. The obtained samples had BET surface areas of 250-350 $\text{m}^2 \text{g}^{-1}$ and pore volumes of 0.2-0.4 $\text{cm}^3 \cdot \text{g}^{-1}$, which are larger than that of bulk $\text{Nb}_2\text{O}_5 \cdot 3\text{H}_2\text{O}$. More importantly, mesoporous $\text{Nb}_2\text{O}_5 \cdot 3\text{H}_2\text{O}$ exhibited much higher catalytic activity for the hydrolysis of cellobiose than supermicroporous and bulk $\text{Nb}_2\text{O}_5 \cdot 3\text{H}_2\text{O}$. However, no significant difference was observed between the activity of bulk and mesoporous $\text{Nb}_2\text{O}_5 \cdot 3\text{H}_2\text{O}$ samples for Friedel-Crafts alkylation. The results suggest that mesopores consisting of hydrophilic niobium oxide are advantageous for hydrophilic reactions, but not hydrophobic ones.

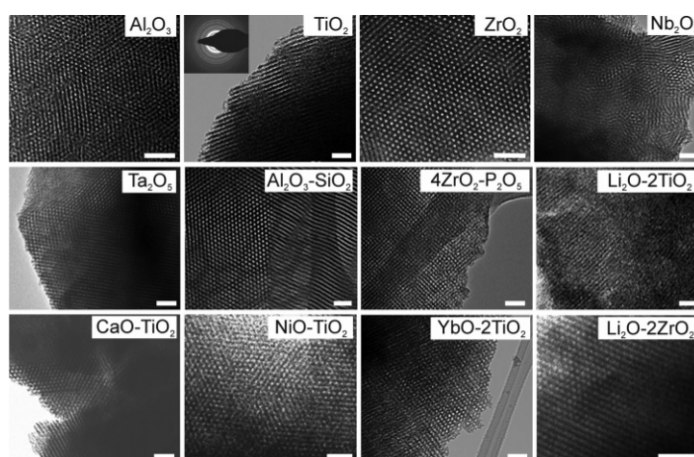


Figure 1.4: TEM images of calcined mesoporous materials. Mesoporous Metal oxides are calcined at 350°C in air for 5 h to remove organic polymer templates. Al_2O_3 , Nb_2O_5 , and 4 $\text{ZrO}_2\text{-P}_2\text{O}_5$ samples are calcined at 500°C [91]. Chen *et al.* have [95] prepared mesoporous titanium dioxide using TiCl_4 and $\text{Ti}(\text{OBU})_4$ and Pluronic P123 following the nonhydrolytic evaporation-induced self-assembly (EISA) method. Recovered solids exhibited three-dimensional mesostructure with pore walls composed of both anatase and rutile phases with a narrow pore size distribution (3.4-4.5 nm), a specific surface area of 91.6 $\text{m}^2 \cdot \text{g}^{-1}$ and pore volume of 0.187 $\text{cm}^3 \cdot \text{g}^{-1}$. Such solids were shown to be as active as Degussa P25 for the photodegradation of phenol (yield of 100% vs. c.a. 90%) instead of ca. 90% under UV light. High contents of TiCl_4 were shown to favor the formation of regular mesostructures and a proper weight ratio of anatase/rutile for a good photoactivity.

$\text{TiO}_2\text{-SiO}_2$ composites can be used instead of TiO_2 . Hence, Dong *et al.* [96] have reported a controllable and reproducible approach to synthesize thermally stable ordered 2-D hexagonal mesoporous crystalline $\text{TiO}_2\text{-SiO}_2$ composites based on an ethanolic EISA process by using titanium isopropoxide (TIPO) and tetraethyl orthosilicate (TEOS) as precursors and triblock copolymer P123 as a template. It was observed that a large amount of acidity (HCl) lowers the condensation and

polymerization rates of TIPO and accelerates the rates for TEOS molecules. According to the authors, the resulting materials were highly stable (over 900°C), had large uniform pore diameters (~6.8 nm) with a pore volume of 0.43 cm³. g⁻¹, and had a high specific surface area (~ 290 m².g⁻¹). Such solids turned to be excellent photocatalysts for the degradation of rhodamine B in aqueous suspension, which was ascribed to the bifunctional effect of highly crystallized anatase nanoparticles and high porosity.

Nanocrystalline Bi₂O₃/TiO₂ materials [97] with ordered mesoporous structure have been prepared by the EISA method using P123 surfactant as a template. The Bi₂O₃-photosensitization of TiO₂ shifted the spectral response from UV to visible region making the Bi₂O₃/TiO₂ photocatalyst easily activated by visible light for the degradation of p-chlorophenol. According to the authors, the ordered mesoporous channels facilitate the diffusion of reactant molecules. Furthermore, the large surface area enhances the Bi₂O₃ oxide nanoparticles dispersion, the light harvesting as well as the adsorption of the reactants. Furthermore, it was found that the highly crystallized anatase may promote the transfer of photo-electrons from bulk to surface and thus inhibit their recombination with photo-holes and increase the quantum efficiency.

Another way is grafting. Earlier, Aronson *et al.* [98] have reported on the grafting of titanium dioxide onto the pore surface of MCM-41 and FSM-16 silicas by treating *as-synthesized* mesostructured silicates with TiCl₄ in hexanes. Resulting composites characterized by a large surface area (683 < S_{BET} < 1018 m². g⁻¹) and pore volumes (*c.a.* 0.7 cm³.g⁻¹) exhibited good catalytic performances in photobleaching of rhodamine-6G (50% conversion) and for the oxidation of R-terpineol (25% at conversion) under UV irradiance. Interestingly, titania formed well-dispersed isolated (TiO₂)_n clusters (~30-70 Ti atoms per cluster) which were attached to the silicate walls via Si-O-Ti bonds. It was concluded that an organic moiety such as surfactant present in the pores, or a physical constraint, such as the pore walls, prevents the creation of large TiO₂ agglomerates and enable the formation of nanosized TiO₂ clusters.

Recently, Tamiolakis *et al.* [99] reported that a mesoporous binary CdS-TiO₂ heterostructure prepared by a surfactant-assisted evaporation induced self-assembly method can work in selective photo-oxidation with visible-light using molecular oxygen as oxidant. The kinetic study of the activity of para-X-substituted benzyl alcohols (X = H, MeO, Me, Cl, NO₂) emphasized higher conversion rate when X was an electron donor group, while alcohols with electron acceptor groups such as chloro- and nitro- benzyl alcohols were converted in slower reaction rates. These results support the idea that a positive charge or a radical cation intermediate could be formed in the transition state of the rate-determining step. The latter would be better stabilized by an electron donating substituent.

Such a radical cation has been suggested to be an active intermediate in side-chain oxidation reaction of aromatic alcohols proceeding via an electron transfer.

Most studies related to mesostructured TiO_2 were focused on bulk materials but, more recently, some works also reported the preparation of titania thin films with well-defined mesoporous structures. For example, Zhao *et al.* [100] prepared a mesoporous titania film using nonionic triblock copolymer as surfactant template, the latter being removed by ethanol extraction followed by calcination at 400°C giving rise to an ordered mesostructured film with high thermal stability. Different groups, including Wang *et al.* [101], have reported that high-quality mesostructured titania thin films can be prepared on silicon substrates using spin coating. Their thermal stability could be improved by applying a supercritical fluid post-treatment process. In this case, high-temperature calcination of the films led to the formation of nanocrystals of anatase within the pore walls without causing collapse of the mesoporous structure. High crystalline TiO_2 thin films were obtained and their higher efficiency could be explained by their high porosity and the presence of highly photoactive anatase nanocrystalline structure. Without stearic acid treatment, calcination at temperatures above 550°C inevitably led to the collapse of the ordered mesoporous structure and formation of rutile crystallites in the walls of the TiO_2 thin films from the transformation of anatase nanocrystals (Fig. I.5).

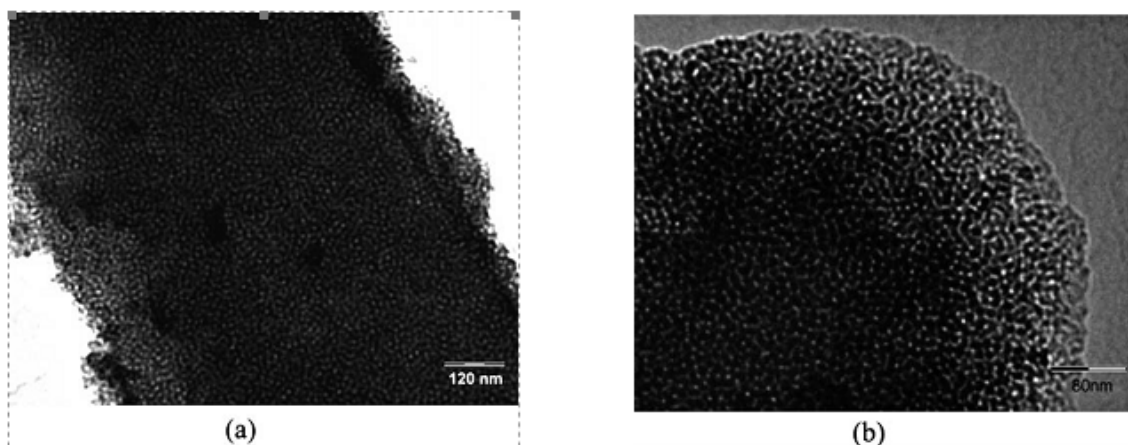


Figure I.5: TEM images of mesoporous titania thin films calcined at (a) 750°C and (b) 850°C , respectively, modified with stearic using spin coating method [101].

II.2. Use of hard templates

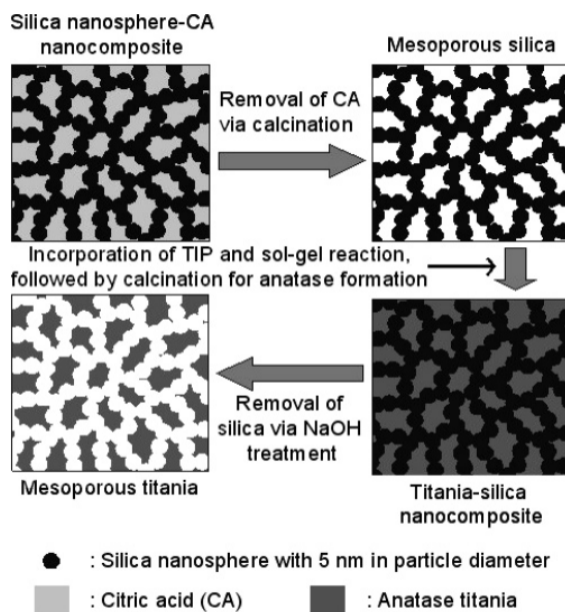
Another possibility to get porous non siliceous monocrystalline transition metal oxides consists in using hard templates such as mesoporous silicas (SBA-15, KIT-6, SBA-16, etc. [102-104]). Hence, porous crystals of Co_3O_4 , In_2O_3 , Cr_2O_3 , WO_3 etc have been prepared from pre-formed SBA-15 silica [105-107]. Among these porous oxides, cubic oxides such as Co_3O_4 and In_2O_3 were also templated by

cage-containing SBA-16. Using this kind of strategy, Yue *et al.* [108] have also described the synthesis of mesoporous monocrystalline rutile via a fabrication at low temperature using mesoporous silicas SBA-15 or KIT-6 as hard templates. They first introduced a solution of titanium nitrate into the pores of the template and allowed it to dry, dehydrate, decompose, and finally, form TiO₂ crystals. According to the authors, the reaction temperature and the concentration of HNO₃ in the used precursor had great influence on the crystallization of TiO₂.

Three key synthetic parameters play important roles in the formation of crystalline porous materials. These are the precursor/template ratios, the calcination temperatures and the immersion time in alkaline medium, to remove template. By this way, Zhang *et al.* [109] have prepared mesoporous crystalline anatase TiO₂ using the nanocasting method with mesoporous silica KIT-6 as the hard template and titanium alkoxide as the precursor. Owing to the template confinement effect, mesoporous anatase TiO₂ instead of rutile phase was obtained at the calcination temperature of 750°C. This exhibited a surface area 207 m². g⁻¹ and pore volume of 0.16 cm³. g⁻¹ with average pore size of 3.1 nm. The H₂ evolution activity of the mesoporous anatase sample hence prepared turned out to be 5.5 times (1852 mmol g⁻¹ h⁻¹) faster than that of bulk anatase TiO₂.

Similarly, Lee *et al.* [110] have reported a novel synthesis of bimodal mesoporous titania via replication of citric acid (CA)-templated mesoporous silica composed of a silica-nanospheres framework. The obtained materials were constituted by a thermally stable anatase-nanocrystal framework-meso TiO₂ as seen in scheme I.11. Interestingly, these ones were characterized by high surface area values (180-240 m². g⁻¹) and pore volumes (0.26-0.45 cm³.g⁻¹) and kept their bimodal mesostructured up to 900°C. Moreover, the anatase to rutile phase transformation of the mesoporous titania was not observed up to 900°C (instead of 700°C). The authors of the paper showed that upon impregnation with Pt the resulting solids were much more active for the water-gas shift reaction than the Pt-impregnated Degussa P25. Such differences were attributed to the three-dimensionally interconnected mesopores and the bimodal mesostructure.

Another possibility involving silica and titania to get mesoporous titania at the end consists in the exploitation of interactions between silica nanoparticles (1.5 nm in diameter) with titania nanoparticles (anatase, 4 nm or 6 nm in diameter) in a gel. In these conditions, the mesopore size could be systematically controlled in a wide mesopore range by simple control of Si/Ti (see Figure I.6) [111]. Such synthesis strategy based on a facile sol-gel synthesis in the absence of expensive organic surfactant templates enabled a systematical control of the pore dimensions, the wall thickness and the specific surface area, in the range of 2-35 nm, 3-6 nm and 180-250 m². g⁻¹, respectively. More importantly, the products have crystalline walls, the pore properties are resistant to heat up to 700°C.



Scheme I.11: Synthesis of the KRICT-MT via replication of the CA-templated mesoporous silica [110].

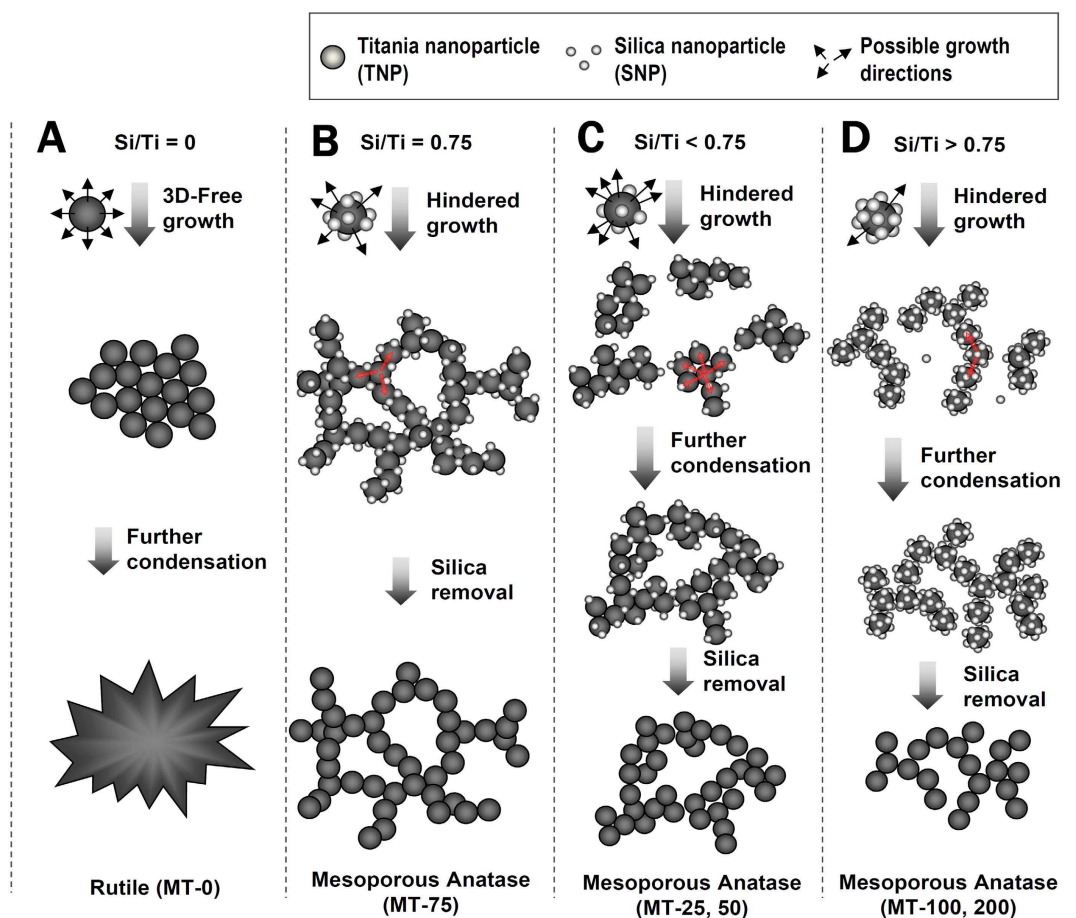


Figure I.6: Formation of mesoporous titania by the action of silica nanoparticles on titania nanoparticles under different Si/Ti ratios: $Si/Ti = 0$ (A), $Si/Ti = 0.75$ (B), $0 < Si/Ti < 0.75$ (C) and $Si/Ti > 0.75$ (D) [111].

II.3 Doping of mesoporous TiO₂ photocatalysts

Anatase TiO₂ can be excited by UV irradiation ($\lambda < 380$ nm) because of its large band gap energy of 3.2 eV. However, a rapid recombination of photoinduced electrons and holes occurs which lowers the quantum efficiency. The implementation of semiconductor heterostructures has been shown (part I) to be one of the effective methods to improve the generation and separation of photoinduced electron-hole pairs in TiO₂ for photoreaction applications.

Doping of mesoporous TiO₂ photocatalysts with noble metals such as Pt, Au, Pd and Ag has been tested frequently. Hence, deposition of Au NPs into mesostructured materials performed by Li *et al.* [112] resulted in a significant improvement of the photonic efficiency due to the generation of Schottky barriers, which inhibit the recombination of electron-hole pairs. In particular, these authors prepared nanoporous organic-inorganic hybrid films with Au-TiO₂ nanobowls using di-block copolymers as templates in combination with a sol-gel process and showed that the resulting solid is an efficient photocatalyst for visible-light.

Doping with metal ions is another possibility. Hence, Dai *et al.* [113] have prepared La-doped mesoporous TiO₂ using Ti(SO₄)₂ and La(NO₃)₃ as precursors in the presence of CTAB. Under UV irradiation, the obtained solid exhibited higher photocatalytic activity for the degradation of phoxim (an organophosphate insecticide) in emulsion than undoped samples and P25, respectively due to its large surface area, highly crystallized mesoporous wall and the presence of more active sites. In the same kind of approach, Kong *et al.* [114] have prepared mesoporous bismuth titanate photocatalyst with large pore diameter (of 6 nm) and low band gap energy (*c.a.* 2.5 eV) via a modified EISA procedure. These materials also exhibited visible-light photocatalytic reactivity.

Another promising procedure is the doping of TiO₂ with nonmetals such as nitrogen, carbon, fluoride and iodine. This sensitization of TiO₂ toward visible light is the result of the generation of newly midgap states or the narrowing of the band gap. Physically such changes can be ascribed for substitution of lattice oxygen by the anion or formation of species in vacancies that give rise to surface or near-surface states. For example, Pan *et al.* [115] have proceeded to the hydrothermal treatment of TiF₄ in H₂SO₄ aqueous solution to prepare mesoporous F-TiO₂ hollow microspheres which showed higher photocatalytic activity in the degradation of methylene blue than P25. In another case, Huang *et al.* [116] have synthesized mesoporous TiO₂ starting from TiCl₄ and diethanolamine precursors. Resulting materials doped with carbon after a phase carbonization exhibited much better activity in removal efficiency of NO than TiO₂ P25. In the same direction, Wang *et al.* [117] [133] have prepared mesoporous TiO_{2-x}N_x/ZrO₂ by sol-gel method and revealed that nitrogen was introduced in the lattice of TiO₂ as the result of the thermal treatment of the hydrous

gels containing NH_3 converting it into a visible-light responsive catalyst. Resulting solids showed good photocatalytic activity for the decomposition of ethylene in air under visible light ($\lambda > 450 \text{ nm}$) illumination.

III. Conclusion

The mild oxidation of benzylic alcohol by O_2 in the presence of photocatalysts has been studied mainly in water and acetonitrile with UV irradiation. A rather poor selectivity to carbonyl compounds was observed in water, which generates more non-selective OH radicals. The photoreaction rate is strongly dependent on factors such as substrate adsorption, intermediates reactivity, irradiation intensity and the nature of catalysts employed. Rapid recombination rate of the photogenerated electrons and holes greatly affects the photoreaction rate. Thus, to overcome this, a metal can be deposited on the TiO_2 surface, or hole/ electron scavengers can be added to the reaction system. Despite significant reports, several important issues could not be solved, such as the low rates of most photocatalytic oxidation reactions. Moreover, the photogenerated holes formed in photocatalytic oxidation processes have a high oxidative potential and may oxidize organic molecules randomly, leading to a poor product selectivity. To date, a few interesting attempts involving TiO_2 photocatalysis in acetonitrile, water, or solvent-free systems using dioxygen as a sole oxidant have been achieved for green oxidation reactions. The role of O_2 during photocatalytic processes, both in the scavenging of conduction band electrons to effectively prevent their recombination with valence band holes and in the formation of active oxygen radicals, as well as, the effect of dissolved dioxygen are still questionable.

The different strategies used for the preparation of pure mesoporous titania photocatalysts or metal-doped mesoporous titania were presented as well as their photocatalytic activities under visible and UV irradiance. Usually, the ordered pore networks, the large surface areas, pore volumes and the small crystal sizes of the building units appear to be beneficial to the separation of the photogenerated hole and electron pairs, as well as to the diffusion of reactants, thus, facilitating the diffusion of excited electrons and holes, and promoting the photocatalytic activity.

It is commonly observed that heterogeneous catalysts undergo deactivation or loss in activity mainly due to catalytic poison or change in surface area, crystal phase or size. Currently, although there are numerous reports on formation of novel photocatalysts, very few discussed and studied their recyclability.

References

- [1] A. R. A. Sheldon, I. W. C. E. Arends, A. Dijkstra, *Catal. Today*, 57 (2000) 157.
- [2] A. R. Sheldon, I. W. C. E. Arends, G. J. Ten Brink, A. Dijkstra, *Acc. Chem. Res.*, 35 (2002) 774.
- [3] P.S. Saud, B. Pant, A.M. Alam, Z.K. Ghouri, M. Park, H.Y. Kim, *Ceram. Int.*, 41 (2015) 11953.
- [4] Z. Xiong, X.S. Zhao, *J. Am. Chem. Soc.*, 134 (2012) 5754.
- [5] K. Honda and A. Fujishima, *Nature*, 238 (1972) 37.
- [6] R. A. Sheldon, J. K. Kochi, *Metal-Catalyzed Oxidations of Organic Compounds*, Academic Press, New York, 1981.
- [7] C. L. Hill, *Advances in Oxygenated Processes*, ed. A. L. Baumstark, JAI Press, London, 1 (1988) 1.
- [8] M. Hudlucky, *Oxidations in Organic Chemistry*, ACS Monograph Series, American Chemical Society, Washington, DC, 1990.
- [9] A. Fujishima, T.N. Rao, D.A. Tryk, *J. Photochem. Photobiol. C*, 1 (2000) 1.
- [10] A. Fujishima, X. Zhang, D.A. Tryk, *Surf. Sci. Rep.*, 63 (2008) 515.
- [11] A. Fujishima, K. Hashimoto, T. Watanabe, *TiO₂ Photocatalysis: Fundamentals and Applications*, BKC, Tokyo, 1999.
- [12] H. Sakai, R. Baba, K. Hashimoto, A. Fujishima, A., *J. Phys. Chem.*, 99 (1995) 11896.
- [13] A. Fujishima, X. C. R. Zhang, *Chimie*, 9 (2006) 750.
- [14] A. Fujishima, X. Zhang, D.A. Tryk, *Int. J. Hydrogen Energy*, 32 (2007) 2664.
- [15] V. Augugliaro, G. Camera-Roda, V. Loddo, G. Palmisano, L. Palmisano, J. Soria, S. Yurdakal, L. Palmisano, J. Soria, S. Yurdakal, *J. Phys. Chem. Lett.*, 6 (2015) 1968.
- [16] J. C. F. Rodríguez-Reyes, C. M. Friend, R.J. Madix, *J. Surf. Sci.*, 606 (2012) 1129.
- [17] S. Higashimoto, N. Kitao, N. Yoshida, T. Sakura, M. Azuma, H. Ohue, Y. Sakata, *J. Catal.*, 266 (2009) 279.
- [18] S. Higashimoto, N. Suetsugu, M. Azuma, H. Ohue, Y. Sakata, *J. Catal.*, 274 (2010) 76.
- [19] M. Zhang, Q. Wang, C. Chen, L. Zang, W. Ma, J. Zhao, *Angew. Chem. Int. Ed.*, 48 (2009) 6081.
- [20] O. S. Mohamed, A. M. Gaber, A. A. Abdel-Wahab, *J. Photochem. Photobiol. A, Chemistry*, 148 (2002) 205.
- [21] L.i Zhao, B. Zhanga, X. Xiao, F. L. Gu, R. Q. Zhang, *J. Mol. Catalysis A: Chemical*, 420 (2016) 82.
- [22] M.I. Litter, *Appl. Catal. B: Environ.*, 23 (1999) 89.
- [23] R. Marotta, I. Di Somma, D. Spasiano, R. Andreozzi, V. Caprio, *Chem. Eng. J.*, 172 (2011) 243.
- [24] D. Spasiano, R. Marotta, I. Di Somma, D. Spasiano, R. Andreozzi, V. Caprio, *Photochem. Photobiol. Sci.*, 12 (2013) 1991.
- [25] C. Meng, K. Yang, X. Fu, R. Yuan, *ACS Catal.*, 5 (2015) 3760.
- [26] S. Vijaikumar, N. Somasundaram, C. Srinivasan, *Appl. Catal. A: General*, 223 (2002) 129.
- [27] Z. M. Wang, E. S. Demessie, A. A. Hassan, *J. Nanotechnol.*, 20 (2011) 11.
- [28] Q. Wang, M. Zhang, C. Chen, W. Ma, J. Zhao, *Angew. Chem. Int. Ed.* 49 (2010) 7976.
- [29] S. Yurdakal, G. Palmisano, V. Loddo, V. Augugliaro, L. Palmisano, *J. Am. Chem. Soc.*, 130 (2008) 1568.
- [30] S. Yurdakal, G. Palmisano, V. Loddo, O. Alagoz, V. Augugliaro, L. Palmisano, *Green Chem.*, 11 (2009) 510.
- [31] J.C. Yu, G. Li, X. Wang, X. Hu, C. W. Leung, Z. Zhang, *Chem. Commun.*, (2006) 2717.
- [32] H. Kisch, S. Sakthivel, M. Janczarek, D. Mitoraj, *J. Phys. Chem. C*, 111 (2007) 11445.
- [33] R. Asahi, T. Morikawa, T. Ohwaki, K. Aoki, Y. Taga, *Science*, 293 (2001) 269.
- [34] N. Zhang, S. Liu, X. Fu, Y.-J. Xu, *J. Mater. Chem.*, 22 (2012) 5042.
- [35] V. Subramanian, E.E. Wolf, P.V. Kamat, *J. Am. Chem. Soc.*, 126 (2004) 4943.
- [36] L. L. Peng, T. F. Xie, Y. C. Lu, H. M. Fan, D. J. Wang, *Phys. Chem. Chem. Phys.*, 12 (2010) 8033.
- [37] D. Pei, J. Luan, *Int. J. Photoenergy*, 2012 (2012) 262831.
- [38] P. Chowdhury, H. Goma, A. K. Ray, *Chemosphere*, 121 (2015) 54.
- [39] F. Al-Zahra, G. Gassima, A. N. Alkhateeb, F. H. Hussein, *Desalination*, 209 (2007) 342.
- [40] S. Higashimoto, K. Okada, T. Morisugi, M. Azuma, H. Ohue, T.H. Kim, M. Matsuoka, M. Anpo, *Top Catal.*, 53 (2010) 578.
- [41] S. Higashimoto, R. Shirai, Y. Osano, M. Azuma, H. Ohue, Y. Sakata, H. Kobayashi, *Journal of Catalysis*, 311 (2014) 137.
- [42] R. Long, K. Mao, M. Gong, S. Zhou, J. Hu, M. Zhi, Y. You, S. Bai, J. Jiang, Q. Zhang, X. Wu, .Y. Xiong, *Angew. Chem. Int. Ed.*, 53 (2014) 3205.
- [43] Q. Hao, B. K. Juluri, Y. B. Zheng, B. Wang, I. K. Chiang, L. Jensen, V. Crespi, P. C Eklund, T. J. Huang, *J. Phys. Chem. C*, 114 (2010) 18059.
- [44] Y. Shiraiishi, D. Tsukamoto, Y. Sugano, A. Shiro, S. Ichikawa, S. Tanaka, T. Hirai, *ACS Catal.*, 2 (2012) 1984.
- [45] X. Q. Gong, A. Slloni, O. Dulub, P.Jacobson, U. Diebold, *J. Am. Chem. Soc.*, 130 (2008) 370.
- [46] K. Yamada, K. Miyajima, F. Mafun, *J. Phys. Chem. C*, 111 (2007) 11246.

- [47] S. Link, C. Burda, Z. L. Wang, M. A. El-Sayed, *J. Chem. Phys.*, 111 (1999) 1255.
- [48] C. Voisin, N. Del Fatti, D. Christofilos, F. Vallee, *J. Phys. Chem. B*, 105 (2001) 2264.
- [49] S. Sarina, S. Bai, Y. Huang, C. Chen, J. Jia, E. Jaatinen, G. A. Ayoko, Z. Bao. H. Zhu, *Green Chem.*, 16 (2014) 331.
- [50] D. Tsukamoto, Y. Shiraishi, Y. Sugano, S. Ichikawa, S. Tanaka, T. Hirai, *J. Am. Chem. Soc.*, 134 (2012) 6309.
- [51] A. Tanaka, K. Hashimoto, H. Kominami, *Chem. Commun.*, 47 (2011) 10446.
- [52] M. Qamar, R. B. Elsayed, K. R. Alhooshani, M. I. Ahmed, D. W. Bahnemann, *ACS Appl. Mater. Interfaces*, 7 (2015) 1257.
- [53] H. Vidal, J. Kapar, M. Pijolat, G. Colon, S. Bernal, A. Cordon, V. Perrichon, F. Fally, *Appl. Catal., B: Environmental*, 30 (2001) 75.
- [54] H. Wang, L. Zhang, Z. Chen, J. Hu, S. Li, Z. Wang, J. Liu, X. Wang, *Chem. Soc. Rev.* 43 (2014) 5234.
- [55] Q. Xiang, J. Yu, M. Jaroniec, *Chem. Soc. Rev.*, 41 (2012) 782.
- [56] S. Xuan, W. Jiang, X. Gong, Y. Hu, Z. Chen, *J. Phys. Chem. C*, 113 (2009) 553.
- [57] J. C. Colmenares, W. Ouyang, M. Ojeda, E. Kunaa, O. Chernyayeva, D. Lisovytskiya, S. De, R. Luque, A. M. Balu, *Appl. Catalysis B: Environmental*, 183 (2016) 107.
- [58] W. Feng, G. Wu, L. Li, N. Guan, *Green Chem.*, 13 (2011) 3265.
- [59] S. T. Zhang, C. M. Li, H. Yan, M. Wei, D.G. Evans, X. Duan, *surf. J. Phys. Chem. C*, 118 (2014) 3514.
- [60] Q. Jia, D. Zhao, B. Tang, N. Zhao, H. Li, Y. Sang, N. Bao, X. Zhang, X. Xu, H. Liu, *J. Mater. Chem. A*, 2 (2014) 16292.
- [61] F. Zaera, *Chem. Soc. Rev.*, 42 (2013) 2746.
- [62] J. Tian, Z. Zhao, A. Kumar, R. I. Boughton, H. Liu, *Chem. Soc. Rev.*, 43 (2014) 6920.
- [63] M. Ge, C. Cao, J. Huang, S. Li, Z. Chen, K. Q. Zhang, S. S. Al-Deyabd, Y. Lai, *J. Mater. Chem. A*, 4 (2016) 6772.
- [64] J. Tiana, J. Lia, Na. Weia, X. Xuc, H. Cuian, H. Liub, *Ceramics International*, 42 (2016) 1611.
- [65] K. Imamura, H. Tsukahara, K. Hamamichi, N. Seto, K. Hashimoto, H. Kominami. *Appl. Catal. A: General*, 450 (2013) 28.
- [66] J. Zhang, Q. Xu, Z. Feng, M. Li, C. Li, *Angew. Chem., Int. Ed.*, 47 (2008) 1766.
- [67] H. G. Yang, C. H. Sun, S. Z. Qiao, J. Zou, G. Liu, S. C. Smith, H. M. Cheng, G. Q. Lu, *Nature*, 453 (2008) 638.
- [68] M. Kong, Y. Li, X. Chen, T. Tian, P. Fang, F. Zheng, X. Zhao, *J. Am. Chem. Soc.*, 133 (2011) 16414.
- [69] Junqing Yan, Guangjun Wu, Naijia Guan, Landong Li, Zhuoxin Li and Xingzhong Cao, *Phys. Chem. Chem. Phys.*, 2013, 15, 10978.
- [70] E. De la Rosa, S. Sepulveda-Guzman, B. Reeja-Jayan, A. Torres, P. Salas, N. Elizondo, M. J. Yacaman, *J. Phys. Chem. C*, 111 (2007) 8489.
- [71] X. M. Sun, X. Chen, Z. X. Deng, Y. D. Li, *Mater. Chem. Phys.*, 78 (2003) 99.
- [72] D. B. Wang, C. X. Song, *J. Phys. Chem. B*, 109 (2005) 12697.
- [73] S. Cho, S. Kim, K. H. Lee, *J. Colloid Interface Sci.*, 361 (2011) 436.
- [74] M. H. Huang, S. Mao, H. Feick, H. Q. Yan, Y. Y. Wu, H. Kind, E. Weber, R. Russo, P. D. Yang, *Science*, 292 (2001) 1897.
- [75] G. Wang, D. Chen, H. Zhang, J. Z. Zhang, J. H. Li, *J. Phys. Chem. C*, 112 (2008) 8850.
- [76] Zi. Tang, X. Yin, Y. Zhangab, Y. J. Xu, *RSC Adv.*, 3 (2013) 5956.
- [77] T. Sano, Y. Oumi, *Catal. Surv. Asia*, 8 (2004) 295.
- [78] S. J. Miao, Y. Q. Deng, *Appl. Catal. B: Environ.*, 31 (2001) 1.
- [79] P. A. Nelson, J. R. Owen, *J. Electrochem. Soc.*, 150 (2003) 1313.
- [80] T. Hyodo, Y. Shimizu, M. Egashira, *Electrochem.* 71 (2003) 387.
- [81] D. Mehandjiev, E. Nikolovazhecheva, *J. Catal.*, 65 (1980) 475.
- [82] M. J. Danks, H. B. Jervis, M. Nowotny, W. Z. Zhou, T. A. Maschmeyer, D. W. Bruce, *Catal. Lett.*, 82 (2002) 95.
- [83] N. C. King, C. Dickinson, W. Z. Zhou, D. W. Bruce, *Dalton Trans.*, (2005) 1027.
- [84] C. T. Kresge, M. E. Leonowicz, W. J. Roth, J. C. Vartuli, J. S. Beck, *Nature*, 359 (1992) 710.
- [85] G. S. Attard, C. G. Goltner, J. M. Corker, S. Henke, R. H. Templer, *Angew. Chem., Int. Ed.*, 36 (1997) 1315.
- [86] D. M. Antonelli, J. Y. Ying, *Angew. Chem. Int. Ed.*, 34 (1995) 2014.
- [87] U. Ciesla, S. Schacht, G. D. Stucky, K. K. Unger, F. Schuth, *Angew. Chem., Int. Ed.*, 35 (1996) 541.
- [88] P. D. Yang, D. Y. Zhao, D. I. Margolese, B. F. Chmelka, G. D. Stucky, *Nature*, 396 (1998) 152.
- [89] Z. Tian, X. Y. Liu, B. Tu, J. Fan, C. Z. Yu, L. M. Wang, S. H. Xie, G. D. Stucky, D. Y. Zhao, *Nat. Mater.*, 2 (2003) 159.
- [90] R. Li, H. Kobayashi, J. Guo, J. Fan, *J. Phys. Chem. C*, 115 (2011) 23408.
- [91] J. Fan, S. W. Boettcher, G. D. Stucky, *Chem. Mater.*, 18 (2006) 6391.
- [92] K. Tanabe, S. Okazaki, *Appl. Catal., A*, 133 (1995) 191.

- [93] K. Tanabe, *Catal. Today*, 78 (2003) 65.
- [94] K. Nakajima, T. Fukui, H. Kato, M. Kitano, J. N. Kondo, S. Hayashi, M. Hara, *Chem. Mater.*, 22 (2010) 3332.
- [95] L. Chen, B. Yao, Y. Cao, K. Fan, *J. Phys. Chem. C*, 111 (2007) 11849.
- [96] W. Dong, Y. Sun, C. W. Lee, W. Hua, X. Lu, Y. Shi, S. Zhang, J. Chen, D. Zhao, *J. Am. Chem. Soc.*, 129 (2007) 13894.
- [97] Z. Bian, J. Zhu, S. Wang, Y. Cao, X. Qian and H. Li, *J. Phys. Chem. C*, 2008, 112, 6258.
- [98] Blake J. Aronson, C. F. Blanford, A. Stein, *Chem. Mater.*, 9 (1997) 2842.
- [99] I. Tamiolakis, I. N. Lykakis, G. S. Armatas, *Catalysis Today*, 250 (2015) 180.
- [100] L. Zhao, Y. Yu, L. Song, M. Ruan, X. Hu, A. Larbot, *Appl. Catalysis A: General*, 263 (2004) 171.
- [101] K. Wang, B. Yao, M. A. Morris and J. D. Holmes, *Chem. Mater.*, 17 (2005) 4825.
- [102] D. Y. Zhao, J. L. Feng, Q. S. Huo, N. Melosh, G. H. Fredrickson, B. F. Chmelka, G. D. Stucky, *Science*, 279 (1998) 548.
- [103] F. Kleitz, S. H. Choi, R. Ryoo, *Chem. Commun.*, (2003) 2136.
- [104] D. Y. Zhao, Q. S. Huo, J. L. Feng, B. F. Chmelka, G. D. Stucky, *J. Am. Chem. Soc.*, 120 (1998) 6024.
- [105] C. Dickinson, W. Z. Zhou, R. P. Hodgkins, Y. F. Shi, D. Y. Zhao, H. Y. He, *Chem. Mater.*, 18 (2006) 3088.
- [106] K. K. Zhu, B. Yue, W. Z. Zhou, H. Y. He, *Chem. Commun.*, (2003) 98.
- [107] B. Z. Tian, X. Y. Liu, H. F. Yang, S. H. Xie, C. Z. Yu, B. Tu, D. Y. Zhao, *Adv. Mater.*, 15 (2003) 1370. [108] W. Yue, X. Xu, J. T. S. Irvine, P. S. Attidekou, C. Liu, H. He, D. Zhao, W. Zhou, *Chem. Mater.*, 21 (2009) 2540.
- [109] Z. Zhang, F. Zuo, P. Feng, *J. Mater. Chem.*, 20 (2010) 2206.
- [110] D. W. Lee, S. Jun Park, S. Ki Ihm, K. H. Lee, *Chem. Mater.*, 19 (2007) 937.
- [111] H. I. Lee, Y. Y. Lee, D. U. Kang, K. Lee, Y. U. Kwon, J. M. Kim, *Scient. Rep.*, 6 (2016) 21496.
- [112] X. Li, J. Peng, J.-H. Kang, J.-H. Choy, M. Steinhart, W. Knoll, D. H. Kim, *Soft Matter*, 4 (2008) 515.
- [113] K. Dai, T. Peng, H. Chen, J. Liu and L. Zan, *Environ. Sci. Technol.*, 43 (2009) 1540.
- [114] L. Kong, H. Chen, W. Hua, S. Zhang, J. Chen, *Chem. Commun.*, (2008) 4977.
- [115] J. H. Pan, X. Zhang, A. J. Du, D. D. Sun, J. O. Leckie, *J. Am. Chem. Soc.*, 130 (2008) 11256.
- [116] Y. Huang, W. Ho, S. Lee, L. Li, G. Zhang and J. C. Yu, *Langmuir*, 24 (2008) 3510.
- [117] X. Wang, J. C. Yu, Y. Chen, L. Wu and X. Fu, *Environ. Sci. Technol.*, 40 (2006) 2369.

Mild oxidation of alcohols using dioxygen in combination with photocatalysts

D. Obaid, A. Mayoufi, P. Beaunier and F. Launay

^a *Sorbonne Universités, UPMC Univ Paris 06, CNRS, Laboratoire de Réactivité de Surface, 4 place Jussieu, F-75005, Paris, France.*

I. Introduction

Selective oxidation of primary alcohols to the corresponding aldehydes or C-C bond cleavage processes are important organic transformations for both laboratory and industrial synthetic chemistry [1-4], but still a lot of stoichiometric oxidants are used such as compounds based on chromium(VI), manganese (VII), osmium and even lead (IV) [5,7,8,9]. For environmental and economic issues, metal catalyzed reactions using molecular oxygen as oxidant have a great potential due to the inherent properties of O₂ to be cheap, readily available, and ensuring a high atom economy. Moreover, from the thermodynamic point of view, these reactions are favorable. However, examples of selective oxidation reactions involving O₂ are still few, essentially for kinetic reasons. They are actually mostly inspired by enzymes, but, often, their catalytic performances are lower. Among the various strategies of O₂ activation available to chemists, the use of photocatalysts is one which has been very little studied especially for the partial oxidation of molecules [10-14].

Photocatalysis based on semiconductors has attracted much attention since Fujishima and Honda explored water splitting over TiO₂ under ultraviolet illumination in 1972 [15]. However, up to now, semiconductor photocatalysts such as TiO₂, ZnO, CdS are mostly used for the removal of organic pollutants [16], photocatalytic hydrogen generation and the development of new solar cells [17]. Titanium dioxide has been widely used in photocatalysis, due to its morphological, microstructural, optical and hydrophilic properties as well as its low cost, non-toxicity, photostability, but to date, a limited progress has been reported for TiO₂ semiconductor p-type in the synthesis of organic chemicals [18-20]. However, photocatalytic processes are generally able to drive reactions at ambient temperature and pressure, which could be favorable for selective oxidation provided that reactive species formed are different from hydroxyl radicals. More particularly, photocatalysts displaying a high crystalline surface area with a highly efficient electron-hole pair separation are worth to be considered [21-24].

This present work is focused on the use of TiO₂ NPs for the photocatalytic (i) transformation of alcohols to aldehydes (or ketones) and (ii) the oxidative cleavage of C-C bonds in activated compounds such α -hydroxy acids involving O₂ [25-28]. As a reference molecule, benzyl alcohol was first tested in different solvent conditions and in the presence of various forms of TiO₂ materials before investigating the capabilities of the system studied towards a wide range of substrates for

both reactions. The photo-assisted oxidation of some of the tested substrates has been studied very little up to now [29-34]. Other oxides (ZrO_2 , CeO_2 , ZrO_2-CeO_2 , ZnO) and mesoporous TiO_2 materials, prepared by a hard templating method, were investigated too.

II. Experimental part

II.1. Chemicals and reagents

The origin and purity of the chemical reagents used is given in Annex 2. Chemicals and solvents were of the highest available grade and were used without further purification. All the materials tested as photocatalysts have been dried in the oven at $50^\circ C$ overnight at least for 12 h.

II.2. Synthesis of mesoporous crystalline TiO_2 (meso- TiO_2 -S1)

SBA-15, used here as a hard template, was prepared following the method reported by Zhao *et al.* [35] and calcined at $500^\circ C$ for 4 h, with air rate $2^\circ C/min$.

Meso- TiO_2 was synthesized according to the method published by Zhang *et al.* [36]: 1 g of SBA-15 dry silica powder was dispersed into 20 mL of an ethanol solution containing 1.8 mL of titanium isopropoxide. After stirring for 1 h at room temperature, the mixture was transferred in an oven and dried overnight at $85^\circ C$. The obtained white powder was calcined at $500^\circ C$ for 4 h and a white $TiO_2/SBA-15$ composite was obtained. Afterward, to remove the SiO_2 template, the powder was dispersed in 20 mL of a 2 M NaOH solution and the suspension stirred for 2 h. After centrifuging the resulting mixture for 45 min at 7000 rpm, the supernatant solution was discarded. This procedure was repeated 5 more times in the next 8 h. In the final step, the solid residue was immersed in 20 mL of 2 M NaOH and stirred overnight for 14 h. After centrifugation, the supernatant was discarded and the sample was washed with deionized water 4 times and dried at $120^\circ C$ overnight. Resulting solid has been abbreviated as meso- TiO_2 -S1.

II.3. Sol gel synthesis of TiO_2 nanoparticles (TiO_2 -SG)

TiO_2 nanoparticles were prepared using the sol gel method described by Kudhier *et al.* [37] via hydrolysis starting from $Ti[OCH(CH_3)_2]_4$ as follows: Titanium tetraisopropoxide (5 mL) was added slowly to a mixture of 10 mL isopropanol, 10 mL of 68 wt.% acetic acid and 12 mL of water. The reaction was performed at room temperature for 12 h, to form a sol-gel. The final sol-gel solution was then dried at $120^\circ C$ for 1 day, and a dry gel was obtained giving rise to $TiO_2(S-120)$. Eventually, the dry gel was calcined at 350 and $450^\circ C$ for 2 h in air ($5^\circ C/min$) to form $TiO_2(S-350)$ and $TiO_2(S-450)$, respectively.

II.4. Synthesis of ZrO₂ nanoparticles (ZrO₂-h)

ZrO₂-h oxide NPs were prepared by simple hydrothermal process using ZrOCl₂·8H₂O as precursor and then calcined at 160°C according to the procedure reported by Rajendran [38].

II.5. Characterization methods

The solid catalysts were analyzed by X-ray diffraction patterns recorded on a Bruker Advance D8 diffractometer using the Cu K α radiation with steps of 0.02°, a count time of 6 s at each point and an X-ray power of 40 kV and 40 mA. Average crystallite size (d_p) was calculated using the Scherrer formula, $d_p = 0.9\lambda/B\cos\theta$, where λ is the X-Ray source wavelength ($\lambda_{Cu} = 0.15418$ nm), B is the full-width at half maximum of the Bragg diffraction peak and θ corresponds to 12.65° ((101) plane of anatase)).

The textural properties of the solid materials were determined from N₂ sorption data obtained at -196°C using an ASAP 2010 Micromeritics instrument or a Bell Instrument. Prior to the analysis, the samples were outgassed at 300°C for 3 h until a stable static vacuum of 2.10⁻³ Torr was reached. The weight of the sample used (initially around 80 mg) was measured exactly after pretreatment. The BET (Brunauer Emmett Teller) specific surface area was calculated from the adsorption data over a relative pressure range from 0.02 to 0.25. The pore diameter and specific pore volume were determined according to the BJH model using the desorption branch.

Diffuse reflectance UV-Vis. spectra were recorded at room temperature for 2 mm thick samples between 200 and 900 nm with a scanning speed of 600 nm.min⁻¹ on a Varian Cary 5E spectrometer equipped with a double monochromator and an integrating sphere coated with polytetrafluoroethylene (PTFE) as reference. The spectra were plotted in absorbance values, after subtraction of the PTFE signal. The Tauc plots ($(\alpha h\nu)^2 = f(h\nu)$) were performed in order to determine the band gap values (E_g) of the different materials tested, where α is $= [2.303 \log (I_0/I)] / L$ with L corresponding to the path length, I_0 to the input intensity, I to the transmitted intensity [39,40]. The direct band gap values were obtained from the intercept of the straight portion of the plot with the x-axis (see Figure II.1).

The titanium composition of the suspensions and solid catalysts were determined by X-ray fluorescence spectroscopy using a XEPOS spectrometer (Spectro Ametek). Samples were analyzed in their powder form and quantitative data were determined using the MicroPowder method combining the well-established fundamental parameters approach to XRF spectrometer calibration with automatic correction for matrix effects by using the Compton backscatter information from the sample to calculate the matrix interferences.

TEM images were obtained with a JEOL-JEM 2011 microscope operated at 200 kV using an accelerating voltage of 200 kV. The powdered samples had to be first dispersed in ethanol and the resulting suspensions deposited on a copper grid coated with a porous carbon film. The powdered samples had to be first dispersed in ethanol and the resulting suspensions deposited on a copper grid coated with a porous carbon film.

Thermogravimetric analysis (TGA) measurements were carried out using a TA Instruments- Waters SDT Q600 analyzer. The TGA data were collected at $10^{\circ}\text{C}\cdot\text{min}^{-1}$ from ambient 10 to 900°C under air flow of $100\text{ mL}\cdot\text{min}^{-1}$ using an alumina pan.

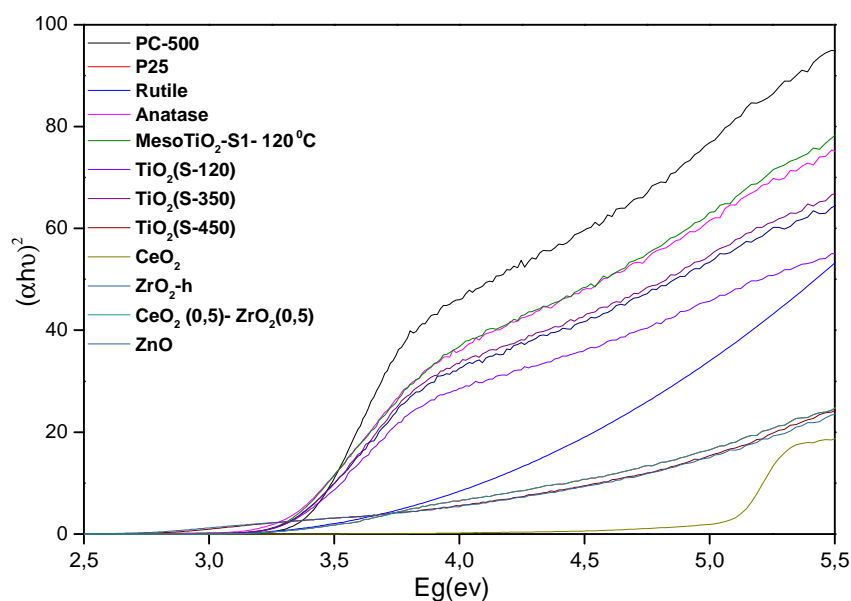


Figure II.1: Tauc plots for the different materials tested in benzylalcohol oxidation under UV irradiance.

The textural and optical data related to the different samples studied are summarized in Table II.1.

Table II.1: Physico-chemical properties of the different photo-materials tested.

Entry	Material	N ₂ physisorption S _{BET} (m ² .g ⁻¹)	Pore vol. (cm ³ .g ⁻¹)	Pore Size (nm)	TiO ₂ XRD Crystallite size (nm)	UV-vis Band gap (eV)
1	Anatase	28	0.04	5.6	72	3.3
2	Rutile	7	0.05	23	51	3.3
3	P25	50	0.25	17.5	21	3.2
4	PC-500	239	0.25	4.2	6.3	3.3
5	SBA-15	449	0.75	6.2	-	-
6	Meso-TiO ₂ -S1	162	0.22	3.8	9	3.25
7	TiO ₂ (S-120)	54	0.2	15	-	3.35
8	TiO ₂ (S-350)	50	0.17	13	7.3	3.3
9	TiO ₂ (S-450)	65	0.23	13	8.2	3.3

10	ZrO ₂	16	0.1	1.5	22	5.0
Entry	Material	N ₂ physisorption S _{BET} (m ² .g ⁻¹)	Pore vol. (cm ³ .g ⁻¹)	Pore Size (nm)	TiO ₂ XRD Crystallite size (nm)	UV-vis Band gap (eV)
11	ZrO ₂ -h	40	0.23	10	6	5.1
12	CeO ₂	122	0.11	3.6	10	2.4
13	ZrO ₂ (0.5)-ZrO ₂ (0.5)	61	0.17	10.8	7	5.0
14	ZnO	9	0.08	6.5	49	3.3

^a Single point of adsorption P/P₀= 0.978, ^b Band gap calculated using Tauc plot, ^c Crystallite size determined from XRD data using Scherrer equation.

II.6. Photocatalytic tests evaluation

II.6.1. Photoreactor setup

A home-made reactor was setup with a photo chamber. As shown in Figure II.2., the reactor has an immersion well with a water inlet and a water outlet. The lamp was housed in this well made of quartz cooled with circulating water thermostated at 15°C. The geometry of the reactor is of significant importance to facilitate photons to be collected in an effective way by the photocatalyst. It is known noted that the irradiance of light decreases inversely with the square of the distance from the source of light. In this case, the maximum distance from the illumination center was around 5 cm.

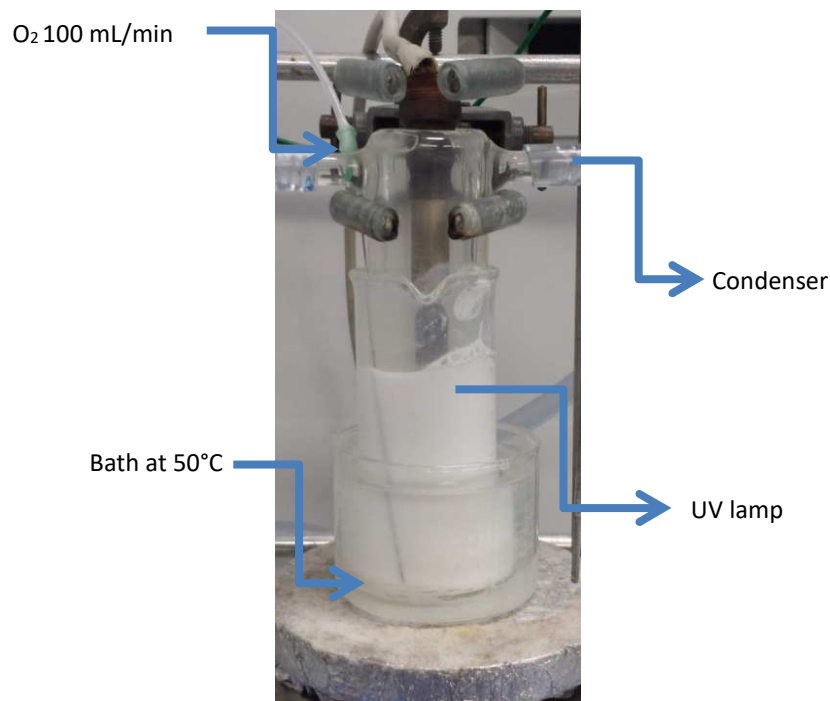


Figure II.2: Reactor set-up used in the photocatalytic experiments.

II.6.1. UV lamp model

As seen in the Figure II.2, the source of UV light used is a HPK 125W mercury lamp from Heraeus Noble light, which is characterized by a continuum from 200 to 600 nm and has a maximum energy at 365 nm with substantial radiation also at 435, 313, 253 and 404 nm (Figure II.3).

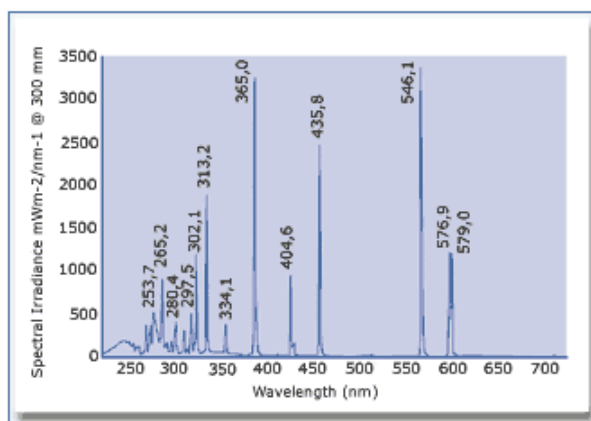


Figure II.3: UV light model as source of irradiance, Mercury Lamp.

II.6.3. Typical experiment of photocatalysis

The photo-catalyst (60 mg) was dispersed in 40 mL of solvent in a test tube made of pyrex glass. Runs were performed at 50°C with 2.9 mmol of the substrate. The suspension was held under constant magnetic stirring at 900 rpm firstly during 1 h without irradiation to reach the adsorption equilibrium of the substrate molecules onto the catalyst, then for 4 h under UV irradiation and O₂ gas flow at 100 mL.min⁻¹.

Quantification of the reactants was performed by gas chromatography on a DELSI NERMAG DN200 instrument equipped with a flame ionization detector (FID) using a 30 m long, 0.25 mm i.d. and 0.25 μm-thick capillary OPTIMA-5-MS column (MACHEREY-NAGEL). To do so, an aliquot of one milliliter of the filtered reaction suspension was mixed with one milliliter of the internal standard solution (0.5 mmol of mesitylene dissolved in 15 mL of methanol). Quantification of acids was done after an esterification treatment of the aliquot (after the addition of 2 drops of concentrated sulfuric acid and a thermal treatment at 60°C for 4 h in an oven). Direct analysis of benzoic acid could also be done by HPLC using a Shim-Pack XR-ODS® 4.6 mm i.d. x 100 mm packed column, with water/ methanol 60:40% v/v and a small amount of acetic acid (0.5% v) as eluent and using a UV detector set at 220 nm.

Conversion of substrates (X) and selectivity for oxidation products ($S_{i,t}$) were calculated as follows: $X(\%) = 100 \times (C_{s,0} - C_{s,t})/C_{s,0}$ and selectivity for product i, $S_{i,t}(\%) = 100 \times (C_{i,t}/(C_{s,0} - C_{s,t}))$ where, $C_{s,0}$, $C_{s,t}$ are the initial and final (after time t) molar concentrations of substrate, respectively and $C_{i,t}$ is the concentration of one of the product after time t of the photocatalytic reaction. In the

present situation, mass balance (MB) values were calculated using the following equation:

$$MB(\%) = \frac{\sum_i^p c_i}{c_p} \times 100.$$

III. Results and discussion

III.1. Synthesized TiO₂ materials

- Case of mesoporous TiO₂

We have synthesized mesoporous TiO₂ using the hard template method described by Zhang *et al.* [36] starting from SBA-15 silica. XRD patterns of the resulting material calcined at 500°C (Meso-TiO₂-S1) and of the intermediate composites are shown in Figure II.4. Main wide angle X-Ray diffraction peaks (101, 004, 200) corresponding to the anatase phase were observed for the TiO₂-SiO₂ composite calcined at 500°C and of course much better for Meso-TiO₂-S1. The adsorption-desorption isotherms of the SBA-15 template and Meso-TiO₂-S1 after treatment with alkaline medium in 2 M NaOH to remove the SiO₂ template are shown in Figure II.5.

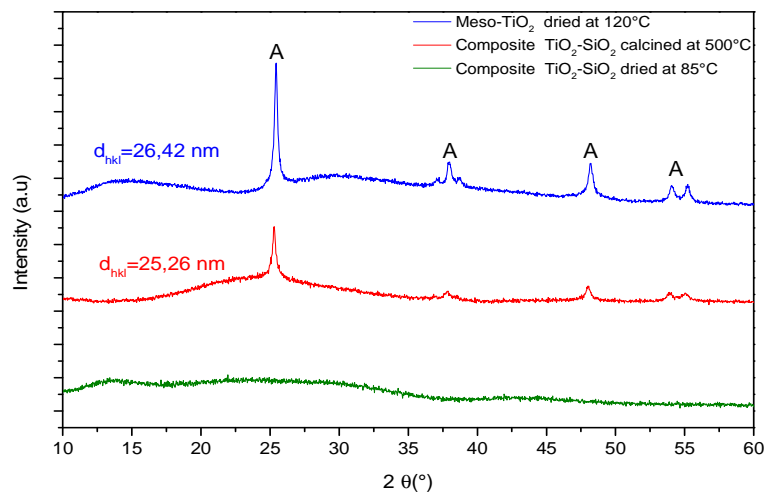


Figure II.4: X-ray diffraction of mesoporous TiO₂ synthesized via the hard template method and its key intermediates: (■) TiO₂-SiO₂ composite dried at 85°C, (■) TiO₂-SiO₂ composite calcined at 500°C before treatment in 2 M NaOH medium and (■) Meso-TiO₂ after treatment in NaOH 120°C.

The curves of SBA-15 are of type-IV with a H1 hysteresis loop characteristic of structured mesoporous materials (Figure II.5). Using the BET and BJH models, the surface area of SBA-15 could be estimated to 449 m².g⁻¹, the pore volume to 0.75 cm³.g⁻¹, with a monodisperse size distribution centered at *c.a.* 6.2 nm. Isotherms of meso TiO₂-S1 are of type-II, forming a H4 hysteresis. Using the same models, the surface area of meso TiO₂-S1 could be estimated to 162 m².g⁻¹, the pore volume to 0.22 cm³.g⁻¹. In this last case, the pore distribution was wider with a maximum around 3.8 nm. The particle size of TiO₂ NPs in meso TiO₂-S1 could be estimated from wide angle XRD measurements

(Figure II.4). It is about 9 nm, which is not so far from the size of the pores of the SBA-15 templates used for the preparation (6.2 nm).

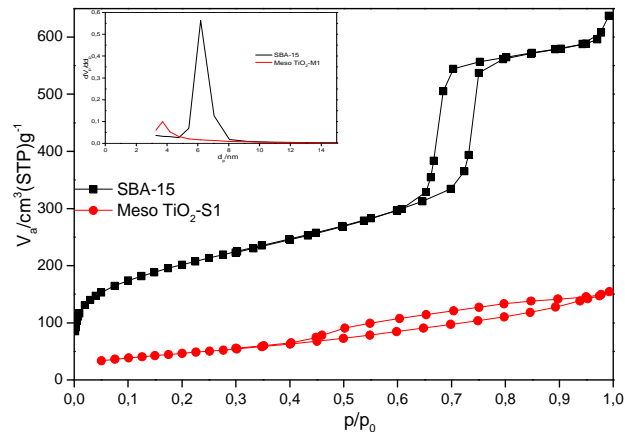
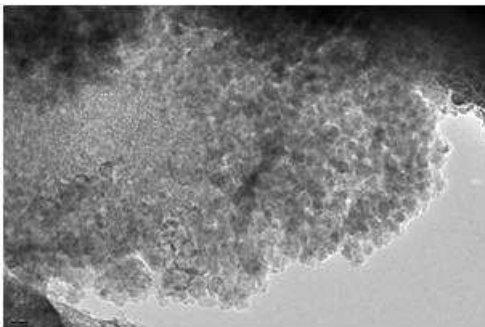


Figure II.5: N₂ adsorption-desorption isotherms at -196°C and pore size distribution of meso TiO₂-S1 and its SBA-15 precursor.

The HR-TEM images of Meso TiO₂-S1 indicate that the latter would be composed of anatase nanoparticles with sizes around 15 nm (Figure II.6A). Their crystallinity is observed in particular in Figure II.6B. The grains of TiO₂ appear to be stucked together, suggesting a small mesoporosity, which seems normal since this porosity should correspond roughly to the walls of the silica SBA-15 starting material that was sacrificed. A finer observation indicates the presence of a veil (2-3 layers) around the NPs which could be phyllosilicates formed after incomplete removal of the silica.

A) Meso TiO₂-S1 (scale bar 20 nm)



B) Meso TiO₂-S1 (scale bar 20 nm)

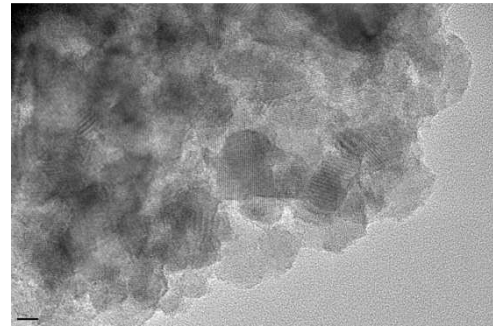
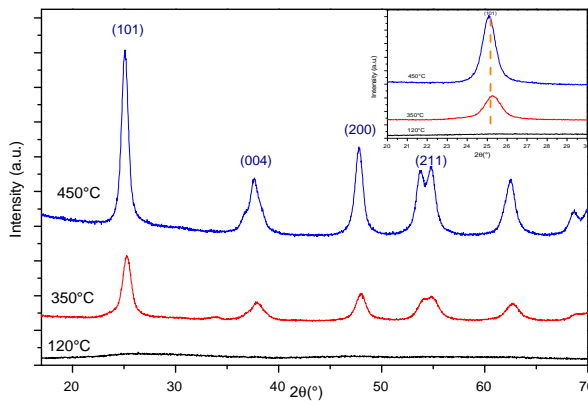


Figure II.6: HR-TEM photographs of MesoTiO₂-S1.

- Case of TiO₂ prepared by sol-gel method (TiO₂-SG)

Samples prepared according to the sol gel method were either dried at 120° C or calcined at 350 or 450°C. According to analyzes carried out by Fluorescence X, only the sample treated at 450°C. contained 100% TiO₂; others contain *a priori* organic matter, undoubtedly isopropyl groups not decomposed. From 350°C, the characteristic peaks of the anatase are present in the diffractograms (Figure II.7) and become more intense at 450°C as the result of the total loss of the organic components. On the other hand, the half-height width of the peaks does not seem to change,

implying that the size of the anatase crystals does not evolve too much (between 7.3 and 8.2 nm according to Scherrer equation).



TiO ₂ sol-gel	TiO ₂ , % FluoX
TiO ₂ (S-120)	43.4
TiO ₂ (S-350)	66.5
TiO ₂ (S-450)	100

Figure II.7: XRD patterns of TiO₂ samples prepared using the sol gel route as a function of the thermal treatment of the recovered solids (120-450°C).

The N₂ sorption isotherms of the different samples grouped in Figure II.8 indicate that the uncalcined material is microporous in nature and characterized by intergranular porosity. After calcination, only this porosity could be preserved but in a lesser proportion than in the as-synthesized material. The textural properties of these samples are almost the same without significant change in surface area or pore diameter. BET surface area values for the three samples are around 55 m².g⁻¹ and the pore volumes around 0.2 cm³.g⁻¹.

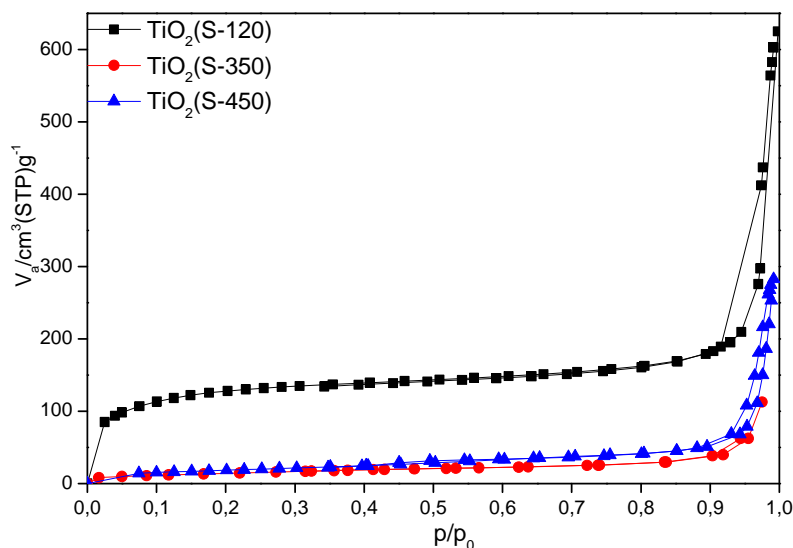


Figure II.8: N₂ adsorption-desorption isotherms at -196°C of TiO₂ samples prepared using the sol gel route as a function of the thermal treatment of the recovered solids (120-450°C).

III.2. Catalysis tests with different semi-conductors

- **TiO₂ photocatalysts**

The photo-oxidation of benzyl alcohol was considered first using P25. Then, results were compared with different commercially available sources of TiO₂ materials, other metal oxides like ZrO₂, CeO₂, ZrO₂-CeO₂, ZnO. The photocatalytic performance of mesoporous TiO₂ (Meso-TiO₂Si1) was also investigated. Typical reactions were performed under UV irradiation with a maximum intensity at 365 nm (see II.6) over 4 h in acetonitrile at 50°C under oxygen flow (100 mL.min⁻¹) with 60 mg of catalyst. As seen in Figure II.9, higher loadings of P25 did not bring significant changes in the reaction rate probably as the result of the decrease of the photo-activated volume of suspension because of scattering of incident light. Both the benzyl alcohol conversion and the benzaldehyde selectivity were significantly lower at 25°C (respectively 48% and 56% instead of 64 % and 92%). Furthermore, an increase in the reaction temperature over 50°C, resulted in reducing the catalytic activity. Flow rate of oxygen at 100 mL.min⁻¹ yielded the best results in terms of formation of benzaldehyde (59% yield). With an increase of the oxygen flow rate, the conversion decreased sharply.

Blank tests carried out in the absence of the catalyst (Table II.2, entry 1) or UV irradiation (case of P25, Table II.2, entry 2) showed negligible benzyl alcohol conversion (< 2%), therefore suggesting that benzyl alcohol oxidation is a photocatalyzed process and neither a photochemical nor a thermal reaction. Before irradiation, a small decrease in the amount of benzyl alcohol was observed which is related to its adsorption on TiO₂ surface, as reported by Higashimoto *et al.* using infrared spectroscopy [41, 42].

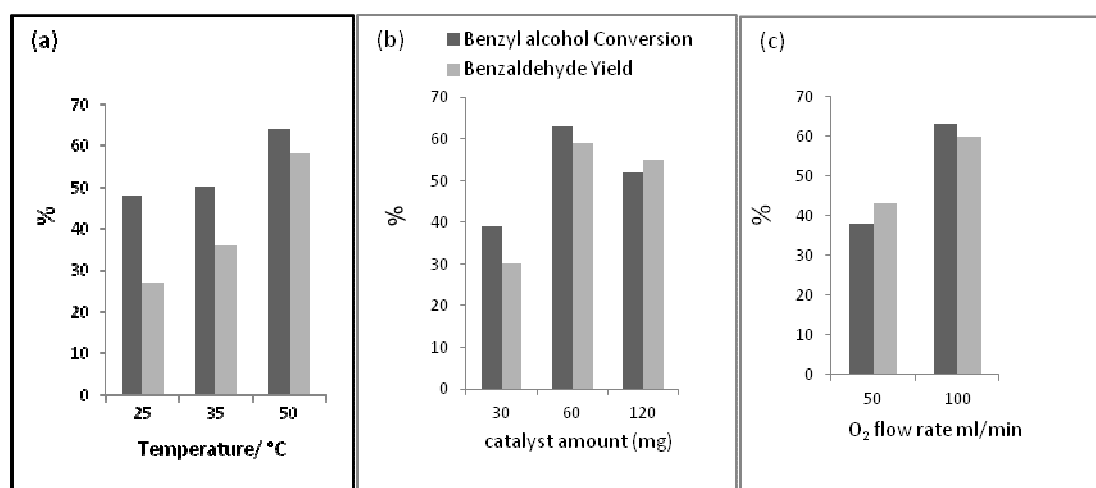


Figure II.9: Influence of a) reaction temperature (b) catalyst loading and (c) oxygen flow rate on the oxidation of benzyl alcohol.

Benzaldehyde and benzoic acid were the only two products identified here. No other by-products such as benzyl benzoate could be detected. A priori, the mass balance was correct (between 97 and

100%), thus, emphasizing the fact that mineralization of organic matter did not occur in the present conditions.

Table II.2: Results of the photo-catalyzed aerobic oxidation tests of benzyl alcohol into benzaldehyde in acetonitrile under UV irradiance.^a

Entry	Materials	Conv. (%) BzOH	Sel. (%) PhCHO	Yield (%) PhCHO	MB (%)
1	No (only hv)	-	-	-	-
2	P25 (no hv)	< 2	-	-	-
3	TiO ₂ - P25	64	92	59	100
4	Rutile	5	100	5	100
5	Anatase	34	73	25	97
6	PC-500	71	83	59	100
7	TiO ₂ (S-120)	67	40	27	100
8	TiO ₂ (S-350)	47	60	28	100
9	TiO ₂ (S-450)	29	100	30	100
10	Meso-TiO ₂ -S1-120 °C	30	96	28	100
11	ZrO ₂	23	70	16	100
12	ZrO ₂ -h	37	84	31	100
13	CeO ₂	28	78	22	100
14	ZrO ₂ (0.5)-CeO ₂ (0.5)	21	92	19	100
15	ZnO	22	100	22	100

^a Reaction conditions: substrate (2.9 mmol), acetonitrile (40 mL), catalyst amount (60 mg), temperature (50°C), exposure time (4 h), O₂ flow (100 mL.min⁻¹), UV lamp irradiance HPK 125W, Max intensity, 365 nm.

In the case of P25, the time dependence of the benzyl alcohol conversion reached a maximum after 4 h of reaction (Figure II.10) with conversion of 64%. Benzaldehyde was formed as the quasi-exclusive product with 94% selectivity. Further conversion of the alcohol was negligible after 4 h whereas the yield of benzaldehyde and mass balance were reduced by *c.a.* 10% after 10 h of irradiation, which stem from overoxidation to benzoic acid, which was detected by HPLC. The invariability of the conversion after 4 h suggests that the photocatalyst deactivates during the reaction. It is highly probable that a deposit was formed on the surface as the reaction progressed. Also, we decided to repeat the test over 1, 5 and 10 h. The catalysts were recovered systematically by filtration and washed extensively with acetonitrile before being dried at 80°C. The thermogravimetric analyzes of all the samples and initial P25 are grouped in Figure II.11.

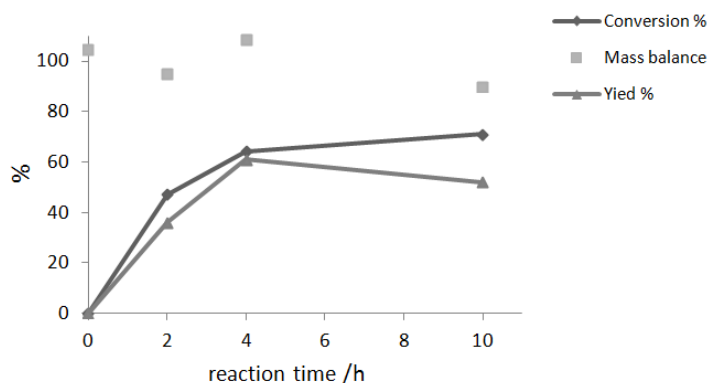


Figure II.10: Time profile of the photocatalytic oxidation of benzyl alcohol over P25 in acetonitrile at 50°C under oxygen flow rate of 100 mL.min⁻¹.

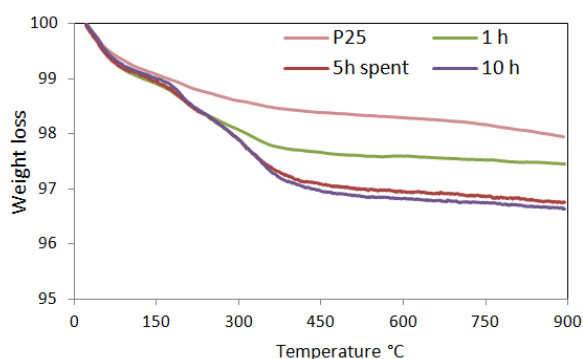


Figure II.11: TGA measurements of the P25 catalyst recovered after 1, 5 and 10 h of benzyl alcohol oxidation in acetonitrile at 50°C under oxygen.

The results show that, indeed, organic matter is present from 1 h of reaction and reaches its maximum amount around 5 h which corresponds roughly to the time when the conversion of the alcohol reaches its maximum value. We hypothesize that highly polar molecules such as benzoic acid remain adsorbed on P25. XRD measurements (Figure II.12) were also performed showing that the size of P25 particles did not change tremendously with time.

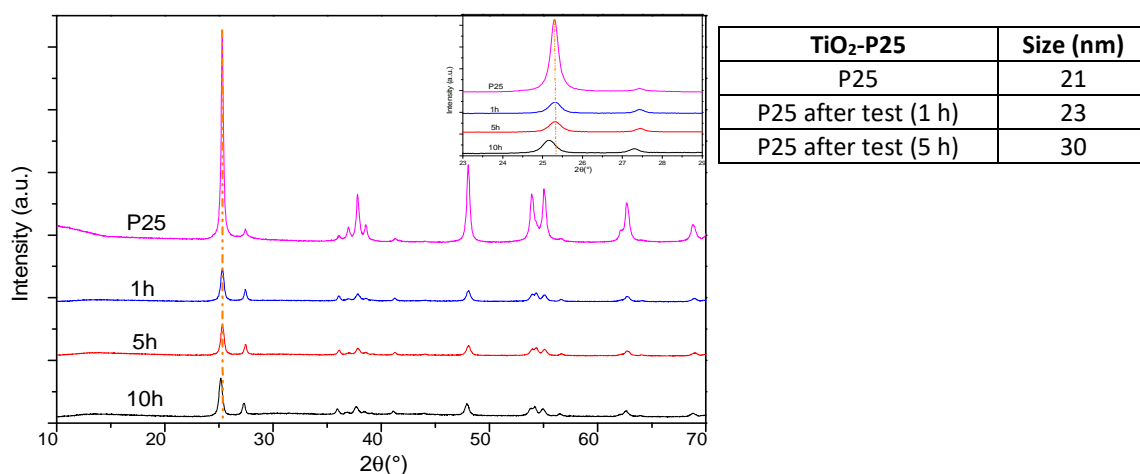


Figure II.12: XRD patterns for P25 after photo-oxidation of benzyl alcohol for different times (1, 5, 10 h).

Recyclability tests

The recyclability of P25 was investigated in the context of the photocatalytic oxidation of benzyl alcohol driven by ultraviolet light. The TiO₂ catalyst was recovered after 5 h either by filtration or centrifugation, then washed with acetonitrile, dried at 60°C and calcined at 300°C for 3 h. The purpose of this treatment was to eliminate the above-mentioned organic contaminants. In the first run, the conversion of benzyl alcohol was 60%. However, it was 54% in the second run, and only 30% after three runs. This sharp decrease in the catalytic activity in the recycling process of catalyst could be attributed to agglomeration of particles of catalysts.

If we now consider all the set of catalysts based on titanium dioxide, it appears that best results in terms of conversion and aldehyde selectivity were obtained for P25 (Table II.2, entry 3) and PC-500 (Table II.2, entry 6). Actually, both materials led to a benzaldehyde yield close to 60 %, but due to better aldehyde selectivity (92% for P25 and 83% for PC-500), P25 can be considered as the most active photocatalyst among those evaluated here. Interestingly, PC-500 (anatase, BET= 239 m².g⁻¹) provided the best benzyl alcohol conversion rate (71%), which could be attributed for its high surface area compared to P25 (50 m².g⁻¹). Better reactivity of P25 is often explained by a synergistic effect between the anatase and rutile [43-47]. A plausible explanation is that rutile plays a key role in separating electrons from holes. In fact, electrons obtained by the photoexcitation of rutile would migrate to the conduction band of anatase, then the holes would remain in the rutile phase, thereby, the recombination would be effectively suppressed as observed by Hurum *et al.* [48]. Pure anatase and pure rutile with different crystal sizes and specific surface areas were tested separately. The anatase phase (Table II.2, entry 4, 28 m².g⁻¹) turned out to be a more efficient catalyst than rutile (Table 2, entry 4, 7 m².g⁻¹). Indeed, the benzaldehyde yield for anatase (25%) was higher than with rutile (5%) but much lower than that obtained with P25 (Table II.2, entry 3, 50 m².g⁻¹) and PC500 (Table II.2, entry 6, 239 m².g⁻¹). Anatase was more efficient than rutile having low surface area too. This is usually explained by a conjunction between a higher fermi level, a lower rate of electron-hole recombination and a higher degree of hydroxylation of anatase [49]. Benzyl alcohol conversion with meso-TiO₂-S1 (Table II.2, entry 10) was only 30% with 96% benzaldehyde selectivity. For TiO₂ samples prepared by the sol gel method, either dried at 120°C (TiO₂(S-120)) or calcined at 350 or 450°C (TiO₂(S-350) and TiO₂(S-450)) (see Table II.2, entries 7-9), it was found that conversion dropped from 67 to 29% with the increase of the temperature treatment from 120 to 450°C while the selectivity increased sharply from 40 to 100% despite these materials have very similar physicochemical properties (specific surface area around 55 m².g⁻¹, pore volume about 0.2 cm³.g⁻¹ with a little change in crystallite size with range of 12.5-13.5 nm).

It has to be noted that Higashimoto *et al.* [41] reported higher photocatalytic performances than us in benzyl alcohol oxidation using an ultraviolet illuminated suspension of TiO₂ dispersed in acetonitrile. Benzyl alcohol conversion and benzaldehyde selectivity values were close to 100% within 1 h. Such differences are not simple to explain. They may be related to the crystal phase of their TiO₂ sample, ST-01, which was an anatase powder made of titania sulfonate displaying a very large surface area (320 m².g⁻¹) compared to P25 or PC500 considered here. Differences may be also due to the variation of the density of hydroxyl groups, in the particle size (*c.a.* 7 nm for ST-01 and 20 nm for P25 approximately), the preparation method and/or to the photo-intensity of the UV lamp employed. At least, the comparison between ST-01 (7 nm, 320 m².g⁻¹) and PC-500 in our case (6.3 nm, 239 m².g⁻¹) both made of anatase with similar particular sizes seems to emphasize that a larger surface area is beneficial for the photoactivity.

- **Other photocatalysts**

None of the other oxides tested (CeO₂, ZrO₂, CeO₂ (0.5%)-ZrO₂(0.5%) and ZnO, table II.2, entries 11-15) led to higher yields of benzaldehyde than TiO₂ P25 or PC-500. The low performance of these oxides is apparently more related to low conversion rates than aldehyde selectivity values. Indeed some of them, CeO₂-ZrO₂ (Ce : Zr=1 : 1 composition), CeO₂ and ZnO led to a benzaldehyde selectivity even better than that obtained with P25-TiO₂. Interestingly, ZrO₂-h prepared by hydrothermal method (Table II.2, entry 12, conv. 37 %, Sel. 84 %) displaying small sized nanocrystallites exhibited much higher activity than commercial ZrO₂ (Table II.2, entry 11, conv. 23%, Sel. 70%). Such improvement of the catalytic performance could be attributed to an increase in the surface area (see Table II.1, entries 10/11, 40 vs 16 m².g⁻¹) and/or nanoparticles crystallite size (see Table II.1, entries 10/11, 6 vs 22 nm).

III.3. Further studies with P25

- **Role of the solvent and of dioxygen**

Acetonitrile is a fairly widespread solvent for catalytic oxidation tests. This is related to its relatively high stability and that is the reason why, it was tested in the first part of this work. Acetonitrile is a by-product of the production of acrylonitrile, so the trend for acetonitrile production follows that of acrylonitrile. However, the demand for acrylonitrile has declined for the plastics and fiber industries leading to the lowering of its production. So, we considered that it was worth to test other solvents, including water for the photocatalytic oxidation of benzylalcohol in the presence of P25. Figure II.13 gathers the results obtained with hexane, ethylacetate, N,N-dimethylformamide (DMF), toluene, methanol and water as well as with two solvent mixtures : MeCN:H₂O (4:1) and iPrOH:H₂O (4:1). In all cases, it was first verified that problems of solubility did not arise in the benzylalcohol concentration domains tested. Dramatic influence of the solvents on benzyl alcohol oxidation could be emphasized.

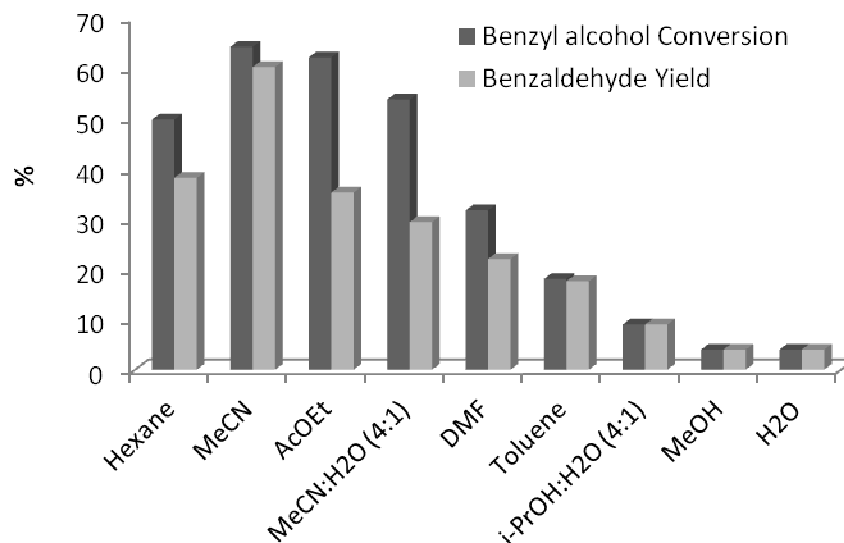


Figure II.13: Effect of solvents on the P25 photocatalyzed aerobic oxidation of benzyl alcohol under UV irradiation (Same conditions as in Table II.3).

Yields of benzaldehyde varied from 3 to 64%. Acetonitrile emerged as the best choice since leading to both rather high aldehyde selectivity value (94%) and alcohol conversion rate (64%). Acetonitrile was apparently not oxidized directly by the holes generated after UV photons like water which gives hydroxyl radicals generally considered to be the cause of non-selective oxidations. According to Table II.3, water as solvent gave 3% yield for benzaldehyde (against 60% for acetonitrile) due to the very low conversion rate of benzylalcohol. For a mixture of acetonitrile / water with a volumetric ratio of 4 / 1, the benzaldehyde selectivity decreased sharply with a value of 57%, which is much lower than with pure acetonitrile (94%). With other solvents such as toluene, hexane, ethyl acetate and DMF, the aldehyde yield values were in between 18 and 38%. The origins for these low yields are different. In the case of toluene, oxidation was very selective but the alcohol conversion was low. Perhaps the test should have been carried out over a longer period of time. In other cases, nor the conversion, nor the selectivity values were optimal, which makes it difficult to improve since the selectivity values were already low for moderate values of the conversion rates.

Table II.3: Effect of solvents on the P25 photocatalyzed aerobic oxidation of benzyl alcohol under UV irradiation^a

Entry	Solvent	Conv. (%)	Sel. (%) PhCHO	Yield (%) PhCHO
1	Acetonitrile	64	94	60
2	Methanol	4	100	4
3	Toluene	18	98	18

Entry	Solvent	Conv. (%)	Sel. (%) PhCHO	Yield (%) PhCHO
4	Hexane	50	76	38
5	Ethylacetate	62	57	35
6	DMF	32	69	22
7	Water [1,82]	3	100	3
8	Acetonitrile : water (4 : 1)	62	57	35
9	Isopropanol	9	100	9
10	Acetonitrile : water (4 : 1) and Cu ²⁺ ^b	14	100	14

^a Reaction conditions: substrate (2.9 mmol), solvent (40 mL), catalyst amount (60 mg), temperature (50°C), exposure time (4 h), O₂ flow (100 mL.min⁻¹), UV irradiance HPK 125 W.

^b [Cu²⁺] = 0.004 mmol L⁻¹.

Methanol (Table II.3, entry 2) and isopropanol (entry 9) seemed to compete with benzylalcohol, thus giving rise to virtually no conversion. Such results can be ascribed to the competitive adsorption of these alcohols on the TiO₂ surface, which blocks the adsorption sites for benzyl alcohol. Methanol, and more generally alcohols can be easily oxidized and are often used as holes scavengers [50-53].

In Figure II.14, we have tried to find some correlations between the conversion rates of benzyl alcohol and, either the solubility of dioxygen (A), or the values of the dielectric constant (B) or those of the polarity of the solvents (C). According to the graphs plotted, it is clear that no straight correlation appears with the polarity or the dielectric constant values. The factors determining the conversion rate seem to be rather complex.

Table II.4: Physicochemical properties of the solvents vs. P25 photo-assisted benzylalcohol oxidation under UV irradiation.^a

Entry	Solvent	O ₂ solubility ^{b,c}	Polarity (Debye)	Dielectric constant	Conv. (%) ^a	Sel. (%) PhCHO ^a	k, °OH, M ⁻¹ .s ⁻¹ ^d
1	Acetonitrile	8 mM [58] ^c	3.92	37.5	64	94	2.2 .10 ⁷
2	Methanol	4.15 .10 ⁻⁴	2.87	32.7	4	100	9.7 .10 ⁸
3	Toluene	9.81 .10 ⁻⁴	0.43	2.38	18	98	3 .10 ⁹
4	Hexane	2.05 .10 ⁻³	0	1.8	50	76	6.6 .10 ⁹
5	Ethylacetate	8.7 .10 ⁻⁴	1.88	6.02	62	57	4 .10 ⁸
6	DMF	3.89 .10 ⁻⁴	3.82	36.7	32	69	1.7 .10 ⁹
7	Isopropanol	7.82 .10 ⁻⁴	1.66	17.9	9	100	1.9 .10 ⁹
8	Water	0.29 .10 ⁻⁴	1.84	80.1	3	100	-

^a Reaction conditions: substrate (2.9 mmol), acetonitrile (40 mL), catalyst amount (60 mg), temperature (50°C), exposure time (4 h), O₂ flow (100 mL.min⁻¹), UV irradiance HPK 125 W. ^b Solubility of molecular oxygen in pure organic solvents at 298.2 K and 101.3 kPa measured using static method. Gas solubilities are expressed in terms of the Ostwald coefficient according to the following equation: $X_G = (RT / PV_L L + 1)^{-1}$ where R, T, P, and V_L are the gas constant, temperature, standard pressure, and molar volume of the solvent before gas dissolution, respectively. ^c Mole fraction solubility of dioxygen in alcohols at 101.325 kPa partial pressure $\times 10^4$) [54-56,58]. ^d Kinetic data for the °OH radicals in aqueous solution and rate constants obtained from this reference [57].

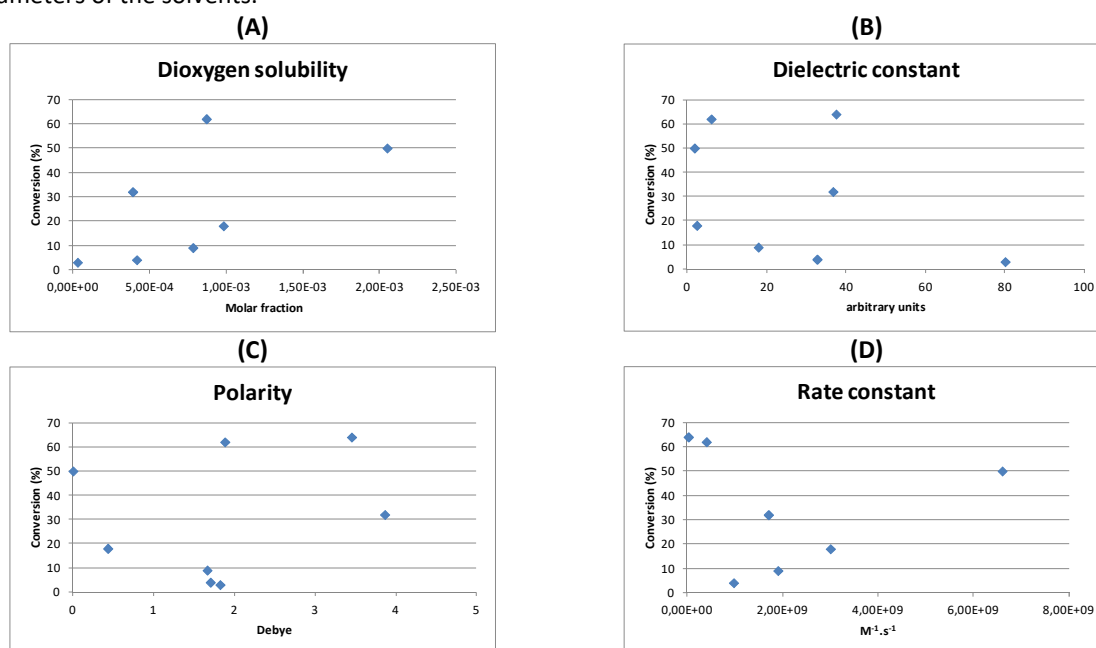
In fact, the best correlation was obtained with the solubility of dioxygen (Figure II.14A). In this case, it could be observed that the data are divided into two series:

- on one hand, water, methanol, isopropanol, toluene and hexane (series 1)
- on the other hand, DMF and ethyl acetate (series 2).

for which the conversion values increase with the solubility of O_2 . However, conversion values of the series 2, are much higher than those of the series 1. Hence, the use of DMF leads to a conversion of 32% when methanol leads to 4% whereas these two solvents are characterized by close values of O_2 solubilities ($3.89 \cdot 10^{-4}$ for DMF and $4.15 \cdot 10^{-4}$ for MeOH). The same is true for ethyl acetate (series 2, $8.7 \cdot 10^{-4}$) and isopropanol (series 1, $7.82 \cdot 10^{-4}$) which lead respectively to 62 and 9% of benzylalcohol conversion. A priori, solvents of the series 2 come less in competition with the oxidation of benzylalcohol than those of the series 1. Dioxygen is an electron acceptor that prevents the recombination holes and electrons. If primary reaction of O_2 with electrons reaching the surface is not favored due to the low concentration of O_2 close to the TiO_2 surface, electrons will recombine with holes.

The classification in these same two series of solvents is also effective when the evolution of the degree of conversion of benzyl alcohol is plotted as a function of the rate constant values of the reaction of OH radicals with the solvent. In the series 1, the higher, the rate of reaction of the solvent with the hydroxyl radicals, the higher, the conversion of benzyl alcohol. For series 2, the opposite is true. The best conversion rates are obtained for the solvents which react least easily with the HO radicals.

Figure II.14: Attempt of correlations between benzylalcohol conversion rates with the physicochemical parameters of the solvents.



Water, acetonitrile and methanol have also been compared by other groups. According to literature [58-60], dioxygen solubility values in water, acetonitrile and methanol are 1, 8.1, and 9.4 mM at room temperature. Exploiting the *in situ* EPR spin trapping technique, Dvoranová *et al.* [60] have shown that the increased solubility of molecular oxygen plays an important role in the photo-oxidation processes together with the stabilization effect of the aprotic solvents on the superoxide radical anions. More precisely, it was emphasized that the spin-adduct ${}^{\bullet}\text{DMPO-O}_2^-$ was dominating the EPR spectrum in CH_3CN . The use of dried CH_3CN solvent indicated that the hydroxyl radicals are generated by the oxidation of $\text{OH}^-/\text{H}_2\text{O}$ adsorbed on the TiO_2 surface via the photogenerated holes. A lower reactivity of the photogenerated hydroxyl radicals towards acetonitrile (Table II.4, entry 1) allowed the hydroxyl radicals to be trapped by DMPO giving rise to ${}^{\bullet}\text{DMPO-OH}$. However for methanol, which is well known as an efficient scavenger of photogenerated holes, it was found that radical intermediates *i.e.* $\text{O}_2^{\bullet-}$ and ${}^{\bullet}\text{OCH}_3$ could be detected after the reaction of electrons with O_2 and holes with CH_3OH . The latter are produced from the interaction of electrons and holes with O_2 and methanol, respectively.

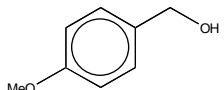
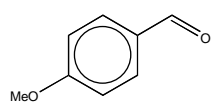
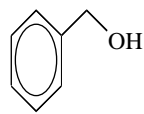
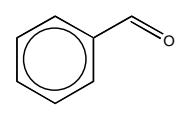
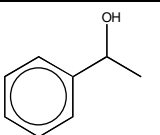
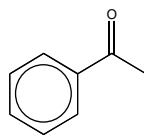
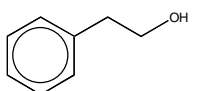
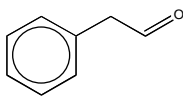
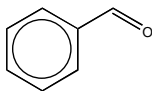
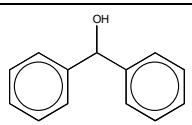
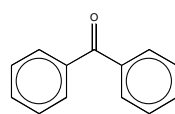
One additional test consisting in the introduction of oxidizing species (Cu^{2+}) was carried out in water : acetonitrile (1:4 v/v). The results are reported in Table II.3 (entry 10). Cu^{2+} ions are often introduced because they can be reduced (in Cu^+) in competition with dioxygen by the photogenerated electrons lowering their participation in the global process but also the hole/electron recombination [61,62]. This addition was performed in the case of the reaction carried out in acetonitrile / water for reasons of solubility and using the optimum concentration recommended in the literature [62]. Here, the addition of copper salt resulted in a significant decrease in the conversion of benzyl alcohol but benzaldehyde selectivity increased. The conversion of benzylalcohol fell from 62% (Table II.3, entry 8) to 14% (Table II.3, entry 10), whereas the benzaldehyde selectivity increased sharply from 57 to 100%. Such results suggest that superoxides initially produced by the reduction of O_2 have a beneficial effect from the point of view of conversion but unfavorable from the point of view of the selectivity.

- **Other substrates**

Other aromatic alcohols were tested in the presence of P25 in acetonitrile at 50°C under UV irradiance (see Table II.5). Very good results have been obtained with 4-methoxy benzyl alcohol (Table II.5, entry 1) since the p-anisaldehyde yield approached 99%. The difference in reactivity between benzyl alcohol and 4-methoxy benzyl alcohol is *a priori* related to the mesomer donor effect of the methoxy substituent in the para position of the $-\text{CH}_2\text{OH}$ group to be oxidized in 4-methoxy benzyl alcohol. This seems to indicate that the oxidizing species have a marked electrophilic character, hence explaining their sensitivity to the electron density of the substrate. These results

also support that positive charge or a radical cation intermediate could be formed in the transition state of the rate determining step which is better stabilized by an electron donating substitute. Hogashimoto *et al.* [63] have tried to draw a relationship between the photocatalytic activities and the oxidative potentials of benzylic alcohols. They did also a comparison between 4-methoxy benzyl alcohol and benzyl alcohol. Measuring cyclic voltammograms in the range of 0-3.0 V vs. SCE in the dark, they found that benzyl alcohol, exhibits an irreversible curve. First oxidative potential (E_p) of benzyl alcohol was at *c.a.* +2.16 V, whereas it was at 1.66 V for 4-methoxy benzyl alcohol. Such observations are in agreement with the easier one-electron oxidation of 4-methoxy benzyl alcohol.

Table II.5: Results of the photocatalyzed aerobic oxidation tests of benzyl alcohol derivatives in acetonitrile under UV irradiance.^a

Entry	Substrate	Conv. (%)	Product desired	Sel. (%) PhCHO
1	 4-methoxy benzyl alcohol	99		99
2		64		94
3	 1-phenyl ethanol	52		98
4	 2-phenyl ethanol	30		15
				84
5	 diphénylméthanol	10		93

^a Reaction conditions: substrate (2.9 mmol), acetonitrile (40 mL), catalyst amount (60 mg), temperature (50°C), exposure time (4 h), O₂ flow (100 mL.min⁻¹), UV irradiance HPK 125 W.

An autocatalytic role of 4-methoxy benzyl alcohol was previously described by Palmisano *et al* [64] in the sense that the photo-oxidation of this specific electron-enriched alcohol worked in aqueous medium under UV, in the presence of O₂ and in the absence of TiO₂. In our case, we checked that, using acetonitrile as a solvent, no autocatalysis could be detected.

Another primary alcohol, 2-phenyl ethanol (Table II.5, entry 4), whose OH group is no longer located at the benzylic position was tested too. The latter, which is less activated than benzyl alcohol, was converted at a rate of 30% over 4 h giving rise, predominantly and surprisingly, to benzaldehyde with a selectivity of 85%; the other product formed being 2-phenyl acetaldehyde (15%). In fact, benzaldehyde originates from the cleavage of the C-C bond between the carbon atoms of the carbonyl function and of the neighbor CH₂. We verified this by carrying out a control test starting with phenyl acetaldehyde. Almost 95% of this compound was then converted to benzaldehyde.

Two other compounds derived more directly from benzyl alcohol since resulting from the substitution of the aldehydic CH bond by a C-CH₃ bond (case of 1-phenyl ethanol, Table II.5, entry 3) or by a C-phenyl bond (case of diphenylmethanol, Table II.5, entry 5) were also tested. Resulting compounds are secondary alcohols and, ketones were expected to be formed. Hence, 1-phenyl ethanol (entry 3) was transformed with moderate conversion (52%) mainly to acetophenone (selectivity of 98%) whereas, only 10% of diphenyl methanol (entry 5) was oxidized to benzophenone (selectivity of 93%). Undeniably, secondary alcohols derived from benzyl alcohol are oxidized with more difficulty than the latter. The increasing difficulty from benzyl alcohol to diphenyl methanol could be explained by a reduced oxidability (increase in the redox potential for ROH⁺ / ROH) or by a more pronounced steric hindrance in the vicinity of the TiO₂ surface.

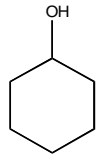
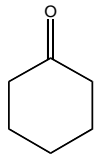
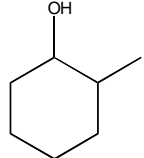
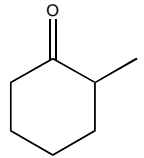
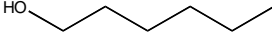
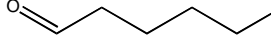
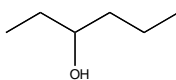
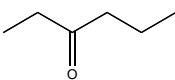
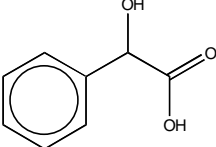
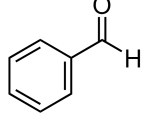
The photocatalytic aerobic oxidation of aliphatic alcohols was also tested under UV light irradiance in acetonitrile (see Table II.6). We chose four substrates: two cyclic alcohols, *i.e.* cyclohexanol and 2-methylcyclohexanol and two alcohols in the form of open chains, *i.e.* 1- and 3-hexanols.

Overall, the results in terms of yield of carbonyl derivatives produced are lower than in the previous series, hence reflecting the lower conversion values obtained. With the exception of cyclohexanol (entry 1), the selectivities are quite good but the formation of heavy by-products, not detected by gas chromatography, cannot be excluded. Cyclohexanol was converted predominantly to cyclohexanone (yield close to 70%). Adipic acid is one of the possible co-products difficult to be analyzed that may arise from the cleavage of the ring. In our conditions, it is worthy to note that the yield of cyclohexanone was higher than in the test performed by Omima *et al.* (45%) in acetonitrile too [12], maybe as the result of shorter irradiance time or of the choice of the lamp (450 W medium pressure mercury lamp in their case).

In the case of 2-methylcyclohexanone (entry 2), the addition of a methyl substituent in the alpha position of the alcohol function has a negative impact on the reactivity of the alcohol since the yield of the carbonyl derivative dropped to around 30%. In this case, the ketone selectivity was particularly high. It seems that the over-oxidation was limited. This can be interpreted by a great difficulty for the

reagents and the products to remain fixed to the surface due to problems of steric hindrance. The donor inductive electron effect of the methyl group is not involved here.

Table II.6: Results of the photocatalytic aerobic oxidation tests of aliphatic alcohols and the oxidative cleavage of C-C bonds.^a

Entry	Substrate	Conv. (%)	Product	Sel. (%)
1		84		85
2		28		99
3		33		95
4		14		98
5 ^b		90		93

^a Reaction conditions: substrate (2.9 mmol), acetonitrile (40 mL), catalyst amount (60 mg), temperature (50°C), exposure time (4 h), O₂ flow (100 mL.min⁻¹), UV irradiance HPK 125 W. ^b Illumination was carried out for 2 h under same conditions.

In the series of open chained alcohol molecules, 1-hexanol (entry 3) gave 33% conversion and selectivity in hexanal was 98% (yield = 32%), whereas, 3-hexanol (entry 4) was selectively (98%) converted to 3-hexanone at 14% conversion rate and (yield = *c.a.* 14%).

The Mandelic acid were tested under the same conditions as benzyl alcohol were readily cleaved allowing the access to benzaldehyde (major compound) and benzoic acid. Interestingly that mandelic acid was selectively oxidized after 2 hr to benzaldehyde at conversion of (90%) with greater selectivity of 93%, while for 5hrs irradiation, the conversion slightly increased (>99%), this could be relied for successive reaction leading for formation of benzoic acid and CO₂.

IV. Conclusion

This study has emphasized the potential of UV-assisted photocatalysis in acetonitrile for the selective oxidation of alcohols as well as the oxidative cleavage of activated C-C bonds in two substrates: 2-phenyl ethanol and mandelic acid.

Benzyl alcohol, used as a reference, was oxidized mainly into benzaldehyde in the presence of P25-TiO₂ and PC-500 but P25 led to a better aldehyde selectivity. The maximum yield of benzaldehyde obtained in this study was *c.a.* 60%. The results with P25 are particularly interesting. They are more particularly related to the composition (mixture of rutile and anatase) rather than to the surface properties of this material since the value of its specific surface area is low compared to that of PC500 and to the different forms of TiO₂ anatase prepared here.

Unfortunately, the conversion of benzyl alcohol appears to be limited in time. It seems that the catalyst is deactivated. We have evidenced the presence of an organic deposit on P25-TiO₂ very early in the reaction. However, it has not hitherto been possible to recover the reactivity of the catalyst after heat treatment.

Tests of different solvents has highlighted the superiority of acetonitrile and the importance of acetonitrile's ability to solubilize O₂, thus emphasizing the role of dioxygen in the whole oxidation process. Other substrates were tested under the best defined conditions for benzyl alcohol. In general, substrates with activated alcohol functions, for example in the benzylic position, have given good results but always with the limitation in terms of the amount converted, except in the case of 4-methoxybenzyl alcohol. Aliphatic alcohols that are more difficult to activate have also been tested. Of these, cyclohexanol yielded cyclohexanone in a yield of about 70%.

References

- [1] R. A. Sheldon, J. K. Kochi, *Metal-Catalyzed Oxidations of Organic Compounds*, Academic Press, New York, 1981.
- [2] C. L. Hill, *Advances in Oxygenated Processes*, ed. A. L. Baumstark, JAI Press, London, 1 (1988) 1.
- [3] M. Hudlucky, *Oxidations in Organic Chemistry*, ACS Monograph Series, American Chemical Society, Washington, DC, 1990.
- [4] *Comprehensive Organic Synthesis*, ed. B. M. Trost and I. Fleming, Pergamon Press, Oxford, U.K., 1991.
- [5] J. A. B. Satrio, L.K. Doraiswamy, *Chem. Eng. J.*, 82 (2001) 43.
- [7] J. LV, Y. Shen, L. Peng, X. Guo, W. Ding, *Chem. Commun.*, 46 (2010) 5909.
- [8] G. Cainelli, G. Cardillo, *Chromium Oxidants in Organic Chemistry*, Springer, Berlin, 1984.
- [9] D. G. Lee, U.A. Spitzer, *J. Org. Chem.*, 35 (1970) 3589.
- [10] A. Costine, B. K. Hodnett, *Applied Catalysis A: General*, 290 (2005) 9.
- [11] G. Palmisano, S. Yurdakal, V. Augugliaro, V. Loddo, L. Palmisano, *Adv. Synth. Catal.*, 349 (2007) 964.
- [12] O. S. Mohamed, S. A. Ahmed, M. F. Mostafa, M. A. Abdel-Wahab, *J. Photochem. Photobiol., A: Chemistry*, 200 (2008) 209.
- [13] S. Higashimoto, N. Suetsugu, M. Azuma, H. Ohue, Y. J. Sakata, *Catal.*, 274 (2010)76.
- [14] S. Furukawa, T. Shishido, K. Teramura, T. Tanaka, *ACS Catal.*, 2 (2012) 175.

- [15] A. Fujishima, K. Honda, *Nature*, 238 (1972) 37.
- [16] C. C. Cheng, W. H. Ma, J. C. Zhao, *Chem. Soc. Rev.*, 39 (2010) 4206.
- [17] A. Kudo, Y. Miseki, *Chem. Soc. Rev.* 38 (2009) 253.
- [18] M. Zhang, Q. Wang, C. C. Chen, L. Zang, W. H. Ma, J. C. Zhao, *Angew. Chem., Int. Ed.*, 48 (2009) 6081.
- [19] X. J. Lang, H. W. Ji, C. C. Chen, W. H. Ma, J. C. Zhao, *Angew. Chem., Int. Ed.*, 50 (2011) 3934.
- [20] T. Shishido, T. Miyatake, K. Teramura, Y. Hitomi, H. Yamashita, T. Tanaka, *J. Phys. Chem. C.*, 113 (2009) 18713.
- [21] Y. Noda, B. J. Lee, K. Domen, J. N. Kondo, *Chem. Mater.*, 20 (2008) 5361.
- [22] J. N. Kondo, K. Domen, *Chem. Mater.*, 20 (2008) 835.
- [23] T. Katou, B. J. Lee, D. L. Lu, J. N. Kondo, M. Hara, K. Domen, *Angew. Chem., Int. Ed.*, 42 (2003) 2382.
- [24] X. Y. Chen, T. Yua, X. X. Fan, H. T. Zhang, Z. S. Li, J. H. Ye, Z. G. Zou, *Appl. Surf. Sci.*, 253 (2007) 8500.
- [25] E. E. Ferapontova, J. Castillo, L. Gorton. *BBA, Biochimica et Biophysica Acta*, 1760 (2006) 1343.
- [26] W. P. Zeng, X. H. Li, J. Du, J. M. Li, P. Zhang, C. W. Hu, X.G. Meng, *Acta Chim. Sinica*, 68 (2010) 27.
- [27] B. Liu, X. G. Meng, W. Y. Li, L. C. Zhou, C. W. Hu, *J. Phys. Chem. A*, 116 (2012) 2920.
- [28] W. F. Yu, X. G. Meng, X. Peng, X. H. Li, Y. Liu, *J. Mol. Catalysis A: Chemical*, 379 (2013) 315.
- [29] O. S. Mohamed, S. Ahmed, M.F. Mostafa, A. Abdel-Wahab, *International Journal of Photoenergy*, 11 pages, 2008.
- [30] F. H. Hussein, G. Pattenden, R. Rudham, J. J. Russell, *Tetrahedron Letter*, 25 (1984) 3363.
- [31] N. Gupta, P. Bansal, B. Pal, *J. Experim. Nanoscience*, 10 (2013) 148.
- [32] S. Nishimoto, B. Ohtani, T. Kagiya, *J. Chem. Soc. Faraday Trans.*, 81 (1985) 2467.
- [33] P. Du, J.A. Moulijn, G. Mul, *J. Catal.*, 238 (2006) 342.
- [34] B. Srinivas, K. Lalitha, P. A. Kumar, R.G. Rajesh, V. D. Kumari, M. Subrahmanyam, B. R. De, *Res. Chem. Intermed.*, 37 (2011) 1069.
- [35] D. Zhao, J. Sun, Q. Li, G.D. Stucky, *Chem Mater*, 12 (2000) 275.
- [36] Z. Zhang, F. Zuo, P. Feng, *J. Mater. Chem.*, 20 (2010) 2206.
- [37] R. S. Sabry, Y. K. Al-Haidarie, M. A. Kudhier, *J. Sol-Gel. Sci. Technol.*, 78 (2016) 299.
- [38] K. Anandan, V. Rajendran, *Journal of Physical Sciences*, 17 (2013) 179.
- [39] A. Kaushal, D. Kaur, *J. Alloys Compd.* 509 (2011) 200.
- [40] K.G. Chandrappa, T. V. Venkatesha, K. Vathsala, C. Shivakumara, *J. Nanopart. Res.* 12 (2010) 2667.
- [41] S. Higashimoto, N. Kitao, N. Yoshida, T. Sakura, M. Azuma, H. Ohue, Y. Sakata, *J. Catal.*, 266 (2009) 279.
- [42] C. J. Pouchert (Ed.), *the Aldrich Library of FT-IR Spectra*, Aldrich Chemical Company Inc., (1985) 1121.
- [43] T. Ohno, K. Sarukawa, K. Tokieda, M. Matsumura, *J. Catal.*, 203 (2001) 82.
- [44] R. I. Bickley, T. Gonzalezcarreno, J. S. Lees, L. Palmisano, R. J. D. J Tilley, *Solid State Chem.*, 92 (1991) 178.
- [45] R. Amal, Y. K. Kho, A. Iwase, W. Y. Teoh, L. Madler, A. J. Kudo, *Phys. Chem. C*, 114 (2010) 2821.
- [46] G. Li, C. P. Richter, R. L. Milot, L. Cai, C. A. Schmuttenmaer, R. H. Crabtree, G. W. Brudvig, V. S. Batista, *Dalton Trans.*, (2009) 10078.
- [47] G. H. Li, S. Ciston, Z. V. Saponjic, L. Chen, N. M. Dimitrijevic, T. Rajh, K. A. J. Gray, *Catal.*, 253 (2008) 105.
- [48] D. C. Hurum, A. G. Agrios, K. A. Gray, T. Rajh, M. C. J. Thurnauer, *Phys. Chem. B*, 107 (2003) 4545.
- [49] O. Carp, C. L. Huisman, A. Reller, *Prog. Solid State. Chem.*, 32 (2004) 33.
- [50] A. N. Ökte, M.S. Resat, *Yüksel Inel Toxicological & Environmental Chemistry* 79 (2001) 3.
- [51] J. Ma, E. Valenzuela, A. S. Gago, J. Rousseau, A. Habrioux, N. Alonso-Vante, *J. Phys. Chem. C*, 118 (2014) 1111.
- [52] B. V. Bogaert, D. Havaux, K. Binnemans, T. Van Gerven, *Green Chem.*, 17(2015) 2180.
- [53] T. Mishara, J. Hait, N. Aman, R.K Jana, S. Chakravarty, J., *Colloid and Interface science*, 316 (2007) 80.
- [54] S. Takashi, H. Yuzo, S. Masaru, A. Sadao, Y. Hideki, *Ind. Eng. Chem. Res.*, 53 (2014) 19331.
- [55] R. Battlno, T. R. Rettich, T. Tominaga, *Journal of Physical and Chemical Reference Data* 12, 2 (1983) 163.
- [56] D. Dvoranová, Z. Barbieriková, and V. Brezová, *Molecules*, 19 (2014) 17279.
- [57] G. Buxton, C. Greenstock, W. Helman, A.B. Ross, *J. Phys. Chem. Ref. Data*, 17 (1988) 513.
- [58] J. Wadhawan, P. Welford, H. McPeak, C. Hahn, R. Compton, *The. Sensor. Actuat. B*, 88 (2003) 40.
- [59] N.J. Turro, V. Ramamurthy, J.C. Scaiano, *Modern Molecular Photochemistry of Organic Molecules*, University Science Books: Sausalito, CA, USA, (2010) 1008.
- [60] I. Golovanov, S. Zhenodarova, *J. Russ. Gen. Chem.*, 75 (2005) 1795.
- [61] M. I. Litter, *Appl. Catal. B*, 23 (1999) 89.
- [62] S. Chen, Y.Z. Liu, *Chemosphere*, 67 (2007) 1010.
- [63] S. Higashimoto, N. Suetsugu, M. Azuma, H. Ohue, Y. Sakat, *J. Catal.*, 274 (2010) 76.
- [64] G. Palmisano, G. Scandura, V. Augugliaro, V. Loddo, A. Pace, B. S. Tek, S. Yurdakal, L. Palmisano, *J. Molecular Cata. A: Chemical*, 403 (2015) 37.

Part II

New photocatalysts for alcohol oxidation based on the deposition of stable TiO₂ colloids onto mesoporous silica

Chapter 3: Bibliographical survey

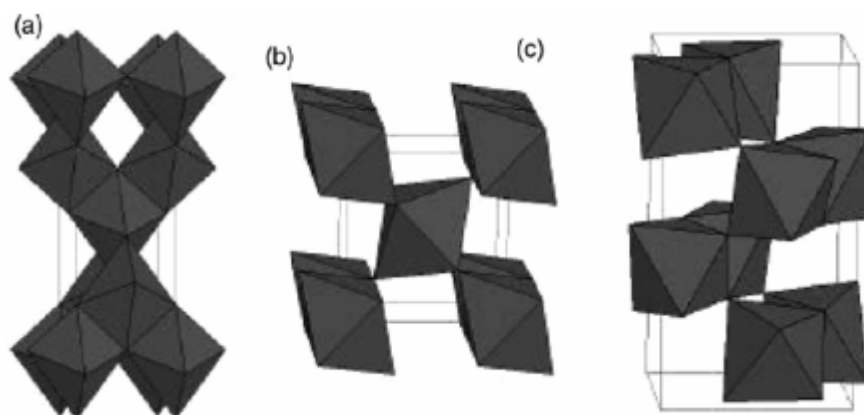
Chapter 4: Experimental results

Synthesis, characterization and use of TiO₂ nanoparticles in photocatalysis

I. Introduction

In different areas of research, and especially in catalysis, there is a strong interest in the synthesis of calibrated nanoparticles (NPs) because such dimension scale affords particular material properties and surface activities that are different from the bulk counterpart. Preparations of NPs suspensions in liquids, also called colloidal suspensions, are particularly interesting due to a very good size, and sometimes morphological, control. Various preparation routes are available and the physical/chemical properties of the resulting nano-objects are extensively studied and characterized. The nanoparticles of interest for catalytic applications can be metallic or in the form of oxides or sulphides.

Here we will focus our attention on titanium dioxide (TiO₂). TiO₂ NPs are particularly important for photocatalysis applications. Herein, this introductory chapter describes what TiO₂ NPs/colloids are as well as their functional advantages. More precisely, we focus on synthesis approaches, phase behavior and surface properties of TiO₂ NPs/colloidal particles as a function of their preparation route. It is known that titanium dioxide can crystallize according to four different structures: anatase, rutile, brookite (Scheme III.1) and TiO₂(B) (monoclinic). In anatase, TiO₆ octahedra share four edges, in rutile, two edges, and in brookite, three edges [1,2]. For TiO₂(B), the fundamental building block is similar to the anatase one, with four octahedra sharing edges. It is also known that the stability of these materials may depend on their particle size. Rutile is the thermodynamically stable form of bulk titania, but anatase is the most stable phase for sizes below 14 nm, whereas, brookite and TiO₂(B) are metastable forms that are not observed in minerals and difficult to synthesize in pure form.



Scheme III.1: Connectivity of TiO₆ octahedral units in (a) anatase, (b) rutile, and (c) brookite [2].

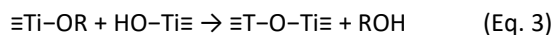
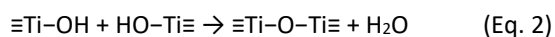
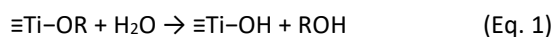
Controlling the morphology of titania nanoparticles may have important effects on the adsorption of molecules and the rate of electron transfer at the particle surface. We will see that spindles, rods, spheres, tetragonal bipyramids, hexagonal nanocrystals, octahedral cages and nanotubes with particle size control can be prepared. Sol gel method is the most used technique to prepare TiO₂ NPs with controlled size and well defined shapes but hydrothermal, solvothermal, surfactant assisted and template methods are also available.

Colloidal particles of titania have been little used in photocatalysis essentially due to their difficult recovery. Another possible exploitation of their well-controlled size (and morphology) consists in their deposition onto UV transparent supports (silica, for example). We will focus a part of this literature survey on methods using pre-formed colloids and pay attention to alternate ways that can be envisaged to control the dispersion.

II. Synthetic routes of colloidal TiO₂ nanoparticles

II.1. Generalities on hydrolysis and condensation of Titania precursors

Sol-gel, hydrothermal, surfactant-assisted solvothermal processes, and templated approaches are the main synthetic techniques used to prepare titania nanoparticles with controlled properties in the nanoscale regime. Some examples are presented in Table III.1 with information dealing with the morphological structures obtained. It can be deduced that various titanium precursors can be used such as halides (TiX₄), salts (TiOSO₄) and alkoxides (Ti(OR)₄). But, the most used ones are titanium alkoxides such as TTIP (R = -CH(CH₃)₂), titanium butoxide (R = -CH₂CH₂CH₂CH₃) and titanium *tert*-butoxide [R = C(CH₃)₃]. All of these compounds are very reactive materials due to the Lewis acidity of the Ti(IV) center. This makes Ti very susceptible to nucleophilic attack, as example from water molecules followed by proton transfer from the water molecule to a coordinating group during a transition state. Then, final removal of the protonated ligand in the form of an alcohol molecule occurs giving rise to the fully hydrolyzed product, Ti(OH)₄. It is worthy noted that the main problems faced in sol-gel process is the proper control of the hydrolysis and condensation rates of titanium precursors, which are too fast because of the presence of water and catalysts in solution. To overcome this problem, it is possible to modify the precursor by extra ligands, for exemple acetylacetonate, that reduces the hydrolysis rate. More generally, the hydrolysis step of a metal complex results in the formation of another metal complex including water in the form of aqua, hydroxo, or oxo ligands, depending on the metal cation and the reaction conditions (Eq. 1). Then, the condensation step (oxolation) is the reaction between two (or more) of the formed complexes to give, here Ti-O-Ti bonds, which are the precursors of the final oxide network (Eq. 2/3) [3,4].



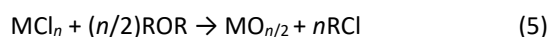
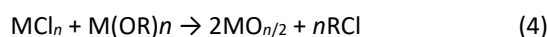
The coordination number of the Ti center in alkoxides is 4, and easily expanded to 6 via the formation of complexes or oxo bridges. Furthermore, TiX_4 and alkoxides, in a lesser extent, are very sensitive for humidity and should be handled carefully to avoid premature hydrolysis. Interestingly, alkoxy groups can be easily replaced by β -diketonates, carboxylic acids, amines, or other organic groups such as cyclooctatetraene, resulting in the formation of complexes whose reactivity can be better controlled. In parallel, these modified precursors can show different reactivities allowing the formation of different phases by guiding the bonding of the octahedral TiO_6 units in a different way compared to the parent alkoxides.

Atrane compounds which are metal precursors formed by the complexation of the metal or semi-metal with triethanolamine have also been used. In this case, triethanolamine acts as a chelating ligand with three alkoxy groups coordinated to the central Ti atom completed by a transannular N-Ti bond. Such compound is very stable toward hydrolysis. Furthermore, the ability of triethanolamine to chelate with the titanium center helps to displace ligands in titanium precursors, such as alkoxide groups, halides, and amides [5-10]. Titanium sulfate $[\text{Ti}(\text{SO}_4)_2]$ was also used as a particularly water-soluble precursor which allowed the formation of the three titania polymorphs under hydrothermal conditions, with a preference for anatase. Complexation with oxalate produces rutile powders at room temperature or brookite by decomposition at 300°C . Titanium oxysulfate (TiOSO_4) has been shown to produce pure anatase powders by precipitation at pH 4-6 with NaOH [11,12].

In the sol gel procedure, it is known that the rate of hydrolysis is increased under acidic conditions. Indeed, protons react with alkoxy groups and favor the nucleophilic attack of H_2O . In basic medium, the hydrolysis steps get progressively faster than the condensation step affording $(\text{OH})_3\text{Si-O-Si}(\text{OH})_3$ giving rise to small and highly branched agglomerates [13]. Regarding halides, it was demonstrated that TiF_4 is a relatively stable compound that can be handled under standard conditions. On the other hand, TiCl_4 , which is widely used for titania synthesis in sol-gel and hydrothermal techniques, easily undergoes hydrolysis with water, forming titanium chlorohydroxy complexes and titanium hydroxide and then releasing HCl. In sol-gel process, a metal alkoxide or inorganic salt is hydrolyzed and then condensation reaction occurs to form colloidal or polymeric sols. Usually, the colloidal route is based on the formation of well-defined particles in aqueous media, where the particles are prevented from agglomeration by mutual repulsion of similar charges at the particle surface. The rapid condensation reaction in the colloidal sol route causes growth and/or the formation of precipitates. Hence,

colloidal sols can be obtained by the control of reaction conditions and/or the peptization of the precipitate by adding acid. In the polymeric route, metal-organic precursors react in alcoholic media where the polymeric particles remain separated because of their small size. In this route, the hydrolysis reaction is slower and is typically achieved by adding a small amount of water, resulting in a partially hydrolyzed alkoxide leading to the formation of a linear inorganic polymer. Experimental parameters such as the hydrolysis ratio of $h = n\text{H}_2\text{O}/n$ alkoxide and the nature of the alkoxy groups are important factors influencing the kinetics of the hydrolysis and condensation reactions for preparation of colloidal suspensions. Here, a stable suspension of Ti clusters can be obtained by hydrolysis of TTIP under low hydrolysis ratios ($h < 1$). However, if ($h > 1.5$), the hydrolysis of TTIP does not result in a stable solution of polyalkoxide, but results in precipitation of titanium dioxide particles. The precipitation takes place after an induction period in which slow particle growths is observed followed by rapid precipitation. The presence and size evolution of nanoparticles (1.5 - 6 nm) in the induction period has been studied by dynamic light scattering (DLS) [14-16]. DLS investigation provides valuable information of the particle size of the titanium clusters present during the time scale of the induction period. Thus, identification of the titanium clusters present during the induction period of titanium alkoxide is of great interest, as the nature of these clusters may determine the properties of the final product. It is known that high crystallinity is obtained upon annealing the materials at temperatures *c.a.* 350°C or higher. For this reason, there is a great challenge to synthesize crystalline TiO₂ nanoscale materials without annealing stage using low-temperature methods. Such an approach allows to drive functional and structural modification with high crystalline phase of NPs at low temperatures lower than 90 °C, which is economically important.

TiCl₄ is also suitable for the following reactions because chloride is a good leaving group in nucleophilic substitution-type reactions. Therefore, two main reactions can produce titania from nonhydrolytic cleavage of the Ti-X bond: i) the alkoxide route and ii) the ether route.



Both reactions are very slow at room temperature, and generally temperatures between 70 and 120°C are required to obtain reasonable rates and crystalline products. NMR studies revealed that numerous reactions are involved, with an initial redistribution of the ligands around the titanium centers and the formation of intermediate oxochloro alkoxides that autocatalyze the reaction. Furthermore, the ether route was found to lead to a faster formation of the gel compared to the alkoxide route [17].

Table III.1: TiO₂ nanoparticles or colloids synthesized under different conditions

Entry	Ti precursor ^a	Surfactant or additives used ^b	NPs morphology	Crystalline phase ^c	Preparation method	Ref.
1	TiCl ₄	HCl, Na ₂ SO ₄	Micrometer-size spheres	R or A+ R	Sol gel	[18]
2	TTIP	NaCl	Sphere	A		[19]
3	TTIP	HCl	Sphere	R or A		[20]
4	Titanium butoxide	HNO ₃ or HCl	Micrometer-size spheres	A		[21]
5	Acetylacetonemodified TTIP	F127-CTAB	Sphere	A		[23,24]
6	Titanium ethoxide	Salts and polymer	Micrometer-size porous +nonporous spheres	amorphous		[25]
7	Acetylacetonemodified TTIP	p-toluenesulfonic acid	Spheres	A		[22]
8	TiOSO ₄	OH ⁻	(spindles) large rods	B		[31]
9	Titanium glycolate	ammonia	irregular	B		[32,33]
10	Titania powder (rutile)	Na ⁺	Nanotubes	titanate		[20,21]
11	TTIP	Oleic acid	Irregular spheres+ small rods	A	Solvothermal	[36]
12	Titanium butoxide	Oleic acid + NaF	Tetragonal bipyramids	A		[37]
13	TiCl ₄	Oleic acid+ oleylamine	Small rods	A	Surfactant-Assisted	[42]
14	TTIP	Tetraalkylammonium cations	Nanorods;hexagonal nanocrystals	A		[43]
15	Ti(COT) ₂	TBPO + TOPO	Spherical	B		[41]
16	TiF ₄	Cu ₂ O templates	Octahedral cages	A	Templated method	[44]
17	Titanium butoxide	Polystyrene spheres	Hollow spheres	A		[45]
18	TiCl ₄	Mesoporous silica	Small particles	A		[46]

^a TTIP: titanium isopropoxide, (COT): cyclooctatetraene

^b CTAB: cetyltrimethylammonium bromide, F127: TBPO tributylphosphine oxide , TOPO trioctylphosphine oxide

^c A: anatase, B :brookite, R: rutile

TiF₄ has been much less used in titania nanocrystals synthesis. Among the examples, we can cite the preparation of anatase titania particles with exposed {001} facets of high-energy. These facets, which represent a small percentage of the entire exposed surface in the most thermodynamically stable morphology of anatase, have been suggested as potentially more reactive than the {101} facets that usually dominate in anatase nanocrystals. It has been found that fluoride can strongly bind the {001} facets at the exposed 5-fold coordinated Ti cations (Table III.1, entry 1,2,3), reducing their surface energy and allowing growth to occur on the {101} facets [18-20].

II.2. Main preparation methods

- Sol-gel pathway

Matijević *et al.* [18] described the preparation of uniform titania spheres by hydrolysis of TiCl₄ contains Na₂SO₄ in highly acidic HCl solutions containing sulfate ions and then aging of this solution for long periods of time (many weeks, Table III.1, entry 1). As seen in Figure III.1, micrometer-size spheres were obtained in these conditions.

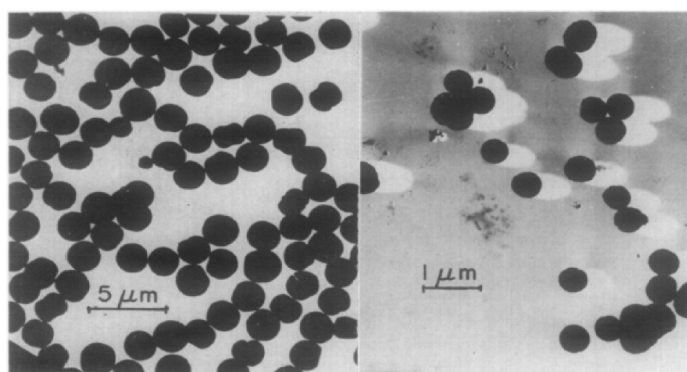


Figure III.1: Electron micrographs of rutile titanium dioxide sol particles obtained by sol-gel synthesis at different ratios of TiCl₄/HCl/Na₂SO₄. [18]

Starting from 0.1 M HNO₃ and titanium butoxide (Table III.1, entry 4), 3.3 nm anatase particles were obtained, however, using of 0.2 to 0.5 M HCL, lead to formation of flowerlike and rodlike TiO₂ rutile nanocrystals, which exhibited high photo-catalytic performance of degradation of methylebe blue which are higher twice than commercial TiO₂ P25 [21]. Conducting the hydrolysis of TTIP in the presence of acetylacetone and p-toluenesulfonic acid (Table III.1, entry 7), Scolan *et al.* were able to obtain in his turn crystalline, monodispersible anatase nanoparticles (1-5 nm) [22]. Using a combination of the F127 and CTAB surfactants (Table III.1, entry 5), Jiu *et al.* managed to drive the hydrolysis of TTIP modified by acetylacetone in order to get anatase particles of 3-5 nm in size, with a high surface area and single phase anatase structure. In this case, a calcinations step at 450°C was necessary to promote crystallization at the end [23,24]. Monodisperse spherical titania particles of

variable sizes distribution from 50 to 2500 nm in diameter of variable porosity are produced in a sol-gel synthesis from $\text{Ti}(\text{EtO})_4$ in ethanol (Table III.1, entry 6) with addition of a salt such as LiCl, NaCl, KCl or a polymer molecules like Lutensol NO.3, or Pluronic PE 430 [25]. Earlier, Bogush and Zukoski *et al.* reported that changes in the ionic strength affect the formation of titania particles. According to these authors, the growth mechanism of the particles can be described by an aggregation model, which implies that the colloidal particles are formed by aggregation of small particles with a size of 5-20 nm (primary particles). This suggests that the formation of primary particles proceeds independently of the existing particles and that the absolute size of the final particles is determined by the size and the aggregation tendencies of the primary particles [26-28]. Okunaka *et al.* reported the preparation of highly stable aqueous titania sols *via* a facile process using titanium tetraisopropoxide in the co-presence of acetylacetone and acetic acid. Titania colloidal particles with diameter values inferior to 10 nm were obtained. The latter, constituted of densely packed anatase TiO_2 , were stable for more than 1 year. They were used to get films with a very good transparency [29].

X.-Q. Chen *et al.* studied the hydrolysis of titanyl organic compounds [$\text{TiO}(\text{OOCCH}_3)_2$ and $\text{Ti}_2\text{O}(\text{OC}_4\text{H}_9)_2(\text{OOCCH}_3)_4$] at low temperature and normal pressure, obtaining stable TiO_2 spherical colloidal particles with a narrow size distribution *ca.* 8.9 nm, its isoelectric point is 6.67, and surface area is $262.7 \text{ m}^2.\text{g}^{-1}$. In particular, they observed that the UV absorbance of the nanocrystalline TiO_2 colloidal solutions increased with a decrease in particle size. The photocatalytic activity of these nanocrystalline TiO_2 colloidal particles was revealed in the degradation of rhodaminee [30].

- Hydrothermal method

The hydrothermal method is similar to the sol gel method, but higher temperature and pressure are often required. For example, such treatments have been used to transform titanate nanotubes into pure brookite nanocrystals (Table III.1, entry 10) under strongly basic conditions and in the presence of Na^+ cations [20,21]. Pure brookite particles could be also prepared through a hydrothermal treatment of a particular titanium glycolate-peroxo complex (Table III.1, entry 9) whose crystal structure resembled that of brookite base units. Other group reported the synthesis of large brookite rods (length 300 nm and diameter 50 nm) via the hydrothermal treatment of TiOSO_4 in the presence of sodium hydroxide (Table III.1, entry 8). This confirms that basic hydrothermal conditions generally favor the formation of brookite nanoparticles [31-33]. Hydrothermal treatment can be favorable to the use of TiO_2 itself as a Ti precursor. Hence, nanotubes composites prepared by this way in NaOH aqueous solution showed efficient photogenerated carriers separation and led to increased light absorption, which improved the photocatalytic degradation of methyl orange [34].

- Solvothermal method

The solvothermal method is very similar to the hydrothermal one except that the primary solvent used is not water. A large variety of surfactants or structure directing agents can be employed in solvothermal methods to drive the shape and morphology of the crystallites. For example, Eiden-Assmann *et al.* reported that monodisperse spherical titania particles of variable sizes were produced in a sol-gel synthesis from $\text{Ti}(\text{OEt})_4$ in ethanol with addition of a salt or a polymer solution (Table III.1, entry 6) [25]. In some cases, hollow and porous titania colloids with amorphous structures were obtained. Du *et al.* showed that octahedral titania particles could be synthesized in toluene whereas spheres were obtained in ethanol starting in both cases from titanium butoxide in the presence of CTAB [35]. A benefit of the solvothermal versus the hydrothermal process is that organic surfactants can be employed allowing the dispersion of the resulting nanocrystals in nonpolar solvents through the formation of reverse micelles. Accordingly, Kim *et al.* used oleic acid to decompose TTIP at 250°C in toluene, resulting in 6 nm crystallites (Table III.1, entry 11) that became elongated upon increased oleic acid concentration [36]. Chen *et al.* (Table III.1, entry 12) used also oleic acid in combination with NaF to drive the formation of specific shapes based on the truncated bipyramidal geometry. Starting from titanium butoxide, oleic acid, NaF, and water, the synthesis was performed via a solvothermal treatment at 250°C for 24 h. The resulting suspension was composed of anatase particles of about 40 nm in length (main axis) with a rhombic projection consistent with truncated tetragonal bipyramidal geometry [37] as seen in Figure III.2.

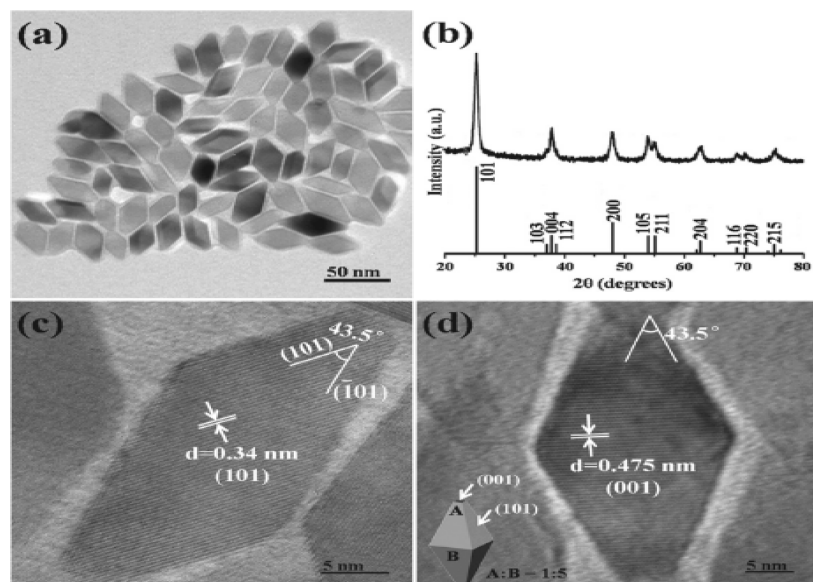


Figure III.2: (a) TEM image of anatase TiO_2 nanobipyramids prepared under solvothermal condition at 250°C for 24 h with a molar ratio of titanium butoxide to NaF of 5:2. (b) XRD pattern of the as prepared TiO_2 nanobipyramids. (c, d) HRTEM images of nanobipyramids. (Inset) nanobipyramid [37].

Q. Wei *et al.* investigated the synthesis of TiO₂ nanoparticles consisting of anatase, rutile and brookite phases under solvothermal condition using different alcohols as solvent, hexamethylene tetramine (HMT) as precipitant, and Ti trichloride as precursor. The effect of the solvent and HMT amount on the phase composition and photocatalytic activity of TiO₂ were studied. Using MeOH, anatase was formed more easily under acidic condition, while rutile and brookite were preferentially formed under basic condition. Photocatalytic degradation of Methyl orange using these materials showed that the mixed crystallites of anatase and brookite led to the best photocatalytic activity [38].

S. Shang *et al.* prepared anatase TiO₂ hollow spheres through a template-free solvothermal route using TiCl₄ as a raw material and a mixture of alcohols-acetone as solvent, demonstrating the aggregation of the anatase TiO₂ nanoparticles and the Ostwald ripening. As-prepared TiO₂ hollow nanostructures exhibited good photocatalytic activity for the degradation of phenol [39]. In another similar approach, a thiobenzoate titanium complex was used as precursor to form 6 nm (diameter) anatase particles in benzyl alcohol under microwave irradiation [40]. Tang *et al.* used an organometallic method based on the reaction of bis(cyclooctatetraene) titanium (Table III.1, entry 15) with dimethyl sulfoxide (DMSO) to provide 5 nm brookite nanocrystals [41].

Surfactants may have also interesting influences. Seo *et al.* used a surfactant-assisted method to prepare anatase rods. This procedure (Table III.1, entry 13) consisted in performing the hydrolysis of TiCl₄ in the presence of oleic acid and oleyl amine [42]. Chemseddine *et al.* pointed out that hydrolysis of titanium alkoxide in the presence of quaternary ammonium hydroxides (Table III.1, entry 14) afforded anatase crystals with hexagonal, rectangular, and rodlike morphology [43].

- Hard templating

Hard templating has also been employed. Such approach consists in utilizing rigid inorganic or polymeric materials as templates, allowing titania to fill the channels of porous materials, to surround polymer spheres, etc. For example, highly uniform titania in the form of hollow structures with octahedral geometry was prepared via the hydrolysis of TiF₄ in the presence of Cu₂O crystals (Table III.1, entry 16) [44]. Similarly, Yang *et al.* obtained hollow spheres by coating polystyrene particles with titanium butoxide, followed by a sol-gel approach to grow a titania layer on the surface followed by a calcination step (Table III.1, entry 17) [45]. Porous SiO₂ materials were also used as templates that were filled with the Ti precursor. As the result, titania NPs were trapped into the mesoporous channels of the silica host (Table III.1, entry 18), as reported for example, by Li *et al.* [46].

III. Deposition of TiO₂ on supports

One of the best photocatalysts listed in the literature is titanium dioxide P-25 which is characterized by a very small surface area. Nanometric TiO₂ could be expected to give better results. We have just described a series of strategies affording nanoparticles of TiO₂ with controlled structures and exposing more surface area. Applications of these nanoparticles already exist in photocatalysis but the implementation of processes with nano-objects is not obvious. Their deposition on a support without loss of their intrinsic properties constitutes an option worth to be studied.

The increase of the specific surface area brought by the support may be of interest from the point of view of heterogeneous catalysis but also because the interaction of the nanoparticles with the support can also be beneficial from a photocatalytic point of view. This is illustrated by the following examples: Hence, G. Zhang *et al.* reported that anatase TiO₂ / diatomite composite based on a mild hydrolysis of titanyl sulfate, where anatase nanoparticles are anchored on the surface of diatomite through Ti-O-Si bonds, gave better photocatalytic activity for formaldehyde oxidation than pure TiO₂. [47]. P. Lei *et al.* reported a facile method to prepare a chemically bonded conjugated-grafted-TiO₂ nanohybrid with high visible-light photocatalytic efficiency [48]. This kind of material was obtained via polymer degradation onto the surface of TiO₂ nanoparticles. According to the authors, interfacial C-O-Ti bonds between TiO₂ and the conjugated structures would act as the pathway for a quick transfer of the excited electrons from the conjugated structures to TiO₂.

In catalysis, deposition of nanometric metal oxides on porous oxide supports is commonly practiced. The challenge, here, is to optimize the dispersion of the metallic precursors on all the surface in order to better use its advantage and obtain, at the end, objects of small size. The methods usually employed involve contacting the porous supports with metal salts in solution. The initial anchoring of metal ions or complexes is based either on ion exchange mechanisms when it is possible (polymers, zeolites, clays etc) and/or the formation of weak or covalent interactions of the metal complexes with the support [49,50]. Ion exchange with lower metal loading tends to give small metal particles [51]. Practically, methods of support impregnation with a solution of salts or metal complexes are the most widespread. One distinguishes "wet impregnations" carried out in the presence of an excess of solution and "dry impregnations" carried out with the quantity of solvent that is just needed to fill exactly the pore volume available. These techniques have been particularly developed in the case of structured mesoporous supports and especially SBA-15 silica. Such supports with a hexagonal array of uniform channels may exhibit area of 500-1000 m².g⁻¹ [52-54]. Their tunable pore diameters of 5-20 nm are also particularly suited to the inclusion of nanometric particles and the diffusion of

relatively bulky organic molecules during the test. However, large surface area and large pore diameters do not guarantee that the final dispersion will be controlled.

An interesting strategy to "force" the inclusion of the desired oxides in the porosity consists in using two immiscible solvents during the impregnation: on the one hand, water to dissolve the metal salts and, on the other hand, an alkane which has no affinity for the mesoporous cavities recognized to be of rather hydrophilic nature. This "Two-solvents" has been extensively applied starting from aqueous metal salts or complexes and with the aim of obtaining supported oxides after a suitable heat treatment [55-57]. Starting from metal salts (iron, cobalt and manganese), such type of impregnation allowed a proper control of both the particle size and the loading of the metal oxides and this method inhibited the growth of metal oxide NPs on the external surface of the support (Figure III.3).

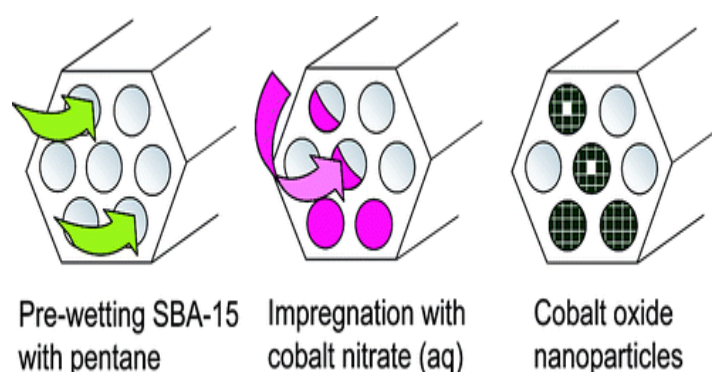


Figure III.3: Principle of the insertion of cobalt oxide in the mesoporosity of SBA-15 using the "Two-solvents" method [57].

Laugel *et al.* [53] also obtained Co_3O_4 and Mn_3O_4 nanoparticles highly dispersed within SBA-15 silica channels using this "Two-solvents" technique which allowed a proper control of the metal oxides loading (7 wt.%) with size of 10-12 nm in diameter. Supported $\text{Co}_3\text{O}_4/\text{SBA-15}$ (7 wt.%) showed the highest catalytic performance in the combustion of methane. Results with this catalyst were quite comparable with perovskites that are usually considered as the most active mixed metal oxides for this reaction (for example, $\text{La}_{0.87}\text{Sr}_{0.13}\text{Mn}_{0.2}\text{Ni}_{0.8}\text{O}_{3-\delta}$)[58,59], suggesting that these materials could be used as novel efficient combustion catalysts at low metal loading. P. Dai *et al.* used also this approach for the preparation of NiO-ZnO photocatalysts encapsulated in mesoporous SBA-15 silica. Hydrophobic alkane solvents (*n*-hexane, *n*-pentane, or cyclohexane) were first used to impregnate SBA-15. This resulted in better wettability and facilitated the introduction of aqueous solutions into the pores which prevented nanoparticle aggregation on the external surface [60].

At the end of this bibliographic chapter, we think that it would be judicious to transpose this "Two-solvents" technique usually used with salts/complexes dissolved in an aqueous medium to aqueous dispersions of preformed colloids. If it works without too much variation in the size of the preformed

nano-objects, this would be a means of controlling not only the final dispersion but also the size of the objects based on the knowledge acquired in the preparation of the colloids (see first part of this chapter).

IV. Conclusion

The synthesis of suspensions of titanium dioxide nanoparticles with size and even controlled morphology is abundantly described in the literature. In the case of TiO_2 , the nature of the crystalline phases obtained (rutile, anatase and brookite) presents an additional challenge in view of their different reactivities. Three main synthetic pathways, *i.e.* the sol-gel method, the hydrothermal and the solvothermal routes were identified. The protocols involve very predominantly alkoxides whose hydrolysis kinetics has to be controlled in aqueous or non-aqueous media. Additives, such as mineral acids and bases, organic ligands or complexing salts, are most often used to obtain the desired sizes. Some of these compounds are adsorbed preferentially on certain crystal faces allowing their stabilization to the detriment of other faces leading selectively to certain morphologies. From reading the literature, it does not always appear that the observed effects are predictable in the current state of knowledge. Another, perhaps more predictable, means of controlling grain morphology, size and spatial positioning is the use of hard templates (polymer beads, porous silicas, etc.). A number of the synthesized nanoparticles were tested as photocatalysts. It is fairly unanimously recognized that the catalytic properties of the latter benefit from the increase of the exposed surface compared to conventional catalysts such as P-25 or PC-500. Other benefits are related to changes in absorption thresholds.

The deposition of pre-formed titanium dioxide colloids on non-photoactive supports should facilitate the implementation of these nanoparticles. This anchorage, if it is stable, should also prevent further agglomeration. In this bibliographical survey, we have recalled that the use of a support with large surface area is not enough, it is also necessary to control the homogeneity of the deposit in order to take full advantage of the initial properties of the colloids. From this point of view, we have highlighted the “two-solvents” impregnation method which has often proved to be efficient at inserting metallic salts initially solubilized in water in the mesoporosity of SBA-15. It seems, however, that no application of this method has been developed starting from colloids dispersed in water.

References

- [1] H. Zhang, F. Banfield, *J. Mater. Chem.*, 8 (1998) 2073.
- [2] O. Carp, C. L. Huisman, A. Reller, *Prog. Solid State Chem.*, 32 (2004) 33.
- [3] T. Sugimoto, X. Zhou, A. Muramatsu, *J. Colloid Interface Sci.*, 252 (2002) 339.
- [4] M. Niederberger, G. Garnweitner, *Chem. Eur. J.*, 12 (2006) 7282.
- [5] H. J. Cohen, *J. Organomet. Chem.*, 5 (1966) 413.
- [6] W. M. P. B. Menge, J. G. Verkade, *Inorg. Chem.*, 30 (1991) 4628.
- [7] A. A. Naiini, W. M. P. B. Menge, J. G. Verkade, *Inorg. Chem.*, 30 (1991) 5009.
- [8] C. R. Bickmore, K. F. Waldner, R. Baranwal, T. Hinklin, D. R. Treadwell, R. M. Laine, *J. Eur. Ceram. Soc.*, 18 (1998) 287.
- [9] M. Bonchio, G. Licini, G. Modena, O. Bortolini, S. Moro, W. A. Nugent, *J. Am. Chem. Soc.*, 121 (1999) 6258.
- [10] P. Sudhakar, C. Valan Amburose, G. Sundararajan, M. Nethaji, *Organometallics* 23 (2004) 4462.
- [11] D. Dambournet, I. Belharouak, K. Amine, *Chem. Mater.*, 22 (2009) 1173.
- [12] S. Sakthivel, M. C. Hidalgo, D. W. Bahnemann, S. U. Geissen, V. Murugesan, A. Vogelpohl, *Appl. Catal. B*, 63 (2006) 31.
- [13] S. Doeuff, M. Henry, C. Sanchez, J. Livage, *J. Non-Cryst. Solids*, 89 (1987) 206.
- [14] A. Soloviev, R. Tufue, C. Sanchez, AV. Kanaev *J. Phys Chem. B.*, 105 (2001) 4175.
- [15] A. Soloviev, D. Ivanov, R. Tufeu, AV. Kanaev, *J. Mater. Sci. Lett.*, 20 (2001) 905.
- [16] D.L. Marchisio, F. Omegna, A. A. Barresi, P. Bowen, *Ind. Eng. Chem. Res.*, 47 (2008) 7202.
- [17] P. Arnal, R. J. P. Corriu, D. Leclercq, P. H. Mutin, A. Vioux, *Chem. Mater.* 9 (1997) 694.
- [18] H. G. Yang, C. H. Sun, S. Z. Qiao, J. Zou, G. Liu, S. C. Smith, H. M. Cheng, G. Q. Lu, *Nature*, 453 (2008) 638.
- [19] X. Q. Gong, A. Selloni, *J. Phys. Chem. B*, 109 (2005) 19560.
- [20] A. Selloni, *Nat. Mater.*, 7 (2008) 613.
- [21] G. Li, S. Zhang, J. Yu, *J. Am. Ceram. Soc.*, 94 (2011) 4112.
- [22] E. Scolan, C. M. Sanchez, *Chem. Mater.*, 10 (1998) 3217.
- [23] J. Jiu, F. Wang, M. Sakamoto, J. Takao, M. Adachi, *J. Electrochem. Soc.*, 151 (2004) 1653.
- [24] J. Jiu, S. Isoda, M. Adachi, F. Wang, *J. Photochem. Photobiol., A*, 189 (2007) 314.
- [25] S. Eiden-Assmann, J. Widoniak, G. Maret, *Chem. Mater.*, 16 (2004) 6.
- [26] G. H. Bogush, C. F. Zukoski, *Ultrastruct. Process. Adv. Ceram.*, (1988) 477.
- [27] V. Privman, D.V. Goia, J. Park, E. Matijevic, *J. Colloid Interf. Sci.*, 213 (1999) 36.
- [28] V. Privman, E. Matijevic, J. Park, *J. Phys. Chem. B*, 105 (2001) 11630.
- [29] S. Okunaka, H. Tokudome, Y. Hitomib, R. Abe, *J. Mater. Chem. A*, 3 (2015) 1688.
- [30] X. Q. Chen, W. H. Shen, *Chem. Eng. Technol.*, 31 (2008) 1277.
- [31] M. Zhao, L. Li, H. Lin, L. Yang, G. Li, *Chem. Commun.*, 49 (2013) 7046.
- [32] K. Tomita, V. Petrykin, M. Kobayashi, M. Shiro, M. Yoshimura, M. Kakihana, *Angew. Chem., Int. Ed.*, 45 (2006) 2378.
- [33] M. Kobayashi, K. Tomita, V. Petrykin, M. Yoshimura, M. Kakihana, *J. Mater. Sci.*, 43 (2008) 2158.
- [34] L. Wu, X. Yang, Y. Huang, X. Li, *Appl. Phys. A*, 123 (2017) 403.
- [35] J. Du, J. Zhang, D. Kang, *J. Cryst Eng Comm.*, 13 (2011) 4270.
- [36] C. S. Kim, B. K. Moon, J. H. Park, B. C. Choi, H. J. Seo, *J. Cryst. Growth*, 257 (2003) 309.
- [37] C. Chen, R. Hu, K. Mai, Z. Ren, H. Wang, G. Qian, Z. Wang, *Cryst. Growth Des.*, 11 (2011) 5221.
- [38] Q. Wei, J. J. Liu, S. Li. Zuo, Y.C. Yu, Z. P. Hao, *J. Inorg. Mater.*, 22 (2007) 931.
- [39] S. Shang, X. Jiao, D. Chen, *ACS Appl. Mater. Interfaces*, 4 (2012) 860.
- [40] M. I. Dar, A. K. Chandiran, M. Gratzel, M. K. Nazeeruddin, S. A. Shivashankar, *J. Mater. Chem. A*, 2 (2014) 1662.
- [41] J. Tang, F. Redl, Y. Zhu, T. Siegrist, L. E. Brus, M. L. Steigerwald, *Nano Lett.*, 5 (2005) 543.
- [42] J. W. Seo, Y. w Jun, S. J. Ko, J. Cheon, *J. Phys. Chem. B*, 109 (2005) 5389.
- [43] A. Chemseddine, T. Moritz, *Eur. J. Inorg. Chem.*, (1999) 235.
- [44] Z. Wang, X. W. Lou, *Adv. Mater.*, 24 (2012) 4124.
- [45] Z. Yang, Z. Niu, Y. Lu, Z. Hu, C. C. Han, *Angew. Chem., Int. Ed.*, 42 (2003) 1943.
- [46] Y. Li, S. J. Kim, *J. Phys. Chem. B*, 109 (2005) 12309.
- [47] G. Zhang, Zhiming Sun, Y. Duan, R. Ma, S. Zheng, *Applied Surface Science*, 412 (2017) 105.
- [48] P. Lei, F. Wang, S. Zhang, Y. Ding, J. Zhao, M. Yang, *ACS Appl. Mater. Interfaces*, 6 (2014) 2370.
- [49] K. Bourikas, J. Vakros, C. Fountzoula, C. Kordulis, A. Lycourghiotis, *Catal. Today.*, 128 (2007) 138.
- [50] C. Wang, S. Lim, G. Du, C. Z. Loebicki, N. Li, S. Derrouiche, G.L. Haller, *J. Phys. Chem. C*, 113 (2009) 14863.

- [51] B. Nohair, C. Especel, G. Lafaye, P. Marecot, L. C. Hoang, J. Barbier, *J. Mol. Catal. A: Chem.*, 229 (2005) 117.
- [52] A. Corma, D. Kumar, *Stud. Surf. Sci. Catal.*, 117 (1998) 201.
- [53] G. Laugel, J. Arichi, H. Guerba, M. Moliere, A. Kiennemann, F. Garin, B. Louis, *Catal. Lett.*, 125 (2008) 14.
- [54] P. A. Buffat, A. Renken, *Catal. Commun.*, 3 (2002) 159.
- [55] M. Imperor-Clerc, D. Bazin, M. D. Appay, P. Beaunier, A. Davidson, *Chem. Mater.* 16 (2004) 1813.
- [56] I. Lopes, N. El Hassan, H. Guerba, G. Wallez, A. Davidson, *Chem. Mater.*, 18 (2006) 5826.
- [57] J. V. D. Meer, B. G. Isabelle, C. Mercier, B. Revel, A. Davidson, R. Denoyel, *J. Phys. Chem. C*, 114 (2010) 3507.
- [58] M. Alifanti, J. Kirchnerova, B. Delmon, D. Klvana, *Appl. Catal. A*, 262 (2004)167.
- [59] TV. Choudhary, S. Banerjee, VR. Choudhary, *Appl. Catal. A*, 234 (2002) 1.
- [60] P. Dai, T. T. Yan, X. X. Yu, Z. M. Bai, M. Z.Wu, *Nanoscale Res. Lett.*, 11 (2016) 226.

New photocatalysts for alcohol oxidation based on the deposition of stable TiO₂ colloids onto mesoporous silica

A. Mayoufi^{a,b}, D. Obaid^a, P. Beaunier^a, V. Peyre^c, A. Haouas^d and F. Launay^a

^a Sorbonne Universités, UPMC Univ Paris 06, CNRS, Laboratoire de Réactivité de Surface, 4 place Jussieu, F-75005, Paris, France.

^b URCMEP (UR11ES85), Faculty of Sciences, University of Gabès, 6029 Gabès, Tunisia

^c Sorbonne Universités, UPMC Univ Paris 06, CNRS, Laboratoire Phenyx, 4 place Jussieu, F-75005, Paris, France.

^d Al Imam Mohammad Ibn Saud Islamic University (IMSIU), College of Sciences, Department of Chemistry, Riyadh 11623, Saudi Arabia

I. Introduction

Titanium dioxide (TiO₂) nanoparticles have received a lot of interest due to their unique physicochemical, optical properties and their use as alternative photocatalysts [1-3]. Anatase, rutile and brookite crystalline phases can be prepared selectively through colloidal approaches. However, the activity of TiO₂ nanoscale catalysts depends also significantly on the surface and the morphology which are strongly related to the synthesis routes. Small nanoparticles with diameter below 50 nm have been reported to improve the adsorption coefficients of organic molecules and the rate of electron transfer, thus the light-absorbing efficiency increased [4]. Many techniques have been reported for the synthesis of TiO₂ nanoparticles including hydrothermal [5-7], precipitation [8] and solvothermal [9,10] pathways. The sol gel route is the most promising method used for the preparation of nanocrystalline TiO₂ materials because of the mild experimental conditions [11-14]. This route is based on titanium alkoxides such as titanium tetraisopropoxide (TTIP). Many factors can influence the rates of hydrolysis and condensation such as the nature of the alkoxy group, the ratio of water to alkoxide, the use of catalysts and the solvent. The preparation of colloidal TiO₂ usually results in particles with diameters between approximately 5 and 20 nm exhibiting physical properties of the bulk [15,16]. Colloidal particles with dimensions below 5 nm are difficult to stabilize. This can be improved by modifying the surface with ligands preventing the aggregation of nanoparticles, but such protection is limited because organic groups used can be lost easily during irradiation [17]. In this context, the confinement of very small TiO₂ nanoparticles within the porosity of mesoporous silica materials which are transparent to UV irradiation represents an interesting challenge.

This article deals with the development of photocatalysts with large specific surface areas combining preformed titanium oxide nanoparticles and transparent silica mesoporous supports. In the first stage, the parameters influencing the stability of the colloids will be investigated and the best

formulation affording particles with sizes < 5 nm will be retained for the deposition step. Two mesoporous supports with different textural properties, one containing more micropores than the other, will be tested. In this work, the colloids will be deposited either by dry impregnation or by the so-called “two-solvents” method [18,19], which appears innovative for this application. In fact, most of the oxides supported within mesoporous silica materials are generally prepared starting from salts and not from colloids.

II. Experimental part

II.1. Chemicals and reagents

The origin and purity of the chemical reagents used is given in Annex 2. Chemicals and solvents were of the highest available grade and were used without further purification. All the materials tested as photocatalysts have been dried in the oven at 50°C overnight at least for 12 h.

II.2. Synthesis of colloidal suspensions

Attempts to prepare titanium oxide colloidal suspensions were carried out in a single process via the hydrolysis of the titanium precursor based on the procedure described by C. Salameh *et al.* [20]. Parameters of the synthesis, such as the nature of the acid, the alcohol, the molar Ti : H₂O and ROH : Ti ratios were modified as shown in Table IV.1.

Table IV.1: Synthesis parameters used for the different preparations ^a.

Name	Alcohol	V _{ROH} (mL)	Ti(OiPr) ₄ (mL)	H ₂ O (mL)	V _{acid} (mL)	[Ti] mol/L	Molar ratio	
							H ₂ O/Ti	ROH/Ti
Ti-M1	MeOH	7.2	3.1	1.25	1.4 HCl	0.8	12.0	16.8
Ti-M2				0.15		0.9	6.2	
Ti-M3				2.50		0.7	18.6	
Ti-M1'				1.7	1.2 HNO ₃	0.8	12.0	
Ti-M1''A^b				2.3	1.1 AcOH	0.8	12.0	
Ti-M1''B^c								
Ti-P1	<i>i</i> -PrOH	7.2	3.1	1.25	1.4 HCl	0.8	12.0	8.9
Ti-P2^d								14.4
Ti-P3		15.5	5	1.5	0	0.8	4.2	12.0
Ti-P4								

^a Normal order of reagents introduction is: Ti precursor + Alcohol + Acid + H₂O (see standard procedure detailed below); ^b Also named Ti-M1'' in this paper; ^c The introduction order was: Ti precursor + AcOH + MeOH + H₂O; ^d The introduction order was: Ti precursor + HCl + *i*-PrOH + H₂O).

The standard procedure was as follows: Titanium tetraisopropoxide, methanol (or isopropanol), 37 wt.% hydrochloric acid (or glacial acetic acid or 68 wt.% nitric acid) and water were introduced successively in the reaction flask. The resulting solution was stirred at room temperature (*c.a.* 25°C),

then, the mixture was heated at 70°C for 4 h. Three series of preparations were undertaken. In the first, *i.e.* Ti-Mx samples correspond to the use of methanol and hydrochloric acid with the molar ROH/Ti ratio = 16.8. In the second, Ti-M1' and Ti-M1'' samples differ from Ti-M1 by the use of other acids. In the third, Ti-Px samples are related to syntheses performed in *i*-PrOH varying both the amounts of alcohol and Ti(OiPr)₄.

II.3. Synthesis of the mesoporous silica precursors

II.3.1. SBA-15

Silica of the SBA-15 type was prepared on a large scale using strongly acidic experimental conditions according to the procedure described by F. Boubekr *et al.* [21]. Homogeneous dilution of 72.3 g of triblock copolymer P123 EO₂₀PO₇₀EO₂₀ was achieved within 6 h in 2150 mL of an aqueous HCl solution (2 mol L⁻¹; 160 mL HCl. 35.5% in wt. per L of water) under constant stirring (600 rpm) at 35°C. Then, 170 mL of tetraethyl orthosilicate were added dropwise in about 45 min. Less than 2 min after the end of TEOS addition, stirring was stopped to favor the formation of fairly monodispersed and individual silica grains. Rapid precipitation of a white powder occurred. The powder and its mother liquor were kept at 35°C for 23 more h. The vessel was left open for the first 6 h to allow ethanol evaporation and the solid was filtered and divided in two parts. One was submitted to a hydrothermal treatment at 95°C, the other one at 130°C for 24 h. The silica powders were then recovered by filtration and washed with water until full elimination of chlorides and dried in air at 60°C. Thus, the resultant powders were calcined at 500°C for 6 h with a heating rate of 2°C.min⁻¹, static conditions in air affording SBA(95) and SBA(130) samples, respectively.

II.4. Deposition of titanium oxide colloids

II.4.1 Incipient wetness impregnation method

Ti-M1/SBA-15(95) and Ti-M1/SBA-15(130) samples were prepared by mixing 1.0 g of the support, *i.e.* SBA(95) and SBA(130) materials with 0.73 (theoretical wt.% Ti = 2.7) and 1.25 mL (theoretical wt.% Ti = 5.1) of the aqueous colloidal suspension (Ti-M1) which corresponds to the exact value of the pore volume available (0.73 and 1.25 cm³.g⁻¹, respectively). The resulting solids were dried overnight at ambient temperature.

II.4.2 "Double-solvents" method (DS)

Ti-M1/SBA-15(95)-DS and Ti-M1/SBA-15(130)-DS samples were synthesized by adding 0.73 (theoretical wt.% Ti = 2.7) and 1.25 (theoretical wt.% Ti = 5.1) mL of the aqueous colloidal suspension (Ti-M1) to 1.0 g of SBA(95) or SBA(130) dispersed in 35 mL of cyclohexane using double solvent route. The volumes of the titanium oxide suspension introduced corresponded again to the exact

value of the pore volume available (0.73 and $1.25 \text{ cm}^3 \cdot \text{g}^{-1}$, respectively). The resulting solids were dried overnight at ambient temperature.

II.5 Characterization

X-Ray diffractograms, N_2 sorption data, Diffuse reflectance UV-Vis. spectra, X-ray fluorescence spectroscopy, thermogravimetric analysis (TGA) and TEM images were performed in the conditions already described in the experimental part of chapter 2.

The hydrodynamic diameter, D_h , of the nanoparticles were measured using a DLS apparatus (Malvern Nano-ZS, wavelength $\lambda = 656 \text{ nm}$, scattering angle $\theta = 173^\circ$). The diffusion coefficient D was related to the radius R of the particles by means of the Stokes-Einstein Equation: $D = k_B T / 6\pi\eta R$, where k_B is the Boltzmann-constant, T the temperature and η the viscosity. The aqueous suspensions of titanium oxide nanoparticles were analysed at 25°C and measurements were started 10 min after the cell was placed in the DLS apparatus to allow the temperature to equilibrate.

II.6. Photocatalytic tests

In a typical experiment, the photocatalyst (60 mg for the solids, 1 mL for Ti-M1 suspension) was dispersed in 40 mL of acetonitrile in a test tube made of pyrex glass. Runs were performed at 50°C with 0.3 mL (2.9 mmol) of benzyl alcohol. The suspension was held under constant magnetic stirring at 900 rpm firstly during 1 h without irradiation to reach the adsorption equilibrium of the substrate molecules onto the catalyst, then for 4 h under UV irradiation (HPK 125 W Mercury lamp with a maximum emission at 365 nm) and O_2 gas flow at $100 \text{ mL} \cdot \text{min}^{-1}$. The lamp was housed in a double-walled immersion well made of quartz cooled with circulating water thermostated at 15°C . Quantification of the reactants after catalysis tests was performed by gas chromatography and HPLC (For details, see chapter 2 and annex 2).

III. Results and discussion

III.1. Study of the hydrolysis of $\text{Ti}(\text{OiPr})_4$ in acidic conditions

The very first synthesis (Ti-M1) was performed starting with the procedure described by C. Salameh *et al.* [20]. Hence, Ti-M1 was prepared by the hydrolysis of 0.8 M $\text{Ti}(\text{OiPr})_4$ in a water / methanol / concentrated hydrochloric acid mixture with $\text{H}_2\text{O}/\text{Ti} = 12$ (molar ratio). In this context, after heating to 70°C , a stable translucent suspension was obtained. Then, no changes were observed visually over a period of 2 months. The hydrodynamic diameter of the Ti-M1 suspension was analyzed by DLS over 1 week and even 3 months. The particle size distribution was Gaussian and centered at 5 nm after

one week and up to one month. Then, it increased up to 13 nm but no precipitation was observed from a macroscopic point of view. Unhydrolysed isopropoxide groups and/or chloride ions on the periphery of the positively charged titanium oxide surface may be involved in the stabilization process. The small sizes of the formed particles and their quasi-spherical morphology after one-month storage were validated by transmission electron microscopy analyzes. Clearly, it was found that the particles of TiO_2 or $\text{TiO}(\text{OH})$ were transformed into objects that crystallized under the electron beam in high resolution transmission electron microscopy. Reticular planes observed are separated by distances of 4.5 nm which are compatible with the anatase form of TiO_2 (101). In the absence of high contrast, these crystalline domains allowed to identify the periphery of the nanoparticles. In spite of these *in-situ* transformations, TEM data tend to show that the nanoparticles of TiO_2 are characterized by average sizes of the order of 3.5-4.5 nm, thus supporting the data obtained by DLS after 1 month as provided in Figure IV.1.

Table IV.2: Effect of the aging time (storage period) on the particle size determined DLS and HR-TEM.

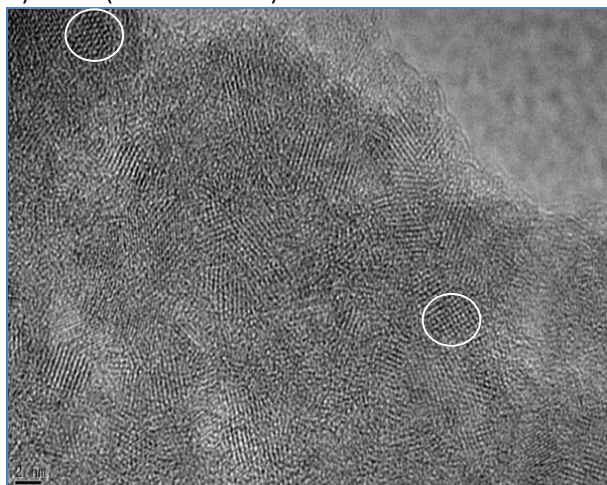
Material	Aging time	Diameter (nm) by DLS	NPs size by HR-TEM
Ti-M1	1 week	5	-
	1 month	5-6	3.5-4.5
	3 months	13	-
Ti-M2	1 month	3	2.5-3.5
Ti-M3		9	3.3-4.5

Other Ti-M_x samples (Ti-M2 and Ti-M3) were synthesized by changing only the amount of water introduced ($6 < \text{molar H}_2\text{O}/\text{Ti} < 18.6$). Stable translucent suspensions were also obtained (Table IV.3). The nanoparticles size distribution measured by DLS was still Gaussian after one month. Mean diameter values were 5-6 nm for Ti-M1 (1.25 mL of H_2O), 3 nm for Ti-M2 (0.15 mL of H_2O) and 9 nm for Ti-M3 (2.5 mL of H_2O). Basically, the greater the amount of water added, the larger the nanoparticles. Differences between Ti-M3 and Ti-M1 were not so obvious using the HR-TEM technique.

The replacement of 37% hydrochloric acid with 68% nitric acid (Ti-M1') or glacial acetic acid (Ti-M1'') with constant quantities of proton and water ($\text{H}_2\text{O}/\text{Ti}=12$) resulted in immediate precipitation in both cases.

Similar experiments carried out in the presence of isopropanol (Ti-Px series) instead of methanol were not conclusive too (Table IV.3) despite of the use of conditions close to those of Ti-M1 sample especially for Ti-P1 or Ti-P2 ($[\text{Ti}] = 0.8 \text{ M}$; $\text{H}_2\text{O}/\text{Ti}$ molar ratio =12 but molar ROH/Ti lower). A gradual precipitation was observed after 1 h, and 2 h for Ti-P1 and Ti-P2 during the treatment phase at 70°C .

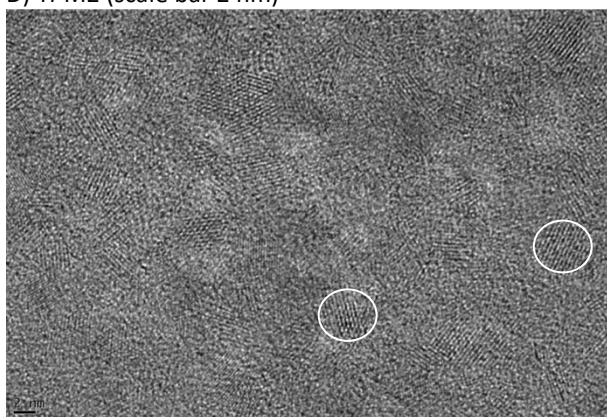
A) Ti-M1 (scale bar 2 nm)



B) Ti-M1 (scale bar 2 nm)



D) Ti-M2 (scale bar 2 nm)



C) Ti-M3 (scale bar 2 nm)

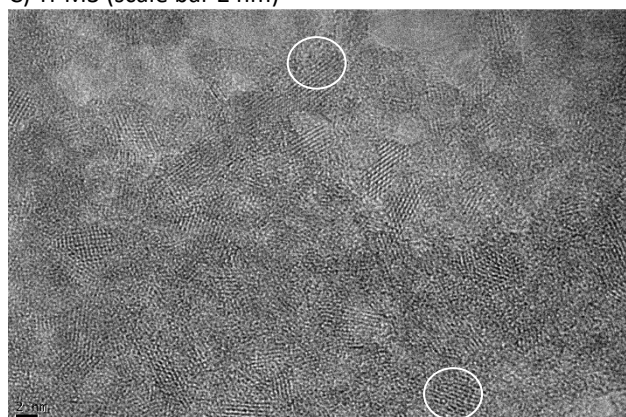


Figure IV.1: HR-TEM photographs of colloidal dispersion of **A and B**) Ti-M1, **C**) Ti-M2, and **D**) Ti-M3 (anatase in white circle after ageing 1 month).

Table IV.3: Observations made for the different attempts of synthesis described in Table IV.1^a.

Name	[Ti] mol/L	Molar ratio		Observations
		H ₂ O/Ti	ROH/Ti	
Ti-M1	0.8	12.0	16.8	Stable
Ti-M2	0.9	6.2		
Ti-M3	0.7	18.6		
Ti-M1'	0.8	12	8.9	Unstable
Ti-M1'' ^b				
Ti-M1'' ^b				
Ti-P1	0.8	12	17.8	Unstable
Ti-P2 ^d				
Ti-P3				
Ti-P4 ^e	0.8	4.2	12.0	Unstable

^a Normal order of reagents introduction is: Ti precursor + Alcohol + Acid + H₂O (see experimental protocol); ^b Also named Ti-M1'' in this paper; ^c The introduction order was: Ti precursor + AcOH + MeOH + H₂O; ^d The introduction order was: Ti precursor + HCl + *i*PrOH + H₂O; ^e No acid used. See table 1, for experimental details.

Without any acid used (Ti-P4), the precipitation occurred instantaneously. It can be concluded that re dispersion is strongly dependent on the type of alcohol used and especially its dielectric constant. It is noteworthy that the dispersion efficiency usually increases with the dielectric constant [22]. Indeed, water (78.5) is expected to be more efficient than methanol (32.6) and, in turn, methanol more efficient than isopropanol (18.1) [22] as observed by Vorkapic and Moon [23,24].

The photocatalytic activities of the colloidal suspensions Ti-M1, Ti-M2 and Ti-M3 aged after 1 month, were evaluated under UV irradiation in the selective oxidation of benzyl alcohol in acetonitrile at 50°C (Figure IV.2).

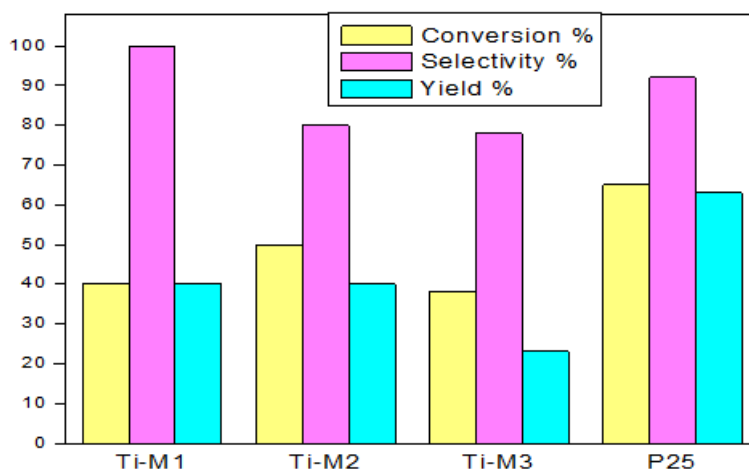


Figure IV.2: Comparison of the photocatalytic activities of 1 month-aged Ti-Mx colloidal suspensions with P25 in the photoselective oxidation of benzyl alcohol under UV irradiance at 50°C.

The results obtained indicate that, with an increase in the water content (from Ti-M2 to Ti-M1, then Ti-M3):

- the conversion rate of benzyl alcohol decreases from 50% (Ti-M2) to about 35% (Ti-M1 and Ti-M3).
- the benzaldehyde yield increases between 38 (Ti-M2) and 43% (Ti-M1), then decreases.

Several explanations are possible. From the point of view of the heterogeneous catalysis, the decrease of conversion could originate from a competitive adsorption of alcohol and water molecules on the surface of the nanoparticles as well as from the decrease of the surface exposed from Ti-M2 (3 nm) to Ti-M3 (9 nm). But other factors related to the NPs phase composition and parameters like the electron-hole recombination should also be considered. The evolution of the benzaldehyde yield is not monotonous meaning that contradictory factors may be involved. To conclude, among the two most efficient colloidal suspensions tested (Ti-M1 and Ti-M2), Ti-M1 would be a little bit more interesting due to the higher benzaldehyde selectivity reached.

Under similar experimental conditions and using equivalent amounts of TiO₂ (1 mL of Ti-Mx 0.8 M corresponds to 60 mg of TiO₂), it is worthy noted that Ti-M1 sample was less active compared to

TiO₂-P25 (see chapter 2 and Figure IV.2). The conversion rate with P25 was higher than with Ti-M1 (43% vs 65%) but in terms of selectivity, the latter was better by about 9% than Ti-M1. The least activity of colloids should be a matter of composition rather than specific surface area. We have seen previously that P25 is a mixture of the rutile and anatase phases while the Ti-M1 colloids are not really crystallized. However, it is necessary to be wary in the interpretations because, once introduced in acetonitrile medium, it is also possible that the size dispersion of the colloids Ti-M1 is strongly impacted.

III.2. Deposition of the colloids onto mesoporous silica supports

The deposition of preformed titanium oxide nanoparticles on such supports is expected to prevent their further aggregation during use, for example in the presence of solvents that are not compatible with their stability. We assumed that a UV-transparent support with large surface area should help to maximize the dispersion of the nanoparticles as well as their accessibility and the adsorption of the substrates. However, it is not easy to predict if the intrinsic photocatalytic activity of the NPs would be strongly disturbed as the result of the variation of electron-hole recombination or trapping of the charge carriers [25-28] in their new environment. The present study will try to bring some answers to the above-mentioned questions.

Deposition experiments were done starting from the one week old Ti-M1 colloidal suspension constituted by highly stable 5 nm nanoparticles displaying reasonable photocatalytic activity. Two mesoporous siliceous materials of the SBA-15 type (SBA(95) and SBA(130)) were considered. The high order of their pore structure was evidenced by low angle XRD measurements (Figure IV.3). More precisely, characteristic peaks at $2\theta=0,82^\circ$, $1,45^\circ$ and $1,67^\circ$ were indexed to the (100), (110) and (200) planes, that correspond to the 2D structure of the p6mm hexagonal symmetry as reported for SBA-15 by other groups [29-31].

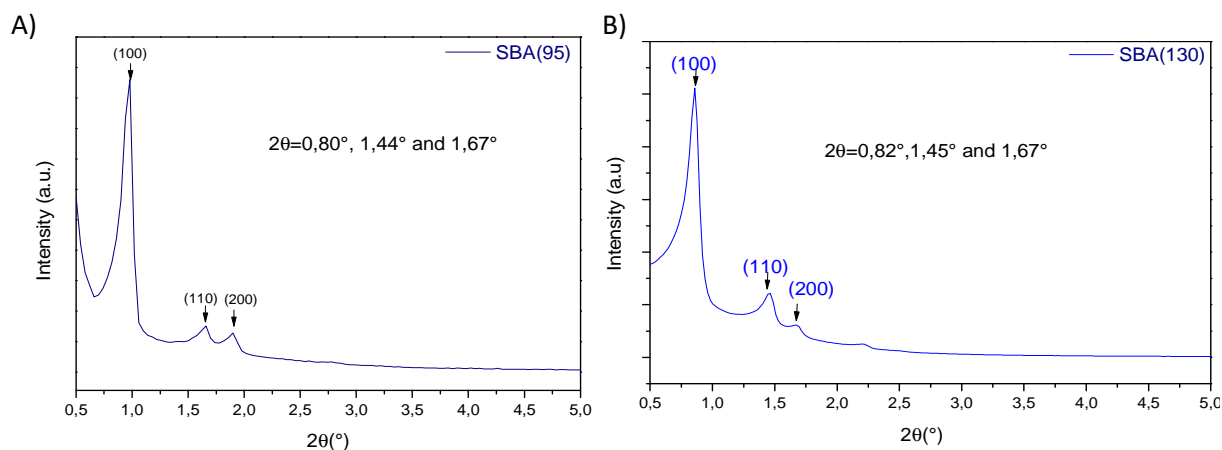


Figure IV.3: Low angle XRD patterns of **A)** SBA(95) and **B)** SBA(130).

N₂ adsorption-desorption isotherms at -196°C for the two SBA-15 solids, shown in Figure IV.4, are characteristic of this type of materials with curves of type IV forming hystereses of type H1 [32]. The sharpness of steps is in agreement with ordered mesoporous materials with relatively large pore sizes and narrow size distribution [33]. The isotherms of SBA(95)/(130) presented a sharp inflection at relative pressure (P/P^0) in the range of 0.6-0.8 which is an indication of the good quality of the starting material. The sample resulting from the hydrothermal treatment at 130°C is characterized by high pore volume ($1.25 \text{ cm}^3 \cdot \text{g}^{-1}$) and pore diameter (*c.a.* 8 nm) compared to SBA (95) ($0.86 \text{ cm}^3 \cdot \text{g}^{-1}$ and *c.a.* 6 nm). Conversely, the value of the specific surface area for SBA(130) is much lower than that of SBA (95) ($550 \text{ m}^2 \cdot \text{g}^{-1}$ vs $730 \text{ m}^2 \cdot \text{g}^{-1}$, see also Table IV.4). In particular, it can be concluded that the pore apertures of both solids are well-adapted to the dimension of the Ti-M1 colloids used.

However, as mentioned in chapter 3, the compatibility of the pores and nanoparticles diameters is not enough to reach the optimum dispersion expected on these selected solids. The challenges lie here i) in locating the titanium oxide nanoparticles within the porosity during the impregnation step and then, ii) in their retention during the drying step. Therefore, the “double-solvent” method was employed to achieve this goal. Indeed, usually the impregnation of mesoporous SBA-15 by the amount of an aqueous solution of metal salts just necessary to fill the porosity in the presence of a non-miscible alkane (cyclohexane here) is used to facilitate the insertion of the metal precursor within the hydrophilic porosity of the mesoporous host. It is then expected that the water with the species it contains, will preferentially be located into the pores due to a lack of affinity with the hydrocarbon chosen as a non-polar solvent. This method has been experimented repeatedly to introduce metal salts but has never been reported for colloidal particles of oxides.

In this work, we have used the fact that the mixture of water / methanol and hydrochloric acid which constitutes the solvent of the colloidal suspension is not miscible with cyclohexane to transpose this double solvent impregnation method to Ti-M1. In the present case, the titanium oxide nanoparticles are pre-formed with a narrow size distribution centered at *c.a.* 5 nm. By using the “Two-solvents” technique, we intend to retain the size control advantage of the colloidal approach, which is not necessarily the case when NPs are formed after the impregnation of the supports by their molecular precursor (here $\text{Ti}(\text{OiPr})_4$). In the following, four samples were prepared:

- two, Ti-M1-SBA(95) and Ti-M1-SBA(130), by the “double-solvents” method,
- two others, Ti-M1-SBA(95)-DS and Ti-M1-SBA(130)-DS, by the incipient wetness impregnation method,

using SBA(95) and SBA(130) as supports, respectively. Resulting solids were dried at room temperature. The Ti concentration of the Ti-M1 colloidal suspension being 0.8 M and the pore

volumes being different ($0.86 \text{ cm}^3.\text{g}^{-1}$ for SBA(95) and $1.25 \text{ cm}^3.\text{g}^{-1}$ for SBA(130)), the theoretical contents of TiO_2 deposited on SBA(95) and SBA(130) are assumed to be equal to 4.5 wt.% in Ti-M1-SBA(95) and Ti-M1-SBA(95)-DS and 7.5 wt.% in Ti-M1-SBA(130) and Ti-M1-SBA(130)-DS samples.

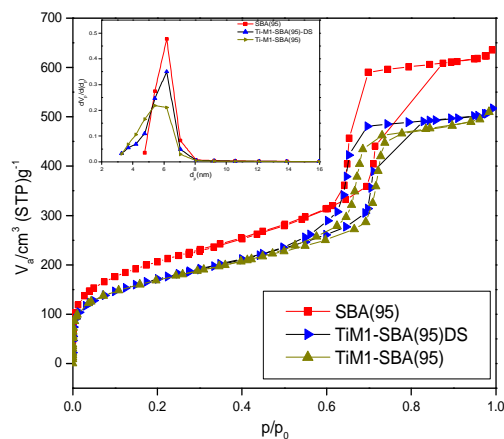
Data related to the composition, the textural properties of the materials and their characteristic properties important for photocatalytic activity are given in Table IV.4.

Table IV.4: Physicochemical properties of the materials before and after Ti-M1 deposition.

Materials	S_{BET} ($\text{m}^2.\text{g}^{-1}$)	Pore vol. BJH ($\text{cm}^3.\text{g}^{-1}$)	Pore diam. (nm)	UV. Vis. band gap ^a
SBA(95)	730	0.86	6.17	3.28
Ti-M1-SBA(95)-DS	600	0.7	6.1	3.65
Ti-M1-SBA(95)	500	0.52	5.5	3.3
SBA(130)	550	1.25	8.05	3.32
Ti-M1-SBA(130)-DS	477	1.1	8.0	3.75
Ti-M1-SBA(130)	540 (?)	1.0	8.0	3.35

The N_2 adsorption-desorption isotherms of the samples recovered after impregnation with Ti-M1 (Figure IV.4) are still characteristic of SBA-15 type materials (typical type IV isotherms with large H1 type hysteresis loop at high relative pressures (0.6-0.8) according to IUPAC classification [49]). Whatever the method used (incipient wetness or “Two-solvents”), the addition of Ti-M1 induced changes of the amount of N_2 adsorbed/desorbed as the result of the modification of the specific surface area, of the pore diameters and of the pore volumes compared to SBA(95) and SBA(130) supports. Similar behavior was reported by Vradman *et al.* for titanium oxide loaded on SBA-15 with the same order of concentration (7 wt.%) [34]. It was observed in particular that the capillary condensation region becomes smaller than for the supports which reflects the filling of SBA-15 channels by the colloidal particles. It can be seen from Table IV.4, that the specific surface area, the pore volumes were decreased with incorporation of titanium oxide colloid in the two samples. The pore size distribution curve for each sample was also shown in Figure IV.4, and the mean values of the pore diameters obtained from the analysis of these isotherms are summarized in Table IV.4.

A)



B)

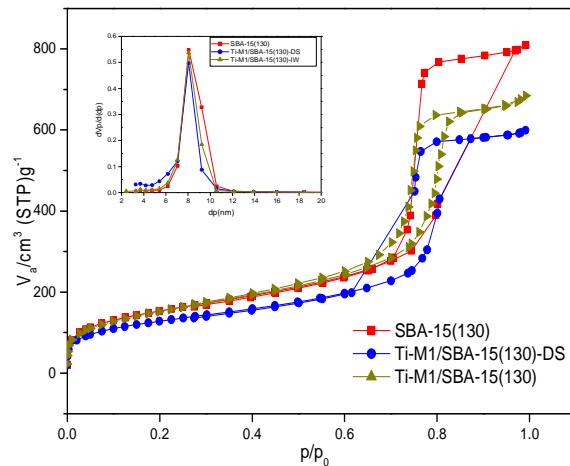


Figure IV.4: N₂ adsorption/desorption isotherms at -196°C of **A)** SBA(95) and **B)** SBA(130) samples superimposed with those of the corresponding materials obtained after Ti-M1 incorporation.

Considering the concentration of Ti in the Ti-M1 colloidal dispersion and assuming that TiO₂ is formed (density of about 4 g.cm⁻³), it appears that the expected evolutions of the pore volumes should be in the range of 1 to 2% compared to the parent supports in the event of the total inclusion of the oxide nanoparticles. In fact, the variations of the pore volumes were much greater: -19% for Ti-M1-SBA(95)-DS, -39% for Ti-M1-SBA(95), -12% for Ti-M1-SBA(130)-DS and -20% for Ti-M1-SBA(130). Except for Ti-M1-SBA(130), the same trend was also observed for the specific surface area. Surprisingly, the variation of the pore volumes for the two supports was more important in the case of the conventional procedure. The pore diameter distributions were quite narrow for the SBA(130) derived material series with an average value around 8 nm. For the series derived from SBA(95), the mean diameter varied more and tended to decrease, the largest variation obtained for the material Ti-M1-SBA(95). In this series, it appears from the distribution curves of the pore diameters that these are less monodisperse; the curves for the solids Ti-M1-SBA(130)-DS and Ti-M1-SBA(130) tend to move towards small diameters. In conclusion, it is not easy to discriminate samples on the basis of physisorption measurements. Direct measurements, by transmission electron microscopy, should be more relevant.

From TGA measurements (Figure IV.5), the SBA(95) and SBA(130) supports used in this study were characterized by mass losses of *c.a.* 2% occurring between 25°C and 100°C. After depositing the colloids and drying, same measurements indicated that the materials obtained contained more organic matter or water (losses of 8 and 10% between 25 and 200°C, for Ti-M1-SBA(130)-DS and Ti-M1-SBA(95)-DS, respectively). Given the appreciable thermal stability of SBA-15-like silica up to 400-

750°C, a possible explanation for weight losses in this range of temperature may involve the formation of Si-O-Ti bridges in Ti-M1-SBA(130)-DS and Ti-M1-SBA(95)-DS samples.

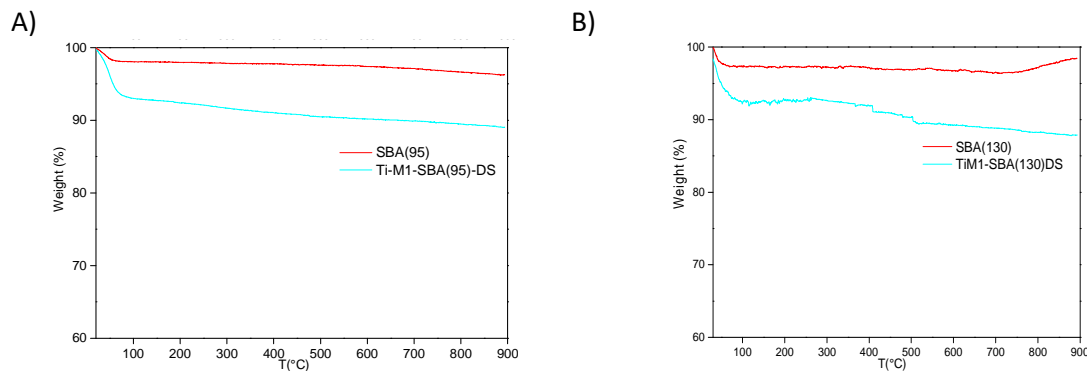


Figure IV.5: TGA curves of **A)** SBA(95) and **B)** SBA(130) samples superimposed with those of some corresponding materials obtained after Ti-M1 incorporation.

The X-ray diffraction patterns of the impregnated materials as well as those of their supports are shown in Figure IV.6. In accordance with the observations of the Ti-M1 colloidal suspension by electron microscopy which showed *in-situ* crystallization, the diffraction patterns of just dried Ti-M1-SBA(95) and Ti-M1-SBA(130) samples did not allow to detect any crystallized nanoobjects. In these two cases, the curves obtained strongly resembled those of the supports. This was not the case for the materials resulting from the deposition following the “two-solvents” method. In these cases, in fact, some rather narrow diffraction peaks emerged. These are characteristic peaks of the anatase crystalline phase. For example, the strongest and clearer peak observed at $2\theta = 25.3^\circ$ would correspond to the (1 0 1) reflection.

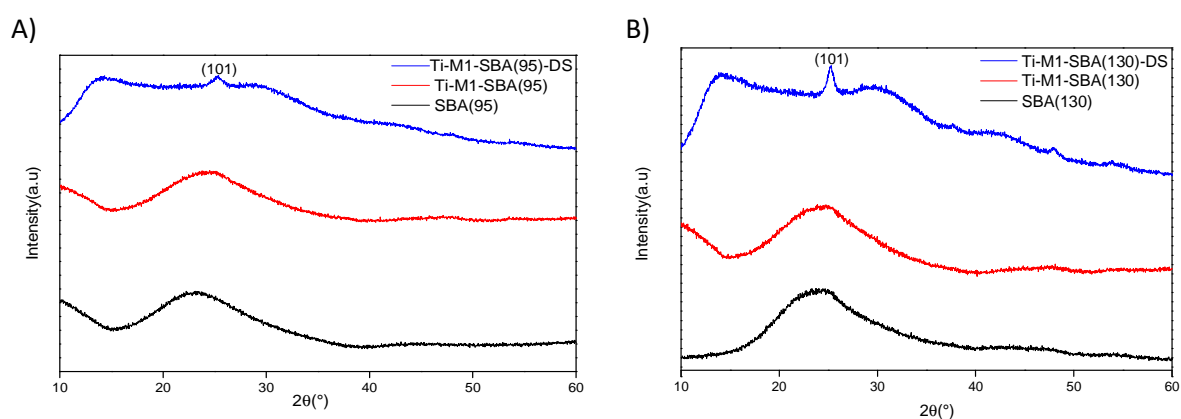


Figure IV.6: X ray diffraction peaks of **A)** SBA(95) and **B)** SBA(130) samples superimposed with those of the corresponding materials obtained after Ti-M1 incorporation

UV-Vis. diffuse reflectance measurements and the corresponding plots of $(\alpha h\nu)^2$ vs. $h\nu$ of both supports (SBA(95) and SBA(130)) and corresponding materials in their dried forms are presented in Figure IV.7.

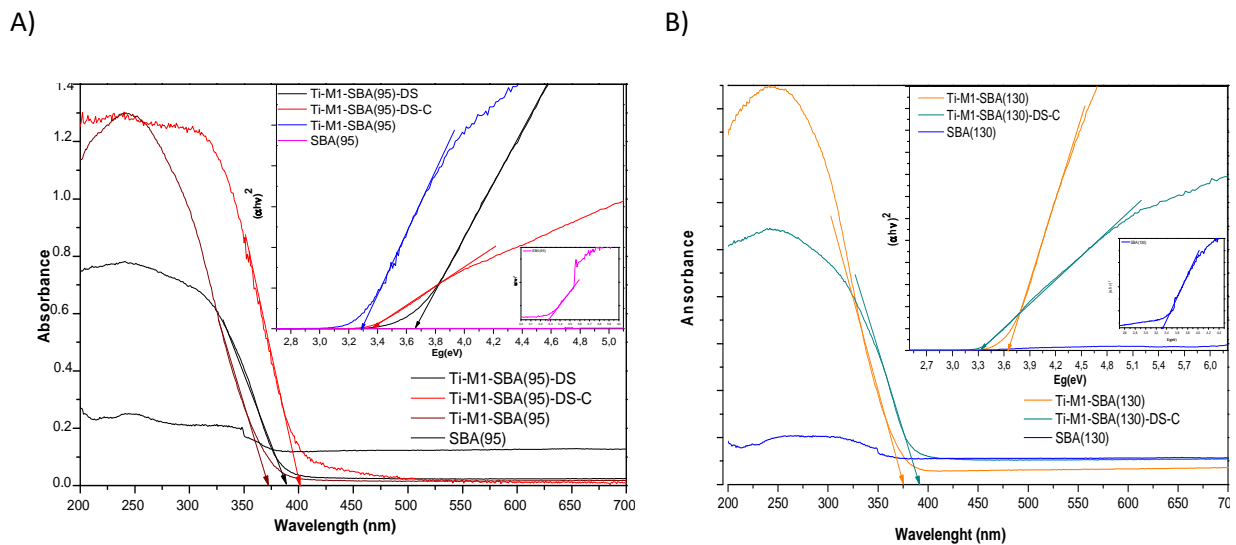


Figure IV.7: DR UV-Vis. spectra and Tauc plots for band gap determination (insets) of A) SBA(95) and B) SBA(130) samples superimposed with those of the corresponding materials obtained after Ti-M1 incorporation. Ti-M1-SBA(95)-DS-C and Ti-M1-SBA(130)-DS-C are the calcined forms (500°C) of Ti-M1-SBA(95)-DS and Ti-M1-SBA(130)-DS.

The band-gap energy (E_g) was determined by Tauc linearization. Resulting E_g values are reported in Table IV.4. All Ti-based materials were characterized by intense absorptions in the UV range. Firstly, the optical band gaps of SBA(95) and SBA(130) were estimated to be 3.28 and 3.32 eV respectively whereas Bouazizi proposed 3.46 eV [35]. Values determined for Ti-M1-SBA(95)-DS and Ti-M1-SBA(95) were 3.65 and 3.3 eV. Those of Ti-M1-SBA(130)-DS and Ti-M1-SBA(130) were 3.75 and 3.35 eV. Clearly, samples prepared using the “Two-solvents” method gave a higher band gap than other samples prepared by a more conventional one. After a calcination treatment, E_g values decreased (see, for example, TiM1-SBA(130)-DS (3.75 eV) vs TiM1-SBA(130)-DS-C (3.3 eV)).

The indirect data cumulated in this study did not allow us to clearly show which of the two impregnation methods used was the most effective to incorporate titanium oxide into the porosity and thus, to take advantage of the specific surface available initially in the SBA-15 supports. We have therefore analyzed three of these solids, Ti-M1-SBA(130)-DS, Ti-M1-SBA(130) and Ti-M1-SBA(95)-DS by high-resolution electron microscopy (Figure IV.8-10).

Regarding Ti-M1-SBA(130) sample (Figure IV.8), this material appeared to be constituted by empty grains and grains containing nanoparticles (Fig. IV.8(A and B)). The filling of the channels was moderate. Some grains were very full (Fig. IV.8(C)), others less (Fig. IV.8(D)). Nanoparticles were

observed outside the grains and within (Fig. IV.8(E)). The nanoparticles inside the channels seemed ill-defined. They contrasted less than in other samples with the walls of the porous support. These observations were valid both on the longitudinal views (Fig. IV.8(F)) and on the transverse views ((Fig. IV.8(D))).

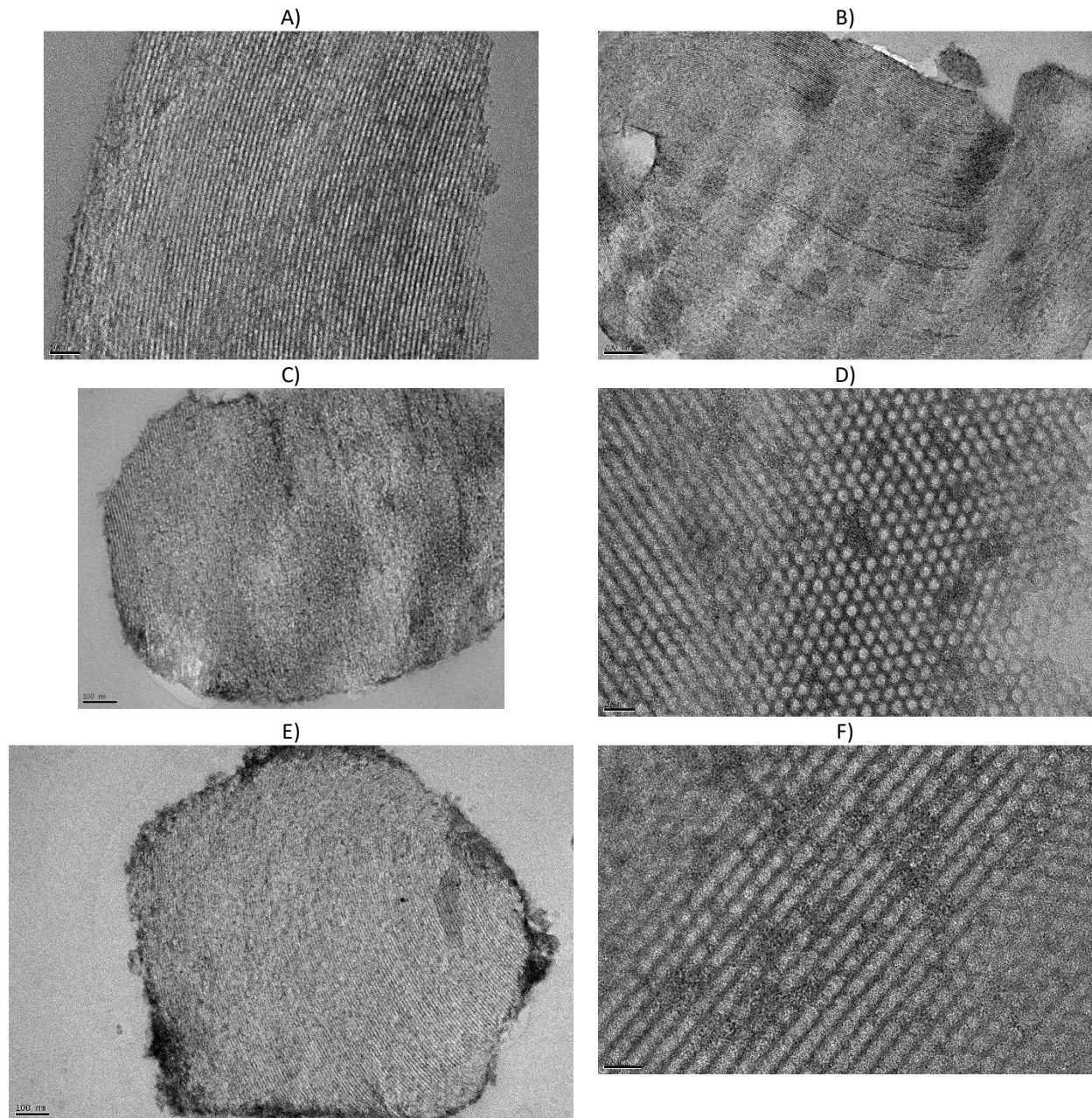


Figure IV.8: Transmission electron micrographs of Ti-M1-SBA(130).

Ti-M1-SBA(130)-DS seemed to be of better quality. On the SBA-15 particles cut by microtomy along longitudinal sections (Fig. IV.9(A)), darker filled areas were observed along the channels. The dark-colored nano-objects were constituted of aligned spots (Fig. IV.9(B)). The filling of the mesoporous solids grains was not optimal. Some grains of SBA-15 appeared empty (Fig. IV.9(C)). On the views

with cross-sections of SBA-15 (Fig. IV.9(D)) or with both transverse and longitudinal sections (Fig. IV.9(E)), nanoparticles included in the pores were clearly observed. Overall, the grains were little surrounded by external deposits of nanoparticles (Fig. IV.9(F)). The more contrasting zones contain TiO_2 .

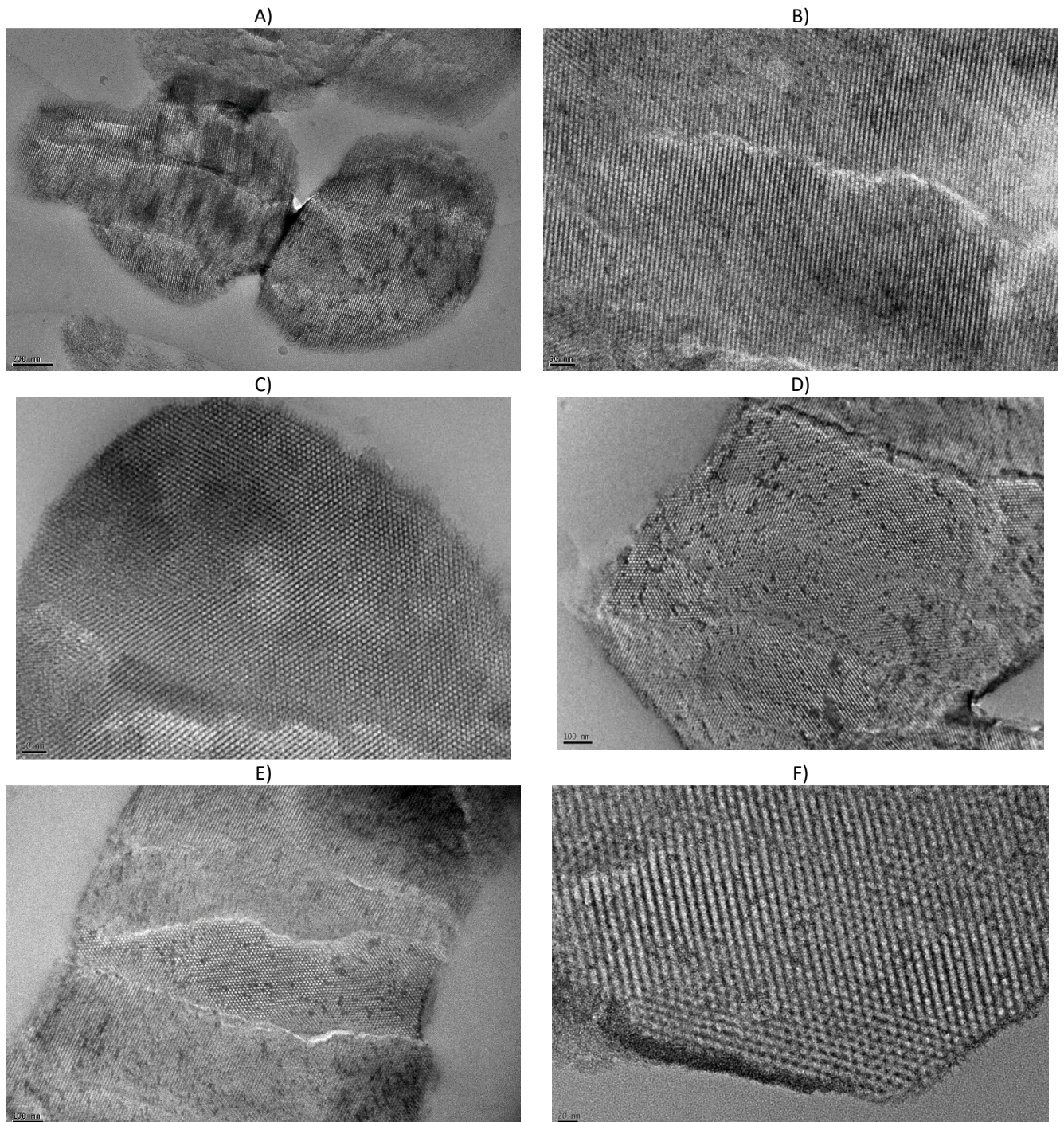


Figure IV.9 : Transmission electron micrographs of Ti-M1-SBA(130)-DS.

In the case of Ti-M1-SBA(95)-DS sample, it was observed on the low-magnification views that a significant amount of nanoparticles accumulate outside the grains (Fig. IV.10(A)). Some SBA-15 silica

grains appeared empty (Fig. IV.10(B)). There were nevertheless grains of the mesoporous solid with nanoparticles inside but in smaller proportions than previously (Fig. IV.10(C)). This was observed both for longitudinal (Fig. IV.10(D)) and transverse sections (Fig. IV.10(C)). The nanoparticles inside the channels appeared to be smaller than the pore diameter (Fig. IV.10(E)). They were crystallized (Fig. IV.10(E) and (F)). Measured sizes were around *c.a.* 2.5 nm.

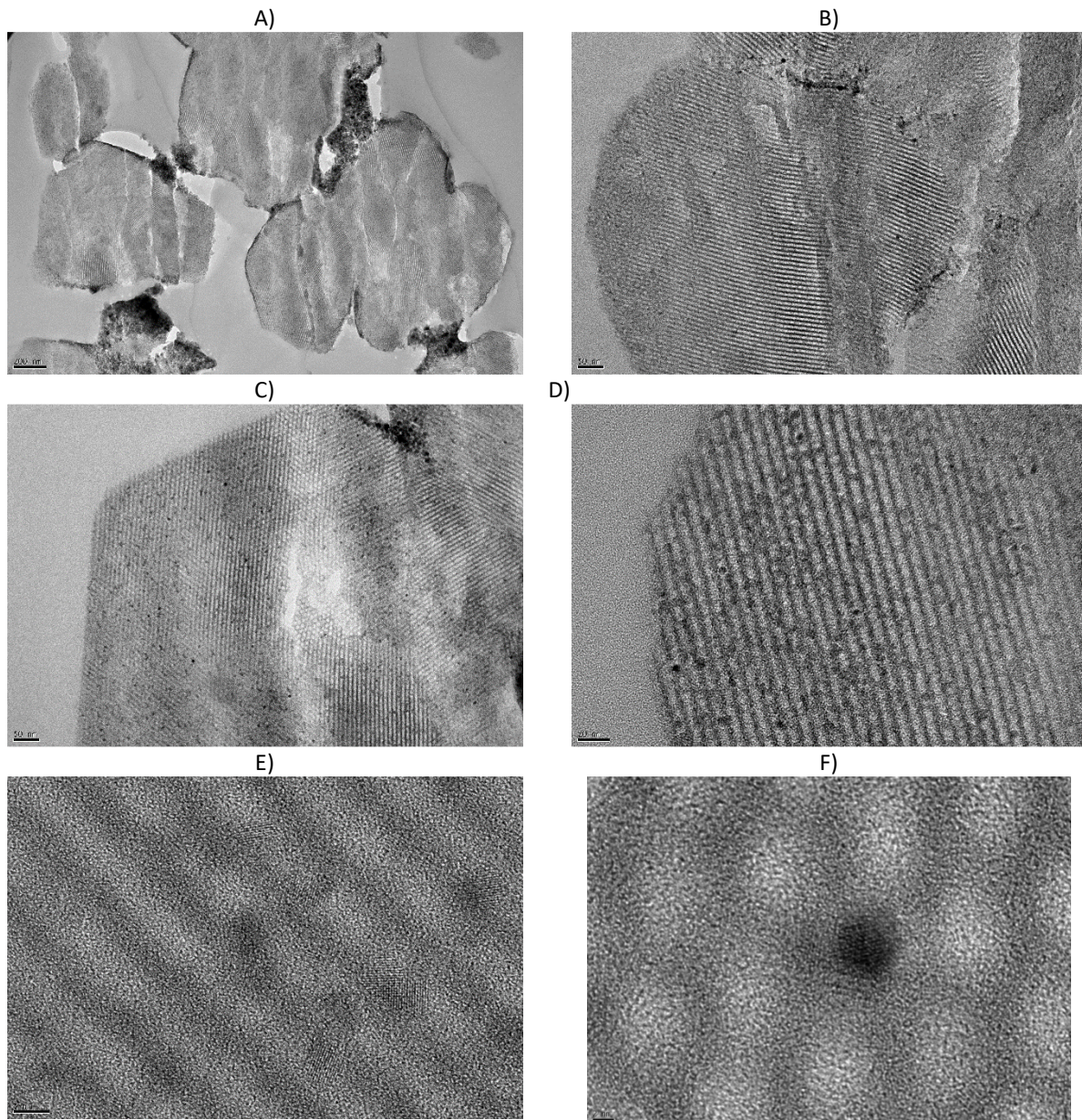


Figure IV.10 : Transmission electron micrographs of Ti-M1-SBA(95)-DS.

From these observations, it appears that in all cases, some titanium oxide was introduced into the pores of the support. The distribution is not optimal and nuances exist between the samples. Hence,

it appears that larger quantities of titanium oxide were detected outside the pores for Ti-M1-SBA(130). The most interesting sample in terms of control of the incorporation of the nanoparticles in the pores appears to be Ti-M1-SBA(130)-DS. The quality of Ti-M1-SBA(95)-DS can be described as intermediate.

In the following, we focused our attention on the photocatalytic properties of the two materials which, from the point of view of microscopy, seemed to contain a maximum of titanium oxide particles within their porosity, *i.e.* Ti-M1-SBA(95)-DS and Ti-M1-SBA(130)-DS. These two solids were tested as photocatalysts in the oxidation of benzyl alcohol in acetonitrile under UV irradiance using molecular oxygen as a sole oxidant at 50°C (Figure IV.11). The tests were performed with 60 mg of each material. Under these conditions, the yields of benzaldehyde were close to 50%, which is much better than starting from the colloidal suspension Ti-M1 alone (Figure IV.2) but less again than using TiO₂-P25. However, it has to be noticed here that the amount of TiO₂ introduced in the present tests (Figure IV.11) is rather low with 3 mg for Ti-M1-SBA(95)-DS (60 mg x 4.5%) and 4.5 mg for Ti-M1-SBA(130)-DS (60 mg x 7.5%) against 60 mg of pure TiO₂ for P25 and Ti-M1 (Figure IV.2). In terms of selectivity, the values obtained with Ti-M1-SBA(95)-DS and Ti-M1-SBA(130)-DS are between 90 and 100% which is quite similar to P25 and Ti-M1.

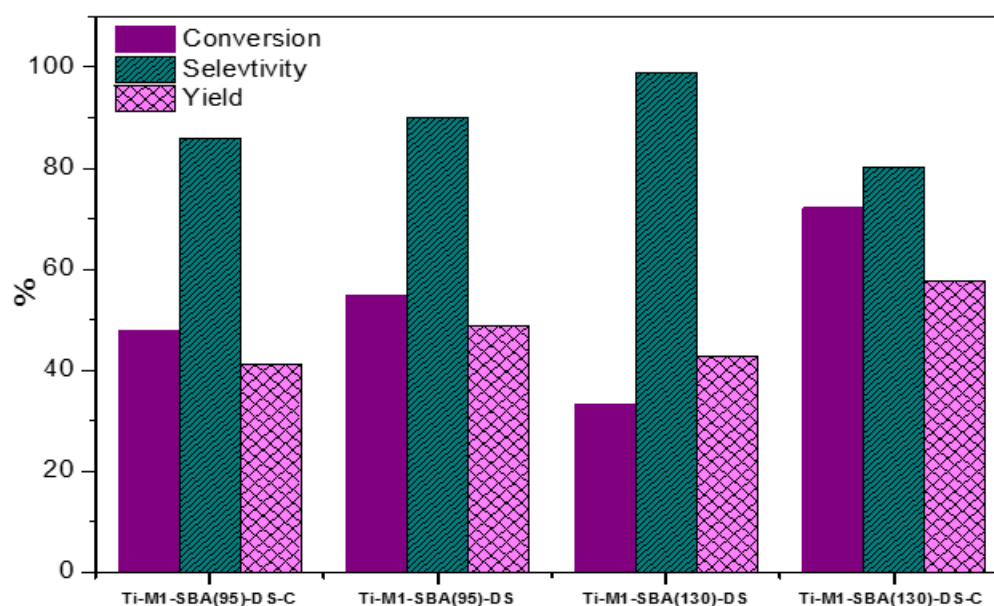


Figure IV.11: Comparison of the photocatalytic activities of the materials prepared by the “Two-solvents” method (in their as-synthesized or calcined forms) in the photoselective oxidation of benzyl alcohol under UV irradiance at 50°C.

We also tested Ti-M1-SBA(95)-DS-C and Ti-M1-SBA(130)-DS-C, the calcined forms of Ti-M1-SBA(95)-DS and Ti-M1-SBA(130)-DS samples, respectively. This post-treatment affected the Ti-M1-SBA(95)-DS and Ti-M1-SBA(130)-DS samples differently. The benzaldehyde yield was lowered in the case of Ti-

M1-SBA(95)-DS-C whereas it was increased in the case of Ti-M1-SBA(130)-DS-C due to a strong effect of the calcination stage on the benzyl alcohol conversion.

IV. Conclusion

The aim of this study was to exploit the colloidal approach for the deposition of titanium oxide nanoparticles on mesoporous silica supports that are transparent to UV in order to take advantage of their important specific surface area and, thus avoid the aggregation of colloids in an environment not suitable for their stability.

After some variations of the parameters of the sol-gel synthesis of the titanium oxide nanoparticles, among which the quantity of water, the nature of the acid or of the alcohol, a protocol resulting in stable nanoparticles at least 1 month was retained and the particles formed characterized in particular by electron microscopy and DLS. It has thus been shown that the nano-objects formed are spherical and non-crystalline with diameters of the order of 5 nm.

Given the pronounced hydrophilicity of the selected suspension, for the first time, it was possible, to carry out impregnation tests of mesoporous silicas of the SBA-15 type by combining the colloidal suspension and an alkane according to the “two-solvents” impregnation method. The tests were carried out starting from two SBA-15 silica samples, one with pores diameters of about 6 nm (SBA (95)); the other having pores diameters of about 8 nm (SBA (130)). The materials obtained, when dried, were compared with reference materials prepared more conventionally by incipient wetness impregnation and characterized by N₂ sorption, XRD, UV-Vis. spectroscopy and by transmission electron microscopy. This last technique allowed us to show, at least qualitatively that, using the “two-solvents” method, the SBA-15 material with the largest pores led to the incorporation of more nanoparticles of titanium oxide in its mesopores than SBA-15 with smaller pore diameters.

The photocatalysis tests carried out with the materials prepared by the “two-solvents” impregnation method were found to be rather efficient despite the small quantities of titanium oxide present in comparison with P25 as well as the poorly defined crystallinity of the oxide. A calcination treatment at 500°C showed positive effects on the activity of the material incorporating less titanium oxide in its pores and negative on the other. Clearly, silica / titanium dioxide interactions appear to play a positive role since lower amounts of TiO₂ lead to improved conversion rates compared to the suspended nanoparticles considered alone. It is not clear at this stage if the confinement of the nanoparticles of titanium oxide in the pores is beneficial to the photocatalytic reactivity.

References

- [1] G. K. Mor, O. K. Varghese, M. Paulose, K. Shankar, C.A. Grimes, *Sol. Energy Mater. Sol. Cells*, 90 (2006) 2011.
- [2] M. A. Khan, M. S. Akhtar, O. B. Yang, *Sol. Energy*, 84 (2010) 2195.
- [3] J. Liu, H. Yang, W. Tan, X. Zhou, Y. Lin, *Electrochim. Acta.*, 56 (2010) 396.
- [4] H. Zhang, F. Banfield, *J. Mater. Chem.*, 8 (1998) 2073.
- [5] B. Li, L. Wang, B. Kang, P. Wang, Y. Qiu, *Sol. Energy Mater. Sol. Cells* 90 (2006) 549.
- [6] M. Sun, W. Fu, H. Yang, Y. Sui, B. Zhao, G. Yin, Q. Li, H. Zhao, G. Zou, *Electrochem. Commun.*, 13 (2011) 1324.
- [7] C. Li, Y. Luo, X. Guo, D. Li, J. Mi, L. Sjø, P. Hald, Q. Meng, B. B. Iversen, *J. Solid State Chem.*, 196 (2012) 504.
- [8] S. M. Yong, T. Nikolay, B.T. Ahn, D. K. Kim, *J. Alloys Compd.*, 547 (2013) 113.
- [9] C. C. Yang, Y. R. Zheng, *J. Power Sources*, 201 (2012) 387.
- [10] M. Grätzel, *J. Photochem. Photobiol. C: Photochem. Rev.*, 4 (2003) 145.
- [11] S. Sahni, S. B. Reddy, B. S. Murty, *Materials Science and Engineering: A*, 452 (2007) 758.
- [12] P. Yang, D. Zhao, D. I. Margolese, B. F. Chmelka, G. D. Stucky, *Nature*, 396 (1998) 152.
- [13] L. Chen, B. Yao, Y. Cao, K. Fan, *J. Phys. Chem. C*, 111 (2007) 11849.
- [14] Y. Sheng, L. Liang, Y. Xu, D. Wu, Y. Sun, *Optical Materials*, 30 (2008) 1310.
- [15] T. Ressler, A. Walter, Z. D. Huang, W. Bensch, *J. Catal.*, 254 (2008) 170.
- [16] R. Mellaerts, R. Mols, J. A. G. Jammaer, C. A. Aerts, P. Annaert, J.V. Humbeeck, G. van den Mooter, P. Augustijns, J. Martens, *A. Eur. J. Pharm. Biopharm.*, 69 (2008) 223.
- [17] P. Łabuz, R. Sadowski, G. Stochel, W. Macyk, *Chem. Eng. J.*, 230 (2013) 188.
- [18] M. Impéror-Clerc, D. Bazin, M.D. Appay, P. Beaunier, A. Davidson, *Chem. Mater.*, 16 (2004) 1813.
- [19] I. Lopes, N.E. Hassan, H. Guerba, G. Wallez, A. Davidson, *Chem. Mater.*, 18 (2006) 5826.
- [20] C. Salameh, J. P. Nogier, F. Launay, M. Boutros, *Catalysis Today*, 257 (2015) 35.
- [21] F. Boubekr, A. Davidson, S. Casale, P. Massiani, *Microporous and Mesoporous Materials*, 141 (2011) 157.
- [22] R. C. Weast, *Handbook of chemistry and physics*, CRC Press, Boca Raton, 1974.
- [23] D. Vorkapic, T. Matsoukas, *KONA Powder and Particle J.*, 18 (2000) 102.
- [24] Y. T. Moon, H. K. Park, D. K. Kim, C. H. Kim, *ibid.*, 78 (1995) 2690.
- [25] JH. Pan, XS. Zhao, WI. Lee. *Chem. Eng. J.*, 170 (2011) 363.
- [26] K. Assaker, B. Lebeau, C. Marichal, C. Carteret, L. Vidal, M. J. Stebe, *RSC Adv.*, 3 (2013) 14970.
- [27] JH. Pan, Z. Lei, WI. Lee, Z. Xiong, Q. Wang, XS. Zhao, *Catal. Sci. Technol.*, 2 (2012) 147.
- [28] J. Wang, Z. Bian, J. Zhu, H. Li, *J Mater. Chem. A*, 1 (2013) 1296.
- [29] V. Meynen, P. Cool, E. Vansant, *Microporous Mesoporous Mater.*, 125 (2009) 170.
- [30] D. Zhao, J. Feng, Q. Huo, N. Melosh, G.H. Fredrickson, B. F. Chmelka, G. D. Stucky, *Science*, 279 (1998) 548.
- [31] D. Zhao, Q. Huo, J. Feng, B. F. Chmelka, G. D. Stucky, *J. Am. Chem. Soc.*, 120 (1998) 6024.
- [32] K. S. W. Sing, D. H. everett, R. A. W. Haul, L. Mosenu, R. A. Pierotti, *Pure Appl. Chem.*, 57 (1985) 603.
- [33] D. Zhao, J. Feng, Q. Huo et al., *Science*, 279, (1998) 548.
- [34] R. Zukerman, L. Vradman, L. Titelman, C. Weidenthaler, M. V. Landau, M. Herskowitz, *Microporous Mesoporous Mater.*, 116 (2008) 237.
- [35] N. Bouazizi, S. Louhichi, R. Ouargli, R. Bargougui, J. Vieillard, F. Le Derf, A. Azzouz, *Applied Surface Science*, 404 (2017) 146.

CONCLUSION AND FUTURE DIRECTIONS

This PhD work, firstly examined the photocatalytic activities of commercially available metal oxides such as TiO₂ (P25 and PC-500), CeO₂, ZrO₂, CeO₂-ZrO₂, ZnO, as well as TiO₂ samples prepared in this work. This study has emphasized the potential of UV-assisted photocatalysis in acetonitrile for the selective oxidation of alcohols as well as the oxidative cleavage of activated C-C bonds in two substrates: 2-phenyl ethanol and mandelic acid.

Benzyl alcohol, used as a reference, was oxidized mainly into benzaldehyde in the presence of P25-TiO₂ and PC-500 but P25 led to a better aldehyde selectivity. The maximum yield of benzaldehyde obtained in this study was *c.a.* 60%. The results with P25 are particularly interesting. They are more particularly related to the composition (mixture of rutile and anatase) rather than to the surface properties of this material since the value of its specific surface area is low compared to that of PC500 and to the different forms of TiO₂ anatase prepared here.

Unfortunately, the conversion of benzyl alcohol appears to be limited in time. It seems that the catalyst is deactivated. We have evidenced the presence of an organic deposit on P25-TiO₂ very early in the reaction. However, it has not hitherto been possible to recover the reactivity of the catalyst after heat treatment.

Tests of different solvents has highlighted the superiority of acetonitrile and the importance of acetonitrile's ability to solubilize O₂, thus emphasizing the role of dioxygen in the whole oxidation process. Other substrates were tested under the best defined conditions for benzyl alcohol. In general, substrates with activated alcohol functions, for example in the benzylic position, have given good results but always with the limitation in terms of the amount converted, except in the case of 4-methoxybenzyl alcohol. Aliphatic alcohols that are more difficult to activate have also been tested. Of these, cyclohexanol yielded cyclohexanone in a yield of about 70%.

In the second part, nonagglomerated colloidal TiO₂ nanocrystals with well defined shape and tinny cluster sizes *ca.* 5 nm in diameter have been directly synthesized via sol-gel route at low temperature without surfactants. Thus, in this study we hypothesized to exploit the colloidal approach for the deposition of titanium oxide nanoparticles on mesoporous silica supports that are transparent to UV in order to take advantage of their important specific surface area and, thus avoid the aggregation of colloids in an environment not suitable for their stability. Among which the quantity of water, the nature of the acid or of the alcohol, a protocol resulting in stable nanoparticles at least 1 month was retained and the particles formed characterized in particular by electron microscopy and DLS. It has

thus been shown that the nano-objects formed are spherical and non-crystalline with diameters of the order of 5 nm.

After some variations of the parameters of the sol-gel synthesis of the titanium oxide nanoparticles, Given the pronounced hydrophilicity of the selected suspension, for the first time, it was possible, to carry out impregnation tests of mesoporous silicas of the SBA-15 type by combining the colloidal suspension and an alkane according to the “two-solvents” impregnation method. The tests were carried out starting from two SBA-15 silica samples, one with pores diameters of about 6 nm (SBA (95)); the other having pores diameters of about 8 nm (SBA (130)). The materials obtained, when dried, were compared with reference materials prepared more conventionally by incipient wetness impregnation and characterized by N₂ sorption, XRD, UV-Vis. spectroscopy and by transmission electron microscopy. This last technique allowed us to show, at least qualitatively that, using the “two-solvents” method, the SBA-15 material with the largest pores led to the incorporation of more nanoparticles of titanium oxide in its mesopores than SBA-15 with smaller pore diameters.

The photocatalysis tests carried out with the materials prepared by the “two-solvents” impregnation method were found to be rather efficient despite the small quantities of titanium oxide present in comparison with P25 as well as the poorly defined crystallinity of the oxide. A calcination treatment at 500°C showed positive effects on the activity of the material incorporating less titanium oxide in its pores and negative on the other. Clearly, silica / titanium dioxide interactions appear to play a positive role since lower amounts of TiO₂ lead to improved conversion rates compared to the suspended nanoparticles considered alone. It is not clear at this stage if the confinement of the nanoparticles of titanium oxide in the pores is beneficial to the photocatalytic reactivity.

Although some attempts to generalize the photocatalytic tests to different types of alcohols were found to be conclusive, under our reaction conditions, the use of TiO₂ was not fully satisfactory. Further studies with TiO₂ should aim at understanding its deactivation mechanism which seems to limit the conversion rate of the alcohols. To be complete, this study should compare the behavior toward deactivation of TiO₂ in its P25 form and TiO₂ dispersed on a silicic support. An interesting development integrating the works in annex 1 showing the interest of Ru NPs for the aerobic oxidation of alcohols would consist in the coupling of TiO₂ and Ru NPs under UV irradiance.

ANNEXES

ANNEX 1

ANNEX 2

Annexe 1

Aerobic oxidation of alcohols using ruthenium supported on DD3 kaolinite

B. Zadam^{a,b}, D. Obaid^b, A. Mayoufi^b, P. Beaunier^b, F. Launay^b, Z. El Berrichi^a

^a Laboratoire de Chimie Physique Appliquée, Guelma, Algérie.

^b Sorbonne Universités, UPMC Univ Paris 06, CNRS, UMR 7197, Laboratoire de Réactivité de Surface
4 Place Jussieu, F-75005 Paris, France

1. Introduction

Mild oxidation of alcohols into the corresponding aldehydes and ketones is an important transformation in organic chemistry that has both academic and industrial relevance [1-3]. However, stoichiometric oxidants such as compounds based on chromium (VI), manganese (VII), osmium and even lead (IV) [4,5] are often used due to their efficiency and for selectivity reasons. In this area, environmentally friendly processes minimizing additional costs of separation and waste removal are particularly needed [6]. More specifically, oxidation of alcohols with molecular oxygen performed in liquid phase in the presence of a solid catalyst achieving the highest possible yield and selectivity is targeted [7-13]. Among the wide variety of metals used, ruthenium is known to catalyze the oxidation of alcohols and other substrates via hydrido-metal or oxo-metal pathways and even radical mechanisms, depending on the oxidation state of the metal, the oxidant used and co-catalysts or additives [3].

Heterogeneous catalysts made of ruthenium nanoparticles on supports like non-natural zeolites or other synthesized inorganic supports have been tested successfully [14-18]. However, low-cost and world widely available porous natural materials with large surface area such as clays should also be considered as alternative supports for the design of heterogeneous catalysts for greener organic transformations [19-22]. Clays provide good dispersions of active sites, especially of metal nanoparticles, leading to better reactivity. Among natural clays, kaolinite which is a phyllosilicate composed of a silica tetrahedral layer $[\text{Si}_2\text{O}_5]_2$ linked through oxygen atoms to an octahedral hydroxide layer $[\text{Al}_2(\text{OH})_4]^{2+}$ may be a good candidate. Algeria possesses in the East an estimated amount of millions of tons of such clays that need to be promoted. Treatments of these natural materials with inorganic acids afford well-defined homogeneous materials ready for use as adsorbents or/and catalysts [23].

Considering the fact that the porous structure of the acid-treated kaolinite makes it a support with

Annex 1

interesting characteristics, we report, here, its use to prepare new and original Ru(0)-based heterogeneous catalysts for the aerobic oxidation of alcohols. These materials obtained by ion exchange of Djebel Debagh « DD3 » Algerian kaolinite [24] with ruthenium precursors and reduction of the metal by sodium borohydride were deeply characterized by X-ray Fluorescence (XRF), X-ray diffraction (XRD), Nitrogen sorption isotherms and TEM. Their performances were also compared with those of more conventional heterogeneous Ru(0)-based catalysts prepared starting from ZSM-5 or hexagonally structured mesoporous silicic supports of the SBA-15 type. It was expected that mineral supports such as clays, zeolites and SBA-15 should disadvantage aggregation of nanoparticles (NPs) often observed with other materials such as activated carbons due to stronger interactions between the NPs and the surface.

2. Experimental part

2.1. Materials

2.1.1. Kaolin sample "DD3"

The commercial raw clay material (DD3) was supplied by the ceramic company ETER (Guelma, Algeria). DD3 was sampled in an active kaolin mine, formed by hydrothermal alteration processes in the region of Guelma (Djebel Debagh, Algeria) [24]. This clay composed of halloysite and kaolinite (with a ratio halloysite/kaolinite = 1.23) has been used previously as an adsorbent in mortars [25] and for the removal of metals [26]. After acid activation, its cation-exchange capacity (CEC) has been estimated to 10.5 meq /100 g using UV-Vis. measurements according to the cobalt hexaammine chloride saturation method. Specific surface S_{BET} is equal to 65 m²/g. In the present study, only the < 2 μm fraction of DD3 kaolin was used after separation using standard sedimentation siphoning process following Stokes' law.

2.1.2. Chemicals and reagents

Chemicals used in Ru-based materials preparation and catalytic tests were RuCl₃ hydrate (36% Ru, 99.9%, ABCR), sodium borohydride NaBH₄ (99%, Aldrich), anhydrous benzyl alcohol (99.8%, Sigma-Aldrich), para-methoxybenzyl alcohol (98%, Sigma-Aldrich), aniline (99%, Sigma-Aldrich), *tert*-butyl hydroperoxide TBHP 5-6 M solution in decane (> 96%, Aldrich), 1,3,5-trimethylbenzene C₉H₁₂ (98%, Sigma-Aldrich) and toluene C₇H₈ (99.3%, Sigma-Aldrich).

The kaolin (DD3), gray in color, was obtained from the Guelma region (Djebel Debagh) in Algeria and supplied and enriched by ceramic company (ETER) (ceramic company, Guelma, Algeria). SBA-15 silica was synthesized according to the method reported by Zhao *et al* [27]. Na-ZSM-5 with Si/Al ratio = 12 was obtained as described by Ghezini *et al* [28]. In order to prepare the exchanged forms of ZSM-5

Annex 1

zeolite, H-ZSM-5, the synthesized material (Na-ZSM-5) was heated up to 550 °C for 5 h under atmospheric conditions.

2.2. Synthesis of ruthenium nanoparticles on DD3

Two ruthenium loadings were considered, 1 and 5 wt.%. In both cases, the support (2 µm fraction of DD3 kaolin) (1.0 g) was dispersed in 25 mL of distilled water for 24 h. Then, for the 1 wt.% sample, RuCl₃ hydrate (0.024 g (0.092 mmol)) was contacted with the solid for 2 h. Reduction occurred instantaneously after NaBH₄ introduction (0.010 g, 0.26 mmol) as shown by a color change. After 2 h, the suspension was filtered, then the catalyst washed and dried at 60°C for 24 h. Similar procedure was implemented for the preparation of Ru-SBA-15(5%), Ru/HZSM-5(5%) and Ru/NaZSM-5(1%).

2.3. Catalytic test

The catalytic reaction was carried out under magnetic stirring in 10 mL of toluene at reflux temperature with 50 mg of catalyst using 1 mmol of alcohol, 1 mmol of mesitylene (internal standard for GC) and 20 µL of 5-6 M TBHP (0.12 mmol). A stream of pure O₂ (10 mL/min) was passed through the mixture during the reaction. In the case of recycling tests, the catalyst was filtered at the end of the first use, washed several times with acetone and dried at 60°C in an oven.

2.4. Characterization

The elemental analysis of the different materials was performed by means of XRF using an energy dispersive XEPOS spectrometer (Spectro Ametek). Samples were analyzed in their powder form. Quantitative data were determined using the MicroPowder method. The X-ray diffraction (XRD) of the random-powdered powders was carried out on a Bruker D8 Advance diffractometer using the CuKα radiation in the 5 to 70° 2θ range. Textural parameters of the different materials were determined from their corresponding N₂ sorption isotherms obtained at -196°C using an ASAP 2010 Micromeritics instrument. Prior to the analysis, the samples were outgassed at 200°C until a stable static vacuum of 2.10⁻³ Torr was reached. The specific surface area was obtained by using the BET equation. Total pore volume was estimated by measuring the volume of gas adsorbed at P/P⁰ = 0.998. The volume distribution in mesopores was obtained from the desorption branch of the isotherm by applying the BJH method. Total micropores volume (< 20 Å) and, micropores size distribution were obtained using Horvath–Kawazoe method. The t-plot method was used to calculate the micropore surface area (< 2 nm) using Harkins–Jura equation. Catalytic tests were monitored by gas chromatography using a Delsi Nermag DN200 instrument equipped with a flame ionization detector and a 30 m long, 0.32 mm i.d and 1.0 µm thick capillary OPTIMA-5 Amin column (MACHEREY-NAGEL). TEM images were obtained with a JEOL-JEM 2011 microscope operated at 200 kV using an

Annex 1

accelerating voltage of 200 kV. The powdered samples had to be first dispersed in ethanol and the resulting suspensions deposited on a copper grid coated with a porous carbon film.

3. Results and discussion

The DD3 clay used as a support mainly contains silicon and aluminum in a 1: 1 molar ratio. The other elements present in large quantities are, in decreasing order, magnesium, iron, calcium, potassium, sulfur and manganese, these six elements representing about 5 wt.% of the material after acid treatment (Table 1). The introduction of ruthenium into the clay in Ru/DD3 (1%) and Ru/DD3 (5%) was quantitative and did not significantly affect the contents of other elements. Of the other supports tested, only HZSM-5 zeolite led to a quantitative inclusion of ruthenium with almost 5% experimentally for 5% expected. Due to the absence of exchange sites, the SBA-15 silica captured very little amount of ruthenium.

Table 1: Composition (%) of natural "DD3" kaolin and Ru/DD3 samples.

Material	Element (wt.%)									
	Si	Al	Mg	Fe	Ca	K	S	Mn	Ru	Si/Al*
DD3	24.6	20.7	2.3	1.15	0.1	0.5	0.3	0.9	-	1.1
Ru-DD3(1%)	25.2	19.7	2.0	1.1	0.2	0.6	0.3	0.9	1	1.2
Ru-DD3(5%)	24.2	19.5	0.5	1.1	0.2	0.6	0.4	0.8	5	1.2
Ru-NaZSM-5(1%)	43.4	3.1	<0.1	0.4	0.1	<0.1	<0.1	<0.1	0.5	13.5
Ru-HZSM-5(5%)	42.6	2.2	<0.1	<0.1	<0.1	<0.1	<0.1	<0.1	4.9	18.7
Ru-SBA-15(5%)	46.5	<0.1	<0.1	<0.1	<0.1	<0.1	<0.1	<0.1	0.3	-

* molar ratio. Na not measured.

The X-ray diffractogram of natural DD3 (Figure 1A) is compatible with a basal reflection at 7.35 Å (halloysite) [29]. Some evidences for illite were observed also.

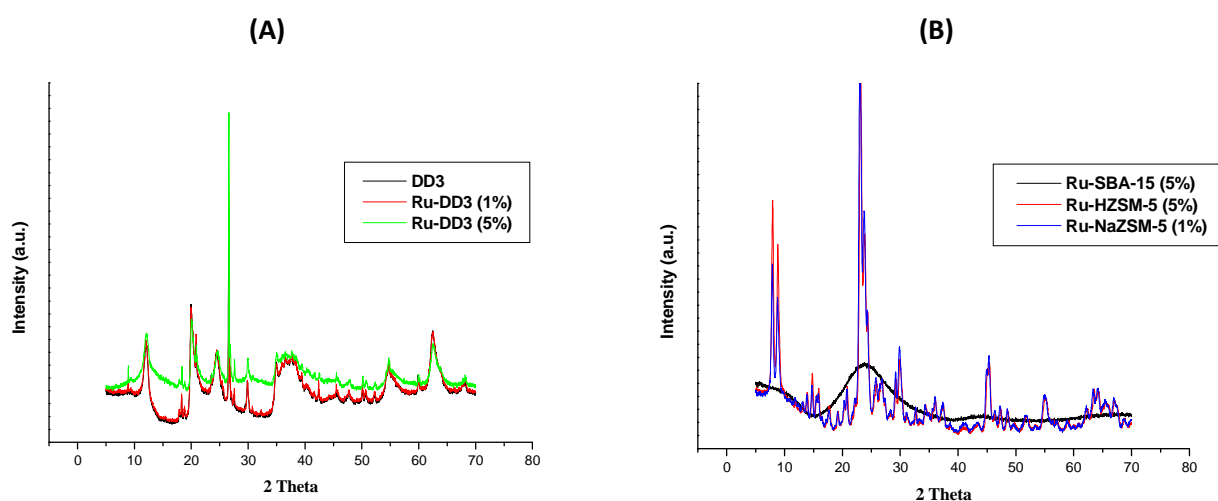


Figure 1: X-ray diffractograms of (A) DD3, (B) SBA-15 and ZSM-5 derived samples.

Annex 1

No significant difference could be detected in the X-ray diagrams of Ru-DD3(1%) and Ru-DD3(5%) samples. Their diffractograms are exactly superimposed with that of DD3. This means that the elaboration process of the nanoparticles did not change significantly the basal spacing of the clay indicating that the crystal structure of kaolinite clay DD3 was retained. There are also no diffraction peaks corresponding to metallic ruthenium, which would indicate that the metallic nanoparticles formed on the DD3 support must be particularly of small size and highly dispersed. Expected values of 2θ would have been 38.5, 44.2, 58.5, 69.7, 78.7 and 86.3° [30]. The same is observed for Ru-NaZSM-5(1%), Ru-HZSM-5(5%) and Ru-SBA-15(5%) (Figure 1B).

TEM images showed that no separate aggregates were observed in Ru-DD3(5%) (Figure 2). Very small particles that are generally well distributed over the whole of the grains are observed in large quantities especially around the periphery of the curled sheets typical for this type of clay. Diameters are in the 1-3 nm range with an average value around 1.6 nm. The ruthenium particles formed by the chemical reduction of the ruthenium(III) salt by NaBH_4 on the other supports (HZSM-5, NaZSM-5 and SBA-15, see Figure 3) are also small. This seems to be more related to the reduction mode and the nature of the metal rather than to a support effect. In the case of Ru/SBA-15(5%), TEM images show that much of the nanoparticles formed are located within the mesopores network.

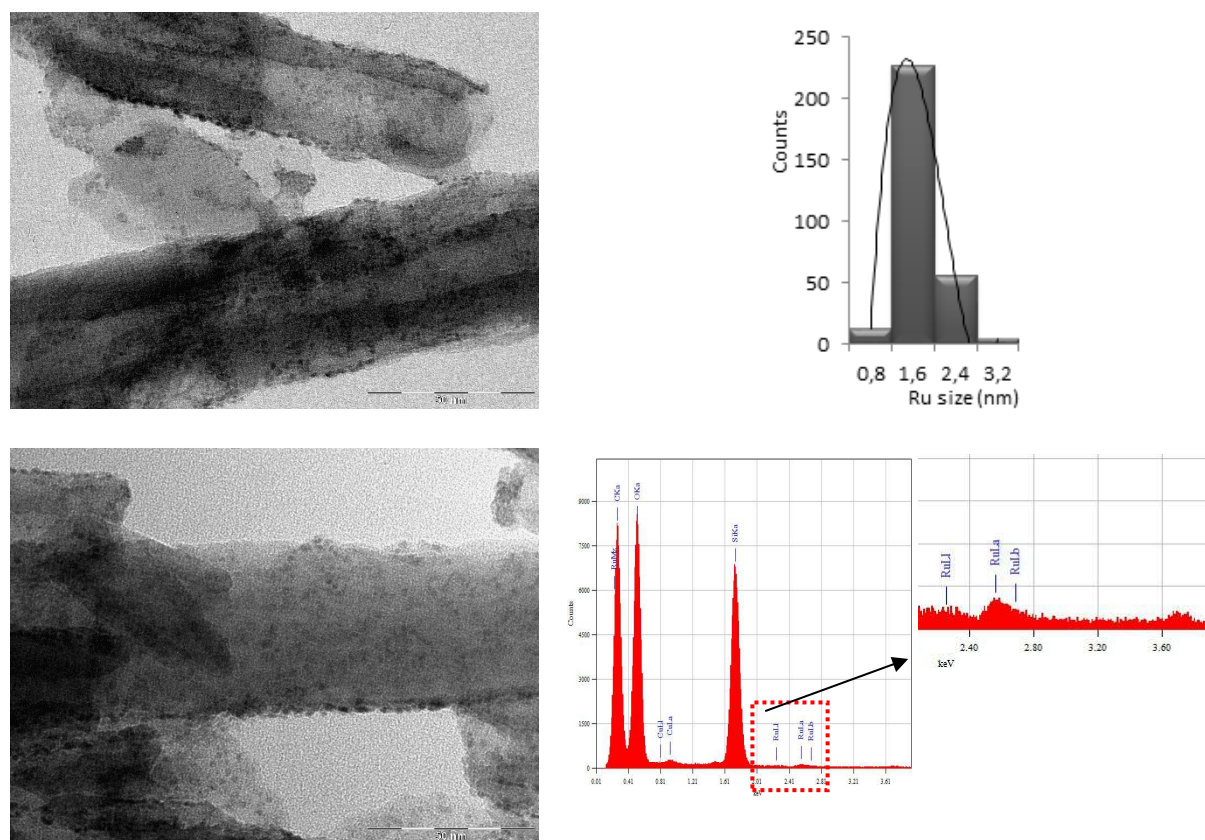


Figure 2: TEM images of Ru-DD3(5%), size distribution of Ru nanoparticles and EDX spectrum emphasizing Ru in the insert.

Annex 1

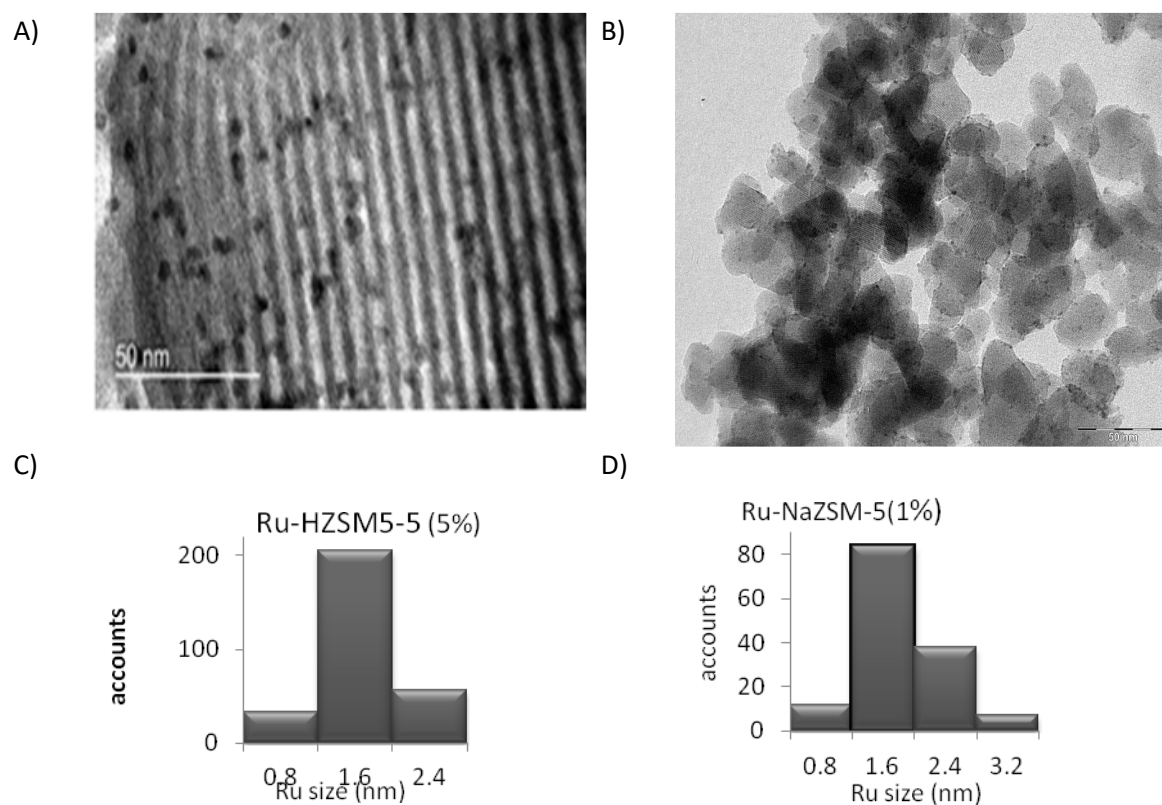


Figure 3 : TEM images of (A) : Ru-SBA-15(5%), (B) : Ru-HZSM5-5(5%) and size distribution histograms (C) : Ru-HZSM-5(5%) and Ru-NaZSM-5(1%).

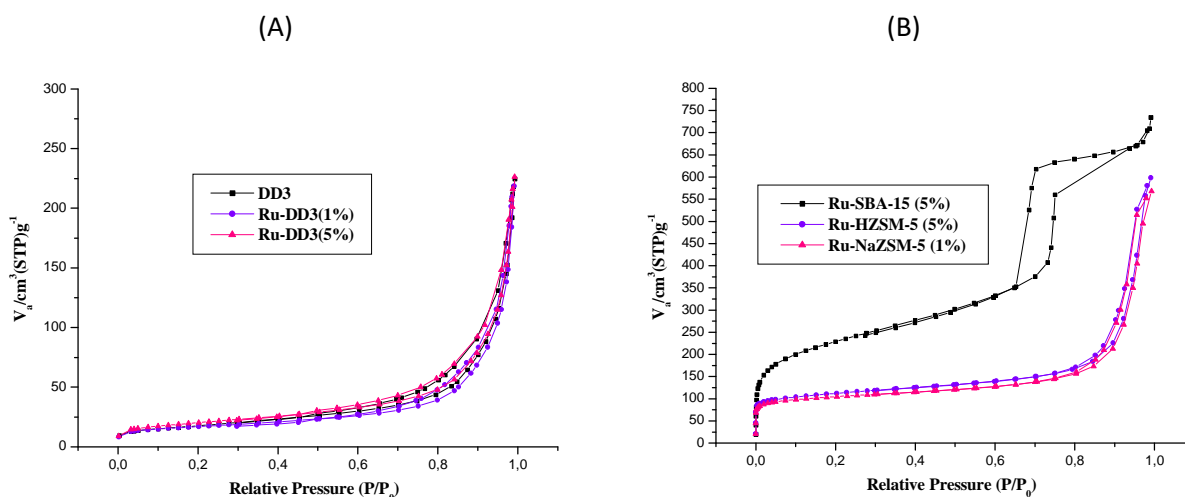


Figure 4: N_2 adsorption-desorption isotherms of (A) DD3, (B) SBA-15 and ZSM-5 derived samples.

Isotherms of DD3 samples (Figure 4A) include a H1 hysteresis loop that is typical of sub-micron materials with interparticle porosity. This one is however present in a lower extent than in the case of the zeolites considered, i.e. Ru-HZSM-5(5%) and Ru-NaZSM-5(1%) (Figure 4B). The step in the low

Annex 1

pressure range is also much less sharp than for the zeolites and even for the SBA-15 type sample emphasizing less microporosity for the clays. As expected, SBA-15 is characterized by the most important mesopore volume of the series.

Table 2. Textural properties of the different DD3 and Ru supported-materials tested.

Materials	S_{BET} ($\text{m}^2\cdot\text{g}^{-1}$)	Total pore volume ($\text{cm}^3\cdot\text{g}^{-1}$) $P/P^0 = 0.998$	$S_{\text{micropores}}$ t-plot	$V_{\text{micropores}}$ t-plot	Micropore diameter HK (nm)
DD3	62	0.37	60	0.001	1.2
Ru-DD3 (1%)	59	0.34	61	0	1.2
Ru-DD3 (5%)	73	0.34	70	0	1.2
Ru-NaZSM-5(1%)	131	0.89	165	0.1	-
Ru-HZSM-5(5%)	138	0.84	164	0.1	-
Ru-SBA-15(5%)	808	1.06	100	0.04	-

The materials thus described were tested in the context of the aerobic oxidation of alcohols and more particularly of benzyl alcohol in toluene at 100°C. The conditions chosen hereafter were defined after optimization of some parameters such as the flow rate of O₂ and the addition of *tert*-butyl hydroperoxide added (Table 3). These preliminary tests were carried starting with the catalyst with the highest loading in Ru, i.e. Ru-DD3(5%) for a substrate / Ru ratio equal to 40 over a period of 3 hours.

Table 3 : Influence of some parameters on the oxidation of benzyl alcohol by O₂ in the presence of Ru-DD3(5%)^a.

Entry	O ₂ flow (mL/min)	TBHP 5.5 M (μL)	Conversion (%)	Selectivity (%)	Yield (%)
1	0	0	100	94.5	94.5
2	0	20	94	93	87
3	10	0	100	96	96
4	10	10	100	96	96
5	10	20	100	97	97
6	20	20	100	96	96

^a Catalyst amount, 50 mg; benzyl alcohol 1 mmol; solvent, toluene 10 mL; reaction temperature 100°C.

Under static air, the oxidation of benzyl alcohol occurred but the reaction was incomplete (Table 3, entry 1). Two approaches have been adopted to improve the performance of the Ru-DD3 catalyst. On the one hand, *tert*-butyl hydroperoxide (TBHP) was added in sub-stoichiometric quantity (10 mol%

Annex 1

relative to the substrate) to serve as radical initiator upon heating to 100°C. The conversion rate of benzyl alcohol of *c.a.* 94% was the worst obtained and the yield of benzaldehyde lower than 90% (Table 3, entry 2). On the other hand, the reaction was carried out under a flow of O₂ at 10 mL / min without TBHP, which resulted in a substantial improvement of the yield of aldehyde (Table 3, entry 3). Other attempts were made using simultaneously TPHP and O₂. In these additional tests, the amount of TBHP was varied between 10 and 20 μL, the O₂ flow rate between 10 and 20 mL / min. Above 20 μL of TBHP 5.5 M in decane (not shown here) and for a flow rate greater than 10 mL / min, it appears that the yield of benzaldehyde no longer increases. The conversion is equal to 100% and the benzaldehyde selectivity is about to 97%. In all cases, the formation of benzoic acid could not be observed directly or after attempts of esterification in the presence of a catalytic amount of sulfuric acid and methanol under reflux.

Then, the activity of the various catalysts based on supported Ru nanoparticles was examined in 3 h catalytic tests carried out at constant weight (Table 4). Reaction conditions of Table 3, entry 5 were used. One of the catalyst, Ru-NaZSM-5(1%) was tested for a longer time, 6 hours instead of 3, but this time extension did not lead to significant changes. After 6 h, the yield of benzaldehyde was approximately the same than after 3 h. Further conversion of benzyl alcohol between 3 and 6 h led apparently to unselective oxidation of the latter.

Table 4: Oxidation of benzyl alcohol into benzaldehyde over Ru based catalysts in toluene suspension using O₂.

Entry	Catalyst	Ru loading (wt. %)	Subst./Ru (mol/mol)	t (h)	Conversion (%)	Selectivity (%)	Yield (%)
1	DD3	0	-	3	46	23	11
2	Ru-SBA-15(5%)	0,33	613	3	19,5	92	18
3	Ru-NaZSM-5(1%)	0,5	396	3 (6)	92 (97)	75 (71)	69 (69)
4	Ru/DD3(1%)	1	200	3	56	77	43
5	Ru-HZSM-5(5%)	5	40	3	100	67	67
6	Ru/DD3(5%)	5	40	3	100	97	97

Catalyst amount, 50 mg; benzyl alcohol 1 mmol; solvent, toluene 10 mL; O₂ flow, 10 mL/min; *tert*-butyl hydroperoxide 0.1 mmol; reaction temperature 100°C.

Regardless of the nature of the support, the values of the conversion of benzyl alcohol increase monotonically with the amount of ruthenium actually introduced into the reaction medium. This is linked a priori to the almost identical size of the NPs obtained on the different materials and to the good accessibility of the latter for all supports considered. However, we note a settlement of the conversion rate for substrate / Ru molar ratio values lower than 200 (i.e. for ruthenium loadings

Annex 1

greater than 1 wt.%). Benzaldehyde is always the major compound obtained. Of all the catalysts tested, only Ru-DD3(5%) led to the quasi-quantitative production of aldehyde, its yield reaching 97% in 3 h (Table 4, entry 6). As expected, the aldehyde selectivity tends to decrease with the increase in conversion rates and hence the ruthenium content. In this trend, Ru-DD3(5%) catalyst distinguished from others by the quasi-exclusive production of benzaldehyde. Between Ru-HZSM-5(5%) (Table 4, entry 5) and Ru-DD3(5%) (Table 4, entry 6), there is almost a 30% difference in benzaldehyde selectivity for Ru-DD3(5%). As shown in Table 1, the natural clay support differs from the synthetic ones by the presence of traces of magnesium, iron, manganese, and in smaller proportions of potassium, calcium and sulfur. The superiority of Ru-DD3(5%) could be related to a synergy between these elements and ruthenium. In any case, DD3 alone does not suitably catalyze the formation of benzaldehyde since the yield does not exceed 11% and the selectivity to aldehyde is very low (Table 4, entry 1 vs. 6).

para-Methoxybenzyl alcohol was also tested with Ru/DD3(5%) in the conditions optimized for benzyl alcohol previously (cf table 4, entry 6) but this alcohol was converted with a much less extent than benzyl alcohol (76% instead of 100%). The yield of para-methoxy benzaldehyde was 71% only compared to 97% for the benzaldehyde production. Such result emphasizes the negative influence of the electron donating properties of the methoxy group on the oxidation performances of such catalyst. Either oxidizing species are not electrophilic in our conditions or more probably, stronger interactions of the aromatic ring of para-methoxybenzyl alcohol with the surface of the NPs compared to benzyl alcohol is detrimental.

The most effective catalyst of this study was further investigated. Thus, Ru-DD3(5%) was tested on five successive runs carried out with the same material. Between each test, the reaction medium was filtered, and the solid recovered washed, then dried overnight before the next test. The results are shown in Table 5.

Table 5: Recyclability of Ru/DD3 (5%) in the aerobic oxidation of benzyl alcohol.

Run	Alcohol conversion (%)	Benzaldehyde selectivity (%)	Benzaldehyde yield (%)
2 nd	99	63	62
5 th	99.5	56	55

Catalyst amount, 50 mg, then recovered amount; benzyl alcohol 0.1 mmol; toluene solvent 10 mL; O₂ flow, 10 mL/min; reaction temperature 100°C; reaction time 3 h.

The test conditions were maintained over all the tests. At no time the conversion into alcohol was

Annex 1

affected. This was constantly equal to c.a. 100%. On the other hand, the selectivity to aldehyde decreased from 97 to 55% over the five runs. In fact, fluorescence X analysis of the catalyst after one test pointed an important loss of rhodium with a loading of 3 wt.% instead of 5 wt.%. Then, throughout the four other tests, the Ru content did not strongly evolve and the activity of the recovered catalysts too, as shown in table 5. The small variation of benzaldehyde selectivity from test n°2 to n°5 could be due to changes in the substrate / Ru ratio which inevitably decreased due to the catalyst losses caused by this protocol. In any case, the benzaldehyde selectivity (between 63 and 56%) turned out to be lower than that (77%) obtained with a unique test of Ru/DD3(1%) (see table 4, entry 4). In the experiment of recyclability of RuDD3(%) (table 5), it is more likely that the change in oxidation state of ruthenium on the surface of nanoparticles over the tests is responsible for the drop of the selectivity to aldehyde. In any case, a significant increase in the size of the nanoparticles cannot be incriminated as evidenced by the TEM images of the recovered material (Fig. 5). Indeed, most of the NPs appear to be still well dispersed and the mean value of their diameter is c.a. 2 nm.

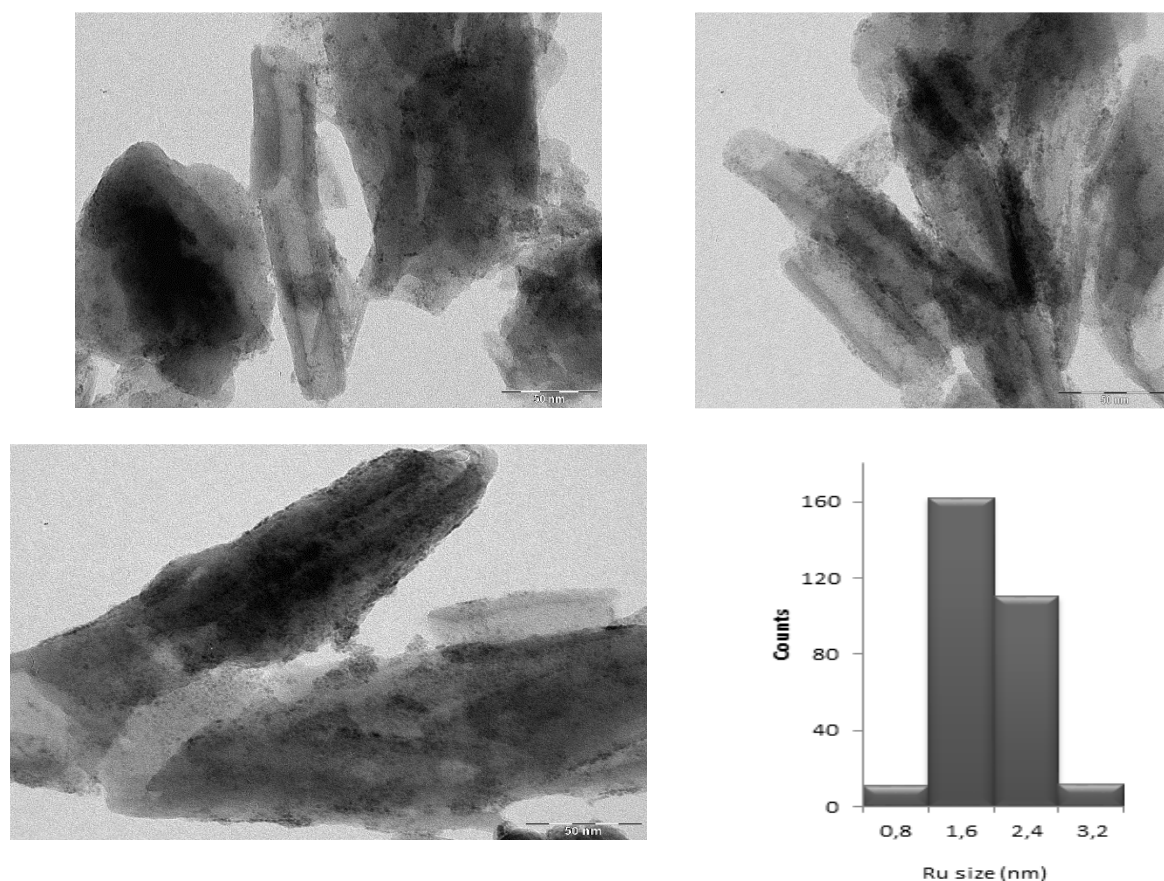


Fig. 5 : TEM image of the Ru-DD3(5%) catalyst after the 5th run and histogram of the Ru NPs size (c.a. 300 counts).

4. Conclusion

In this work, we have shown that Ru(0) nanoparticles can be prepared quasi-quantitatively on natural clays (DD3) consisting essentially in kaolinite. The Ru(0) NPs were obtained by the reduction of Ru(III) ions previously exchanged with the counter-ions of the DD3 material, the latter being activated by a prior acid treatment. Comparison with supports with (ZSM-5) or without cation exchange properties (SBA-15 silica) has highlighted the very good incorporation capacities of the clay. However, the NPs size distribution appeared to be independent of the nature of the support. The materials thus produced were tested in the context of the oxidation of benzyl alcohol. At 100°C, under a stream 10 mL/min O₂ flow and with 10 mol% of *tert*-butyl hydroperoxide with respect to the substrate, the yield of benzaldehyde is c.a. 97%. Unfortunately, the catalysts thus produced suffer from a strong leaching after one test and then, a progressive deactivation linked a priori to the modification of the surface properties of the nanoparticles [14]. RuDD3(5%) also catalyzed the selective oxidation of *p*-methoxy benzyl alcohol into *p*-methoxy benzaldehyde. Recently, Y. Zhang *et al* have shown that the oxidation of alcohols can be coupled to the formation of imines involving the carbonyl derivative produced and an amine present at the start of the reaction [31]. The solvent and temperature conditions were substantially the same as ours. We have therefore carried out an exploratory test by adding a stoichiometric amount of aniline to the reaction medium involving Ru-DD3 (5%) and benzyl alcohol, the whole transformation being performed under the conditions optimized before for the oxidation reaction (Table 4, entry 6), but for 14 h. Under these conditions, the presence of the amine seems to slow down the oxidation of the alcohol, probably by poisoning of the nanoparticles of Ru since the conversion of the benzyl alcohol was greatly reduced. On the other hand, benzaldehyde is no longer present because of its complete transformation *in situ* into the corresponding imine identified by GC-MS, thus underlining the feasibility of the second reaction with the catalysts developed here.

Acknowledgements : One of us, Bisma Zadam thanks the Algerian government and her university for allowing her to spend a two-month scientific stay in France at the Laboratoire de Réactivité de Surface.

References

- [1] J. I. Kroschwitz, Kirk Othmer Encyclopedia of Chemical Technology, vol. 4, 4th edn., Wiley-Interscience Publication, New York, 1992.
- [2] T. Mallat, A. Baiker, Oxidation of alcohols with molecular oxygen on solid catalysts, Chem. Rev. 104 (2004) 3037-3058.
- [3] F. Adam., E.A. Sugiarmawan, A porous ruthenium silica catalyst modified with amino benzoic acid for the

Annex 1

oxidation of butanol with molecular oxygen, *J. Porous Mater.* 16 (2009) 321-329.

[4] G. Cainelli, G. Cardillo, *Chromium Oxidants in Organic Chemistry*, Springer, Berlin, 1984.

[5] D.G. Lee, U.A. Spitzer, *J. Org. Chem.* 35 (1970) 3589.

[6] B.M. Choudary, M.L. Kantam, P.L. Santhi, New and ecofriendly options for the production of speciality and fine chemicals, *Catal. Today* 57 (2000) 17-32.

[7] M. Besson, P. Gallezot, Selective oxidation of alcohols and aldehydes on metal catalysts, *Catal. Today* 57 (2000) 127-141.

[8] I.W.C.E. Arends, R.A. Sheldon, in: E. Bäckvall (Ed.), *Modern oxidation methods of alcohols using environmentally benign oxidants*, Wiley-VCH, Weinheim, 2004, p. 147-186.

[9] B.Z. Zhan, A. Thompson, Recent development in the aerobic oxidation of alcohols, *Tetrahedron* 60 (2004) 2917-2934.

[10] T. Mallat, A. Baiker, Oxidation of alcohols with molecular oxygen on platinum metal catalysts in aqueous solutions, *Catal. Today* 19 (1994) 247-283.

[11] R.A. Sheldon, I.W.C.E. Arends, A. Dijkman, New developments in catalytic alcohol oxidations for fine chemicals synthesis, *Catal. Today* 57 (2000) 157-166.

[12] A.P. Markusse, B.F.M. Kuster, J.C. Schouten, Platinum catalysed aqueous alcohol oxidation: experimental studies and reaction model discrimination, *J. Mol. Catal. A* 158 (2000) 215-222.

[13] J. Muzart, Palladium-catalysed oxidation of primary and secondary alcohols, *Tetrahedron* 59 (2003) 5789-5816.

[14] E.J. García-Suárez, M. Tristany, A.B. García, V. Collière, K. Philippot, Carbon-supported Ru and Pd nanoparticles: Efficient and recyclable catalysts for the aerobic oxidation of benzyl alcohol in water, *Microporous and Mesoporous Materials* 153 (2012) 155-162.

[15] B.-Z. Zhan, M.A. White, T.-K. Sham, J.A. Pincock, R.J. Doucet, K.V. Ramana Rao, K.N. Robertson, T.S. Cameron, Zeolite-Confined Nano-RuO₂: A Green, Selective, and Efficient Catalyst for Aerobic Alcohol Oxidation, *J. Am. Chem. Soc.* 125 (2003) 2195-2199.

[16] V.V. Costaa, M.J. Jacinto, L.M. Rossi, R. Landers, E.V. Gusevskaya, Aerobic oxidation of monoterpenic alcohols catalyzed by ruthenium hydroxide supported on silica-coated magnetic nanoparticles, *J. Catal.* 282 (2011) 209-214.

[17] S.G. Peng, M.R. Weng, J.G. Han, Y.K. Guo, Y.G. Zhang, Shiyou Xuebao, Shiyou Jiagong 25 (2009) 80-83.

[18] M.J. Jacinto, O.H.C.F. Santos, R. F. Jardim, R. Landers, L. M. Rossi, Preparation of recoverable Ru catalysts for liquid-phase oxidation and hydrogenation reactions, *Appl. Catal. A: Gen.* 360 (2009) 177-182.

[19] B.J. Borah, D. Dutta, P.P. Saikia, N.C. Baruah, D.K. Dutta, Stabilization of Cu(0)-nanoparticles into the nanopores of modified montmorillonite: An implication on the catalytic approach for "Click" reaction between azides and terminal alkynes, *Green Chem.* 13 (2011) 3453-3460.

[20] G. Nagendrappa, Organic synthesis using clay and clay-supported catalysts., *Appl. Clay Sci.* 53 (2011) 106-138.

[21] G. Nagendrappa, Organic synthesis using clay catalysts, *Resonance* 7 (2002) 64-77.

[22] R.S. Varma, Clay and clay-supported reagents in organic synthesis, *Tetrahedron* 58 (2002) 1235-1255.

[23] A. Amari, M. Chlendi, A. Gannouni, A. Bellagi, Optimised for toluene activation of bentonite adsorption, *Appl. Clay Sci.* 47 (2010) 457-461.

[24] A. Boulmouk, Y. Berredjem, K. Guerfi, A. Gheid, Kaolin from Djebel Debbaghe Mine Geulma, Algeria, *Res. J. Appl. Sci.* 2 (2007) 435-440.

[25] B. Rabehi, K. Boumchedda, Y. Ghernouti, Study of calcined halloysite clay as pozzolanic material and its potential use in mortars, *Int. J. Phys. Sci.* 7 (2012) 5179-5192.

[26] S. Mellouk, S. Cherifi, M. Sassi, K. Marouf-Khelifa, K.A. Bengueddach, J. Schott, A. Khelifa, Intercalation of halloysite from Djebel Debagh (Algeria) and adsorption of copper ions, *Appl. Clay Sci.* 44 (2009) 230-236.

[27] D. Zhao, Q. Huo, J. Feng, B.F. Chmelka, G.D. Stucky, Continuous mesoporous silica films with highly ordered large pore structures, *J. Am. Chem. Soc.* 120 (1998) 6024-6036.

[28] R. Ghezini, M. Sassi, A. Bengueddach, Adsorption of carbon dioxide at high pressure over H-ZSM-5 type zeolite, *Microporous and Mesoporous Materials* 113 (2008) 370-377.

[29] S. Zen, F. Zohra El Berrichi, Adsorption of tannery anionic dyes by modified kaolin from aqueous solution, *Desalination and Water Treatment ???* (2014) 1-9.

[30] N. Thi Bich Hien, H. Young Kim, M. Jeon, J. Hee Lee, M. Ridwan, R. Tamarany, C. Won Yoon, Ru-N-C Hybrid Nanocomposite site for Ammonia Dehydrogenation: Influence of N-doping on Catalytic Activity, *Materials* 8 (2015) 3442-3455.

[31] Y. Zhang, F. Lu, H.-Y. Zhang, J. Zhao, Activated Carbon Supported Ruthenium Nanoparticles Catalyzed Synthesis of Imines from Aerobic Oxidation of Alcohols with Amines, *Catal. Lett.* 147 (2017) 20-28.

Annexe 2

I. Calibration curves used for the determination of the conversion, selectivity and yield values using the internal standard method.

- Benzyl alcohol oxidation

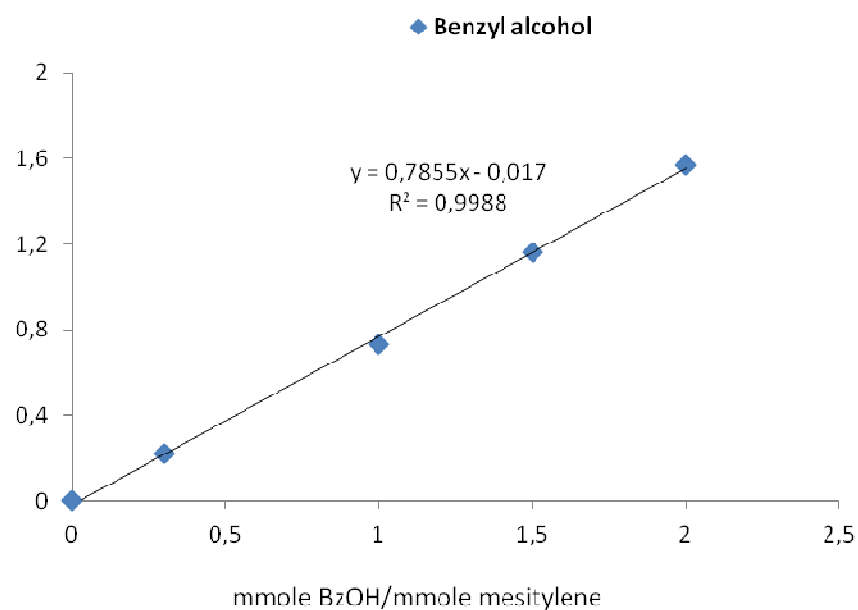


Figure 1: Quantification of benzyl alcohol using mesitylene as internal standard.

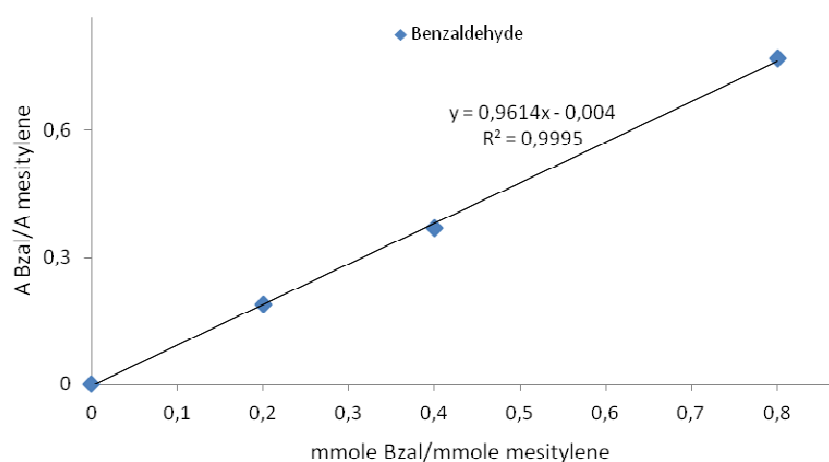


Figure 2: Quantification of benzaldehyde using mesitylene as internal standard.

Annex 2

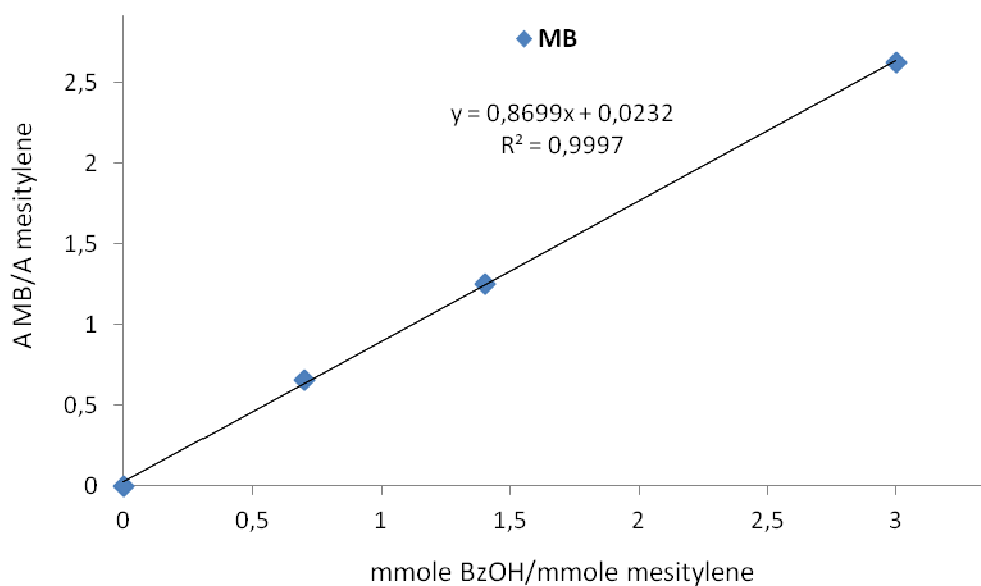


Figure 3: Quantification of methyl benzoate using mesitylene as internal standard.

The amount of methyl benzoate determined by this curve refer to benzoic acid formed after converting it to methyl benzoate via a total esterification of the withdrawn aliquot in the presence of an excess of methanol and 2 drop of concentrated sulfuric acid.

- Cyclohexanol oxidation

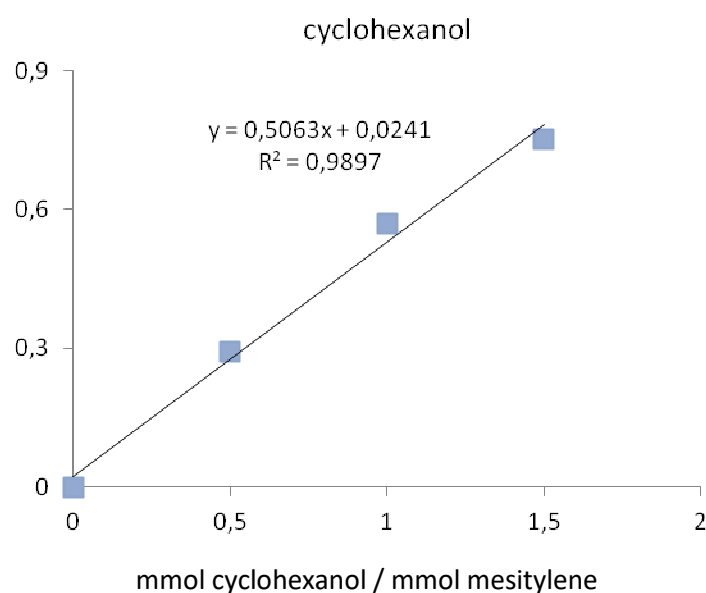


Figure 4: Quantification of cyclohexanol using mesitylene as internal standard.

Annex 2

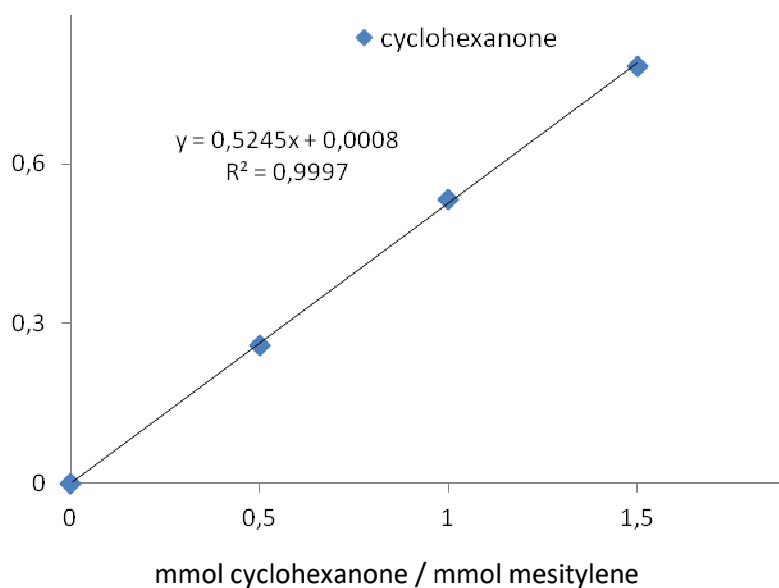


Figure 5: Quantification of cyclohexanone using mesitylene as internal standard.

II. List of reagents and solvents used

- Solvents and acids

Product name	Formula	Purity %	Company
Acetic acid	CH ₃ COOH	68.8%	SIGMA-ALDRICH
Acetone	CH ₃ COCH ₃	99.9%	SIGMA-ALDRICH
Acetonitrile	CH ₃ CN	99.8%	SIGMA-ALDRICH
Cyclohexane	C ₆ H ₁₂	99,5%	SIGMA-ALDRICH
Ethanol	C ₂ H ₅ OH	99.8%	SIGMA-ALDRICH
Ethyl acetate	CH ₃ COOC ₂ H ₅	99.8%	SIGMA-ALDRICH
Hexane	C ₆ H ₁₄	95%	SIGMA-ALDRICH
Hydrochloric acid	HCl	35%	SIGMA-ALDRICH
Mesitylene	C ₆ H ₃ (CH ₃) ₃	99.3%	SIGMA-ALDRICH
Methanol	CH ₃ OH	99.8%	SIGMA-ALDRICH
Nitric acid	HNO ₃	99.9%	SIGMA-ALDRICH
Sulfuric acid	H ₂ SO ₄	98 %	SIGMA-ALDRICH
Toluene	C ₆ H ₅ CH ₃	99.3%	SIGMA-ALDRICH

- Minerals

Product name	Formula	Purity %	Company
Ceria oxide	CeO ₂ HAS-1A	98%	Rhone-Poulenc
Ceria oxide- zirconia oxide	CeO ₂ - ZrO ₂	-	Rhone-Poulenc
Ruthenium trichloride	RuCl ₃	99%	SIGMA-ALDRICH
Titanium dioxide P25 70% Anatase, 30% Rutile	P25-TiO ₂	99 %	Degussa
Titanium dioxide Anatase	TiO ₂	99.9%	Janssen Chimica
Titanium dioxide, Millennium PC500	TiO ₂	99.9%	Millennium Inorganic Chemicals

Annex 2

Titanium dioxide, Rutile	TiO ₂	99 %	Rhodia
Zirconia oxide	ZrO ₂	99%	Rhone-Poulenc
Zinc oxide	ZnO	99%	Vieille Montagne
Zirconium(IV) oxychloride octahydrate	ZrOCl ₂ ·8H ₂ O	98%	SIGMA-ALDRICH

- Organics

Product name	Formula	Purity %	Company
Acetophenone	C ₆ H ₅ COCH ₃	99%	Fluka
Adipic acid	C ₆ H ₁₀ O ₄	99.9%	Jassen
Benzyl alcohol	C ₆ H ₅ CH ₂ OH	99.8%	SIGMA-ALDRICH
Benzaldehyde	C ₆ H ₅ CHO	99.5%	SIGMA-ALDRICH
Benzyl benzoate	C ₆ H ₅ COOCH ₂ C ₆ H ₅	99%	SIGMA-ALDRICH
Benzoic acid	C ₆ H ₅ COOH	99.5%	SIGMA-ALDRICH
Benzophenone	C ₆ H ₅ COC ₆ H ₅	99%	SIGMA-ALDRICH
Cyclohexanol	C ₆ H ₁₁ OH	99%	SIGMA-ALDRICH
Cyclohexanone	C ₆ H ₁₀ (=O)	99.8%	SIGMA-ALDRICH
Diphenyl methanol	(C ₆ H ₅) ₂ CHOH	99%	SIGMA-ALDRICH
1-hexanol	CH ₃ (CH ₂) ₅ OH	99%	SIGMA-ALDRICH
1-hexanal	CH ₃ (CH ₂) ₄ CHOH	99%	SIGMA-ALDRICH
3-hexanol	CH ₃ CH ₂ CH ₂ CH(OH)CH ₂ CH ₃	97%	SIGMA-ALDRICH
3-hexanone	CH ₃ CH ₂ CH ₂ COCH ₂ CH ₃	97%	SIGMA-ALDRICH
Mandelic acid	C ₆ H ₅ CH(OH)CO ₂ H	99%	SIGMA-ALDRICH
Methyl benzoate	C ₆ H ₅ COOCH ₃	99%	SIGMA-ALDRICH
2-methyl cyclohexanol	2-CH ₃ -C ₆ H ₁₁ OH	99%	SIGMA-ALDRICH
2-methyl cyclohexanone	CH ₃ C ₆ H ₉ O	99%	SIGMA-ALDRICH
4-methoxybenzyl alcohol	4-CH ₃ O-C ₆ H ₅ CH ₂ OH	99%	SIGMA-ALDRICH
4-methoxy benzaldehyde	4-CH ₃ O-C ₆ H ₅ CHO	99%	SIGMA-ALDRICH
1-phenyl ethanol	C ₆ H ₅ CH(OH)CH ₃	99%	EGA-Chmie
2-phenyl ethanol	C ₆ H ₅ CH ₂ CH ₂ OH	99%	SIGMA-ALDRICH
Poly(ethylene glycol)-block-poly(propylene glycol) blockpoly(ethylene glycol)	HO(CH ₂ CH ₂ O) ₂₀ (CH ₂ CH(CH ₃)O) ₇₀ (CH ₂ CH ₂ O) ₂₀ H Pluronic (P123)	-	SIGMA-ALDRICH
tert-Butyl hydroperoxide solution, TBHP	(CH ₃) ₃ COOH	6 M in decane	SIGMA-ALDRICH
Tetraethyl orthosilicate (TEOS)	Si(OEt) ₄	98%	SIGMA-ALDRICH
Titanium (IV) isopropoxide	Ti[OCH(CH ₃) ₂] ₄	98%	SIGMA-ALDRICH

Table des illustrations

Part I / Chapitre 1

Figure I.1: Composition of solar energy on earth	7
Figure I.2: Principle of photocatalysis in the presence of excited TiO ₂ [10]	8
Figure I.3: SEM images of (a, b) TiO ₂ NBs and (c) Ru/TiO ₂ NB heterostructures	19
Figure I.4: TEM images of calcined mesoporous materials. Mesoporous Metal oxides are calcined at 350°C in air for 5 h to remove organic polymer templates. Al ₂ O ₃ , Nb ₂ O ₅ , and 4 ZrO ₂ -P ₂ O ₅ samples are calcined at 500°C	23
Figure I.5: TEM images of mesoporous titania thin films calcined at (a) 750 and (b) 850 °C, respectively, modified with stearic using spin coating method	25
Figure I.6: Formation of mesoporous titania by the action of silica nanoparticles on titania nanoparticles under different Si/Ti ratios: Si/Ti = 0 (A), Si/Ti = 0.75 (B), 0 < Si/Ti < 0.75 (C) and Si/Ti >0.75 (D) [111]	27
Scheme I.1: Mineralization <i>versus</i> selective oxidation [15]	8
Scheme I.2: Oxidation reaction pathway of benzyl alcohol (products distribution) [16]	9
Scheme I.3: Two-electron transfer mechanism in the oxidation of alcohols in the absence of O ₂ [19]	10
Scheme I.4: Oxygen transfer process in the TiO ₂ photocatalytic oxidation of alcohols in BTF solvent in the presence O ₂ [19]	11
Scheme I.5: Probable photocatalytic oxidation mechanism of benzyl alcohol into benzaldehyde in the presence of TiO ₂ under UV light [21]	11
Scheme I.6: Probable mechanism of selective oxidation of benzyl alcohol by TiO ₂ /Cu(II)/UV [23]	12
Scheme I.7: Role of proton in acceleration of the disproportionation decomposition [28]	14
Scheme I.8: Surface structures of benzyl alcohol adsorbed-TiO ₂ [40]	15
Scheme I.9: Selective oxidation of alcohols over Au- under Visible light irradiation [49]	16
Scheme I.10: Mechanism of mesoporous TiO ₂ in photooxidation of benzyl alcohol under visible light, with creating new energy levels [90]	22
Scheme I.11: Synthesis of the KRICT-MT via replication of the CA-templated mesoporous silica [110]	27

Part I / Chapitre 2

Figure II.1: Tauc plots for the different materials tested in benzylalcohol oxidation under UV irradiance	36
Figure II.2: Reactor set-up used in the photocatalytic experiments	37
Figure II.3: UV light model as source of irradiance, Mercury Lamp	38
Figure II.4: X-ray diffraction of mesoporous TiO ₂ synthesized via the hard template method and its key intermediates: (■) TiO ₂ -SiO ₂ composite dried at 85°C, (■) TiO ₂ -SiO ₂ composite calcined at 500°C before treatment in 2 M NaOH medium and (■) Meso-TiO ₂ after treatment in NaOH 120°C	39
Figure II.5: N ₂ adsorption-desorption isotherms at -196°C and pore size distribution of meso TiO ₂ -S1 and its SBA-15 precursor	40
Figure II.6: HR-TEM photographs of MesoTiO ₂ -S1	40
Figure II.7: XRD patterns of TiO ₂ samples prepared using the sol gel oute as a function of the thermal treatment of the recovered solids (120-450°C)	41

Figure II.8: N ₂ adsorption-desorption isotherms at -196°C of TiO ₂ samples prepared using the sol gel route as a function of the thermal treatment of the recovered solids (120-450°C)	41
Figure II.9: Influence of a) reaction temperature (b) catalyst loading and (c) oxygen flow rate on the oxidation of benzyl alcohol	42
Figure II.10: Time profile of the photocatalytic oxidation of benzyl alcohol over P25 in acetonitrile at 50°C under oxygen flow rate of 100 mL.min ⁻¹	44
Figure II.11: TGA measurements of the P25 catalyst recovered after 1, 5 and 10 h of benzyl alcohol oxidation in acetonitrile at 50°C under oxygen	44
Figure II.12: XRD patterns for P25 after photo-oxidation of benzyl alcohol for different times (1, 5, 10 h)	44
Figure II.13: Effect of solvents on the P25 photocatalyzed aerobic oxidation of benzyl alcohol under UV irradiation (Same conditions as in Table II.3)	47
Figure II.14: Attempt of correlations between benzylalcohol conversion rates with the physicochemical parameters of the solvents	49
Part II / Chapter 3	
Figure III.1: Electron micrographs of rutile titanium dioxide sol particles obtained by sol-gel synthesis at different ratios of TiCl ₄ /HCl/Na ₂ SO ₄ . [18]	64
Figure III.2: (a) TEM image of anatase TiO ₂ nanobipyramids prepared under solvothermal condition at 250°C for 24 h with a molar ratio of titanium butoxide to NaF of 5:2. (b) XRD pattern of the <i>as</i> prepared TiO ₂ nanobipyramids. (c, d) HRTEM images of nanobipyramids. (Inset) nanobipyramid [37]	66
Figure III.3: Principle of the insertion of cobalt oxide in the mesoporosity of SBA-15 using the “Two-solvents” method [57]	69
Scheme III.1: Connectivity of TiO ₆ octahedral units in (a) anatase, (b) rutile, and (c) brookite [2]	59
Part II / Chapter 4	
Figure IV.1: HR-TEM photographs of colloidal dispersion of A and B) Ti-M1, C) Ti-M2, and D) Ti-M3 (anatase in white circle after ageing 1 month)	78
Figure IV.2: Comparison of the photocatalytic activities of 1 month-aged Ti-Mx colloidal suspensions with P25 in the photoselective oxidation of benzyl alcohol under UV irradiance at 50°C	79
Figure IV.3: Low angle XRD patterns of A) SBA(95) and B) SBA(130)	80
Figure IV.4: N ₂ adsorption/desorption isotherms at -196°C of A) SBA(95) and B) SBA(130) samples superimposed with those of the corresponding materials obtained after Ti-M1 incorporation	83
Figure IV.5: TGA curves of A) SBA(95) and B) SBA(130) samples superimposed with those of some corresponding materials obtained after Ti-M1 incorporation	84
Figure IV.6: X ray diffraction peaks of A) SBA(95) and B) SBA(130) samples superimposed with those of the corresponding materials obtained after Ti-M1 incorporation	84
Figure IV.7: DR UV-Vis. spectra and Tauc plots for band gap determination (insets) of A) SBA(95) and B) SBA(130) samples superimposed with those of the corresponding materials obtained after Ti-M1 incorporation. Ti-M1-SBA(95)-DS-C and Ti-M1-SBA(130)-DS-C are the calcined forms (500°C) of Ti-M1-SBA(95)-DS and Ti-M1-SBA(130)-DS	85
Figure IV.8: Transmission electron micrographs of Ti-M1-SBA(130)	86
Figure IV.9 : Transmission electron micrographs of Ti-M1-SBA(130)-DS	87
Figure IV.10 : Transmission electron micrographs of Ti-M1-SBA(95)-DS	88
Figure IV.11: Comparison of the photocatalytic activities of the materials prepared by the “Two-solvents” method (in their <i>as</i> -synthesized or calcined forms) in the photoselective oxidation of benzyl alcohol under UV irradiance at 50°C	89

Annex 1

Figure 1: X-ray diffractograms of (A) DD3, (B) SBA-15 and ZSM-5 derived samples	100
Figure 2: TEM images of Ru-DD3(5%), size distribution of Ru nanoparticles and EDX spectrum emphasizing Ru in the insert	101
Figure 3: TEM images of (A): Ru-SBA-15(5%), (B) : Ru-HZSM5-5(5%) and size distribution histograms (C) : Ru-HZSM-5(5%) and Ru-NaZSM-5(1%)	102
Figure 4: N ₂ adsorption-desorption isotherms of (A) DD3, (B) SBA-15 and ZSM-5 derived samples.	102
Figure 5: TEM image of the Ru-DD3(5%) catalyst after the 5 th run and histogram of the Ru NPs size (c.a. 300 counts)	106

Annex 2

Figure 1: Quantification of benzyl alcohol using mesitylene as internal standard.	111
Figure 2: Quantification of benzaldehyde using mesitylene as internal standard.	111
Figure 3: Quantification of methyl benzoate using mesitylene as internal standard.	112
Figure 4: Quantification of cyclohexanol using mesitylene as internal standard.	112
Figure 5: Quantification of cyclohexanone using mesitylene as internal standard.	113

Table des tableaux

Part I / Chapter II

Table II.1: Physico-chemical properties of the different photo-materials tested	36
Table II.2: Results of the photo-catalyzed aerobic oxidation tests of benzyl alcohol into benzaldehyde in acetonitrile under UV irradiance	44
Table II.3: Effect of solvents on the P25 photocatalyzed aerobic oxidation of benzyl alcohol under UV irradiation	47
Table II.4: Physicochemical properties of the solvents vs. P25 photo-assisted benzylalcohol oxidation under UV irradiation	48
Table II.5: Results of the photocatalyzed aerobic oxidation tests of benzyl alcohol derivatives in acetonitrile under UV irradiance	51
Table II.6: Results of the photocatalytic aerobic oxidation tests of aliphatic alcohols and the oxidative cleavage of C-C bonds	53

Part II / chapter 3

Table III.1: TiO ₂ nanoparticles or colloids synthesized under different conditions	63
--	----

Part II / chapter 4

Table IV.1: Synthesis parameters used for the different preparations	74
Table IV.2: Effect of the aging time (storage period) on the particle size determined DLS and HR-TEM	77
Table IV.3: Observations made for the different attempts of synthesis described in Table IV.1	78
Table IV.4: Physicochemical properties of the materials before and after Ti-M1 deposition	82

Annex 1

Table 1: Composition (%) of natural "DD3" kaolin and Ru/DD3 samples	100
Table 2. Textural properties of the different DD3 and Ru supported-materials tested	103
Table 3 : Influence of some parameters on the oxidation of benzyl alcohol by O ₂ in the presence of Ru-DD3(5%)	103
Table 4 : Oxidation of benzyl alcohol into benzaldehyde over Ru based catalysts in toluene suspension using O ₂	104
Table 5: Recyclability of Ru/DD3 (5%) in the aerobic oxidation of benzyl alcohol.	105

Résumé

Des oxydes semi-conducteurs, en particulier TiO_2 commercialement disponible ou des échantillons mésoporeux synthétisés, ont été testés comme photocatalyseurs de l'oxydation ménagée et aérobie d'alcools dans l'acétonitrile sous UV. L'alcool benzylique a été oxydé principalement en benzaldéhyde (rendement = 60%) en présence de TiO_2 -P25. Malheureusement, ce catalyseur tend à se désactiver. Le rôle du dioxygène dans le processus d'oxydation a été souligné après avoir testé différents solvants. Les alcools aliphatiques ont également été étudiés. Ainsi, le cyclohexanol a donné principalement de la cyclohexanone (rendement = 70%).

Parallèlement, une approche colloïdale a été développée pour déposer les nanoparticules d'oxyde de titane sur des supports de silice mésoporeux SBA-15 transparents aux UV afin d'éviter les phénomènes d'agrégation lors des tests. Après optimisation de leur synthèse (quantité d'eau, nature de l'acide et de l'alcool), des nanoparticules sphériques non cristallines stables de 5 nm de diamètre ont été obtenues. En utilisant la méthode d'imprégnation à "deux solvants", ces dernières ont été introduites avec succès dans les mésopores de deux échantillons de SBA-15, l'un avec un diamètre moyen des pores de 6 nm, l'autre de 8. Les analyses MET ont souligné que le matériau SBA-15 avec les pores les plus grands a conduit à l'incorporation de davantage de nanoparticules. A priori, les interactions silice / oxyde de titane dans les matériaux résultants semblent favorables puisque les quantités inférieures de TiO_2 dans les tests de photocatalyse correspondants ont conduit à de meilleurs taux de conversion que ceux obtenus avec P25 ou la suspension mère de colloïdes.

Mots clés : [Oxydation photocatalytique sélective; Dioxyde de titane; Oxydation ménagée d'alcools; Imprégnation "double solvants"; Ultra-violet ; Mésoporeux]

[Bulk TiO_2 vs alternative Ti-based photocatalysts for the mild aerobic oxidation of alcohols]

Abstract

A series of metal oxides semiconductors, including commercially available TiO_2 or synthesized mesoporous samples, were tested as photocatalysts for the aerobic mild oxidation of alcohols in acetonitrile under UV. Benzyl alcohol, used as a reference, was oxidized mainly into benzaldehyde. Best yield (60%) was obtained with TiO_2 -P25. Unfortunately, this catalyst tended deactivate with time. The role of dioxygen solubility in the oxidation process was emphasized through the test of different solvents. Aliphatic alcohols were also studied. Among them, cyclohexanol gave mainly cyclohexanone with a yield of 70%.

Parallely, a colloidal approach was developed for the deposition of titanium oxide nanoparticles on UV transparent mesoporous silica supports in order to take advantage of their important specific surface area and avoid aggregation phenomena during the photocatalysis tests. After optimizing the synthesis protocol (amount of water, nature of the acid and alcohol), spherical, non-crystalline stable nanoparticles with 5 nm diameter were obtained. Using the "two-solvents" impregnation method, these particles were successfully introduced in the mesopores of two SBA-15 silica samples differing by their mean pore diameter (either 6 or 8 nm). TEM measurements emphasized that the SBA-15 material with the largest pores led to the incorporation of more nanoparticles in its mesopores. Clearly, silica/ titanium dioxide interactions in the resulting materials appeared to play a positive role since lower amounts of TiO_2 in the corresponding photocatalysis tests led to improved conversion rates of benzylalcohol compared to those performed with P25 or the parent suspension of colloids.

Keywords : [selective photocatalytic oxidation ; titanium dioxide; mild oxidation of alcohols ; « two-solvents » impregnation ; Ultra-violet ; Mesoporous]